FCTUC DEPARTAMENTO DE ENGENHARIA CIVIL
FACULDADE DE CIÊNCIAS E TECNOLOGIA
UNIVERSIDADE DE COIMBRA

Hybrid Lattice-Tubular Steel Onshore Wind Towers: Conceptual Design of Tower and Transition Segment

Dissertação apresentada para a obtenção do grau de Mestre em Engenharia Civil na Especialidade de Mecânica Estrutural

Autor
João Pedro Rocha Resende de Almeida

Orientador
Carlos Alberto da Silva Rebelo
Milan Veljkovic

Coimbra, Julho, 2016

ACKNOWLEDMENTS

RESUMO

A necessidade de lutar contra o aquecimento global tem levado a um constante aumento do interesse em energias renováveis. Consequentemente, o mercado de energia eólica está a crescer exponencialmente. Deste modo, é necessário a melhoria e/ou desenvolvimento de tecnologias no campo das energias renováveis, sendo esse um trabalho de um engenheiro civil.

Com o presente trabalho pretendeu-se desenvolver o conceito de torres eólicas inovadoras, de baixo custo, cujo procedimento de ereção deverá ser inovador e requerem pouca manutenção. Uma vez que estas torres devem resistir a ventos fortes, que, por sua vez, correspondem a uma maior eficiência na obtenção de energia, e por forma a suportar turbinas maiores, a altura da torre deve ser aumentada relativamente aos tamanhos mais convencionais. Assim, as torres de aço híbridas treliça-tubular surgem como uma excelente solução.

Torres de aço híbridas treliça-tubular consistem numa treliça de aço que suporta um segmento tubular. Estas duas partes são ligadas por um segmento de transição. Particularizando para a torre de aço híbrido treliça tubular desenvolvida no presente estudo, esta deve ser colocada em terra e capaz de suportar uma turbina eólica de 5 MW. Além disso, o seu dimensionamento teve em conta a estabilidade global de torre, bem como a estabilidade local de elementos de estrutura de treliça, fadiga e problemas dinâmicos estão também incluídos no dimensionamento. A treliça tem 60 m de altura que suporta um segmento tubular de 90 m de aço.

Com uma altura total de 150 m, a montagem da torre exigiria guindastes de grande porte, o que pode resultar num aumento de preço considerável. Desta forma, foi também objetivo do presente projeto, a conceção de uma solução única para a peça de transição que pode permitir a montagem de peças tubulares através de um procedimento de escorregamento e, ao mesmo tempo, evitar a utilização de grandes guindastes.

ABSTRACT

The need to fight global warming has led to an increased interest in renewable energies and, consequently, the market is undergoing an exponential growth, in particular wind power. Nevertheless, there is a constant need to improve renewable energies technologies, a task and the responsibility of a civil engineer.

At present, work is aimed to develop the concept of innovative wind towers, which should be cost-effective, hold an innovative erection procedure and require low maintenance. Since such towers ought to resist to stronger winds, which correspond to a higher efficiency, and to support bigger turbines, the hub must be heightened, making hybrid lattice-tubular steel towers an excellent solution.

Hybrid Lattice-Tubular steel towers consist of a steel lattice structure, supporting a steel tubular segment in the upper part of the tower, while a transition segment connects the two parts. In particular, the hybrid lattice-tubular steel tower that was developed in the present study is targeted for onshore applications and able to support a 5 MW wind turbine. Moreover, its design took into account the global stability of a tower as well as the local stability of elements in lattice structure, fatigue and dynamic problems. The lattice structure is 60 m tall and supports a 90 m steel tubular segment.

With a total height of 150 m, the tower assembly would require large cranes, which could induce a considerable price increase. This way, it was also a goal of this project to design of a unique solution for the transition piece that could allow the erection of tubular parts by a slide procedure and, at the same time, avoid the use of large cranes.

LIST OF CONTENTS

SYMBOLS

A – Cross section area

A_V – Shear area

a – ratio of web area to gross area

d - outer diameter of circular tubular sections

di – inner diameter of circular tubular sections

E - Modulus of elasticity

fu – Ultimate strength

fy – Yield strength

fy' – Reduced yield strength depending on ρ

G – Shear modulus

GW – Gigawatt

I – Moment of inertia

I_T – Torsional Constants

I_W – Warping Constants

i – properties radius of gyration about the relevant axis, determined using the properties of the gross cross-section

k_{yy} Interaction factor

k_{yz} Interaction factor

k_{zy} Interaction factor

k_{zz} Interaction factor

L_b – Member length braces

L_c – Member length chords

L_{ch} – Buckling length of chord

L_{br} – Buckling length of braces

MW – Megawatt

M - Mass

m – Meter

mm – Millimetre

$M_{c,Rd}$ – Design resistance for bending about one principal axis of a cross-section

$M_{Ed,y}$ – Design bending moment, y-y axis

$M_{Ed,z}$ – Design bending moment, z-z axis

$M_{y,Rd}$ – Design values of the resistance to bending moments, y-y axis

$M_{z,Rd}$ – Design values of the resistance to bending moments, z-z axis

$M_{Ed,z}$ – Design bending moment, z-z axis

$N_{b,Rd}$ - Design buckling resistance of a compression member

N_{cr} – elastic critical force for the relevant buckling mode based on the gross cross sectional

N_{Ed} – Design value of the axial force

$M_{N,Rd}$ – Reduced design values of the resistance to bending moments making allowance for the presence of normal forces

$M_{V,Rd}$ – Reduced design values of the resistance to bending moments making allowance for the presence of shear forces

ΔM_y moments due to the shift of the centroidal y-y axis

ΔM_z moments due to the shift of the centroidal z-z axis

$N_{PL,Rd}$ – Design plastic resistance to normal forces of the gross cross-section

N_{Rd} – Design values of the resistance to normal forces

n – Ratio of design normal force to design plastic resistance to normal forces of the gross cross-section

T_{Ed} – Design value of total torsional moments

T_{Rd} – Design resistance to torsional moments

$T_{t,Ed}$ – Design value of internal St. Venant torsion

$T_{w,Ed}$ – Design value of internal warping torsion

t – Thickness

$V_{Ed,y}$ – Design shear force, y-y axis

$V_{Ed,z}$ – Design shear force, z-z axis

$V_{c,Rd}$ - Design shear resistance

$V_{pl,T,Rd}$ – Reduced design plastic shear resistance making allowance for the presence of a torsional moment

W_{el} – Elastic section modulus

W_{pl} – Plastic section modulus

x-x – axis along a member

y-y – axis of a cross-section

z-z – axis of a cross-section

α – Parameter introducing the effect of biaxial bending

α – Imperfection factor

α – Coefficient of linear thermal expansion

β – Parameter introducing the effect of biaxial bending

ε – Strain

ε – Coefficient depending on fy

γ_{M0} – Partial factor for resistance of cross-sections whatever the class is

γ_{M1} – Partial factor for resistance of members to instability assessed by member checks

γ_{M2} – Partial factor for resistance of cross-sections in tension to fracture

Φ – Value to determine the reduction factor χ

σ – Stress

ν – Poisson's ratio in elastic stage

λ – Slenderness

$\bar{\lambda}$ – Non dimensional slenderness

λ_l – Slenderness value to determine the relative slenderness

$\bar{\lambda}_T$ – Relative slenderness for torsional or torsional-flexural buckling

$\bar{\lambda}_{OV}$ – Overall relative slenderness for complete shell structures

ρ – Reduction factor to determine reduced design values of the resistance to bending moments making allowance for the presence of shear forces

η – Factor for shear area

τ_{Ed} – Design value of the local shear stress

$\tau_{t,Ed}$ – Design shear stresses due to St. Venant torsion

$\tau_{w,Ed}$ – Design shear stresses due to warping torsion

χ – Reduction factor for the relevant buckling curve

χ_y –reduction factor due to flexural buckling (y-y axis)

χ_z –reduction factor due to flexural buckling (z-z axis)

1 INTRODUCTION

1.1 Background

For the time being, global warming is doubtlessly one of the greatest threats to the world that we live in. In order to fight this problem, it is necessary to invest in the development and optimization of the use of renewable energies. A renewable energy is an energy that comes from natural resources, such as sun, wind, rain, tides and geothermal energy, which are naturally replenished. In this thesis, among all the mentioned renewable energies, wind energy will be prioritized.

Wind energy is obtained through the use of wind turbines, which are located in the top of wind towers. The most common wind turbines have three rotor blades. Such blades rotate around a horizontal axis hub, which, in turn, is connected to the power electronics, located in the nacelle at the top of a wind tower. The typical components of a wind turbine are demonstrated in the Figure 1.1. Wind turbines produce electricity by using the natural power of the wind to drive a generator. The wind is a clean and sustainable fuel source, it does not create emissions and it will never run out as it is constantly replenished by energy from the sun [Briefi, 2004].
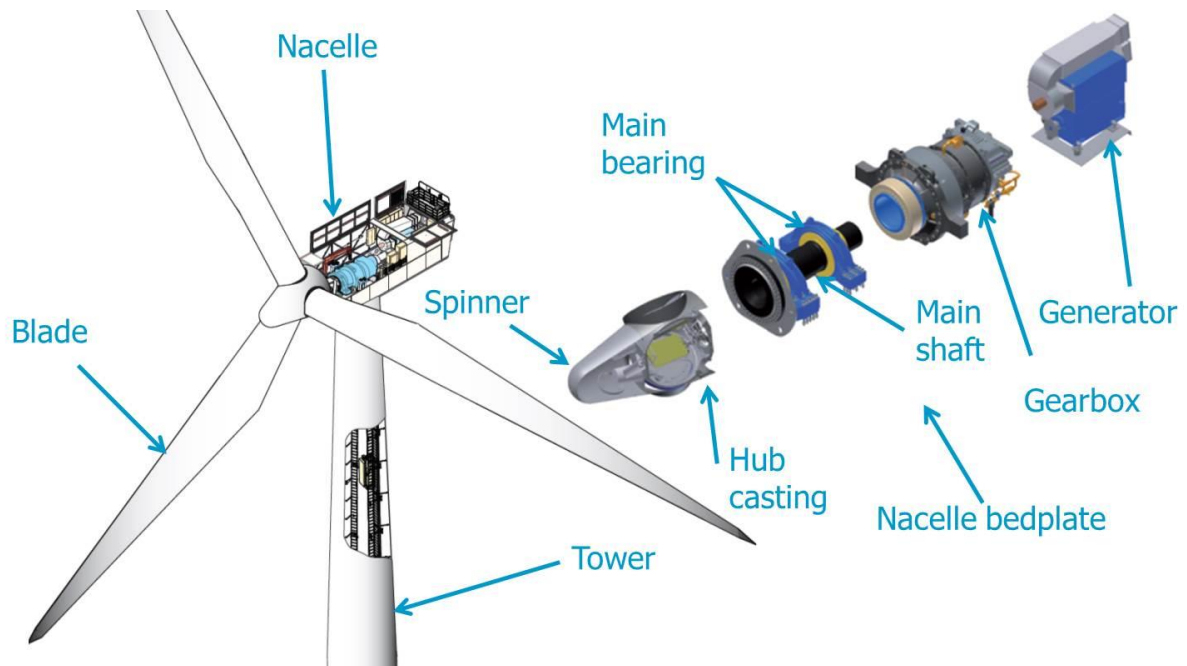
Figure 1.1 – Typical components of a Horizontal Axis Wind Turbine (HAWT)

As technology improved, windmills became wind turbines. Additionally, besides onshore installations, nowadays, there are installations of wind turbines also located offshore. Wind turbines manufacturers are currently developing longer blades and lighter rotors in order to optimize and increase energy production. Currently, the highest wind power is that can be obtained by the wind turbines in use is set at 7.0 MW. Nevertheless, European Wind Energy Association (EWEA) has already planned wind turbines capable of generating 15 MW and states that in the future it will be possible to reach 20 MW.

It is worth noting that wind is a clean and sustainable fuel source; and it does not create any greenhouse gases emissions or toxic substances. The fuel sources do not contribute to air or water pollution, and will never run out as it is constantly replenished by energy from the sun. Therefore, the wind energy market has a significantly influence when it comes to energy installations. According with the EWEA, wind power was the renewable energy with the most capacity installed with a total of 11,791.4 MW, where 10,308.1 MW were onshore and 1,483.3 offshore. Wind power was the energy technology with the highest installation rate of 44 %, in 2014. In Graphic 1A a comparison is presented between the power capacity installations in the European Union (EU) while Graphic 1B shows a similar comparison but only between renewable energies. Nowadays, wind power is the most advanced renewable technology available at large scale. Since 2000 wind power has achieved a Compound Annual Growth Rate of 9.8 % and in 2014 11.8 GW of wind power were installed in the EU. Furthermore, also since 2000, 412.7 GW of new power capacity was installed. As a result of this, wind power represents 29.4 % of the total renewable power capacity installed, which consists in more than 50 % of the overall result of renewable energies.
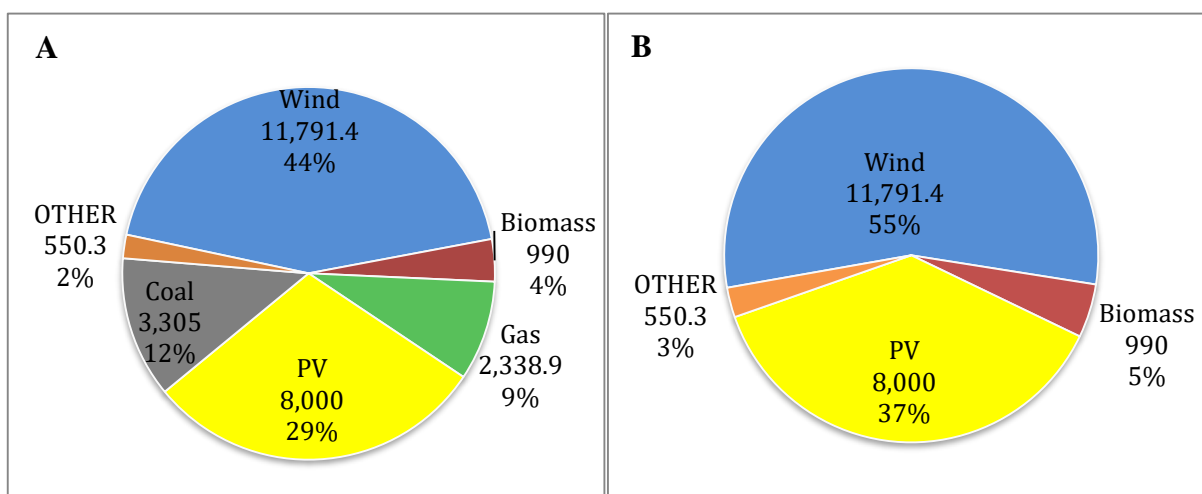
Graphic 1.1 – Power capacity installed a) Power Capacity Installed in EU (MW) - Total 26.9 GW (2014); b) Renewable Power Capacity Installed in EU (MW) - Total 26.9 GW (2014);

OTHER represents the sum of Hydro, Waste, Geothermal and Ocean Energy (Adapted from EWEA, 2014)

Regarding the evolution of wind power installations in the EU (Graphic 1.2) it can be ascertained that it has been increasing over time, though not constantly. Others renewable energies such as biomass, hydro, waste, CSP, geothermal and ocean energies also presented a similar behaviour during the past decade but in a slower rhythm.
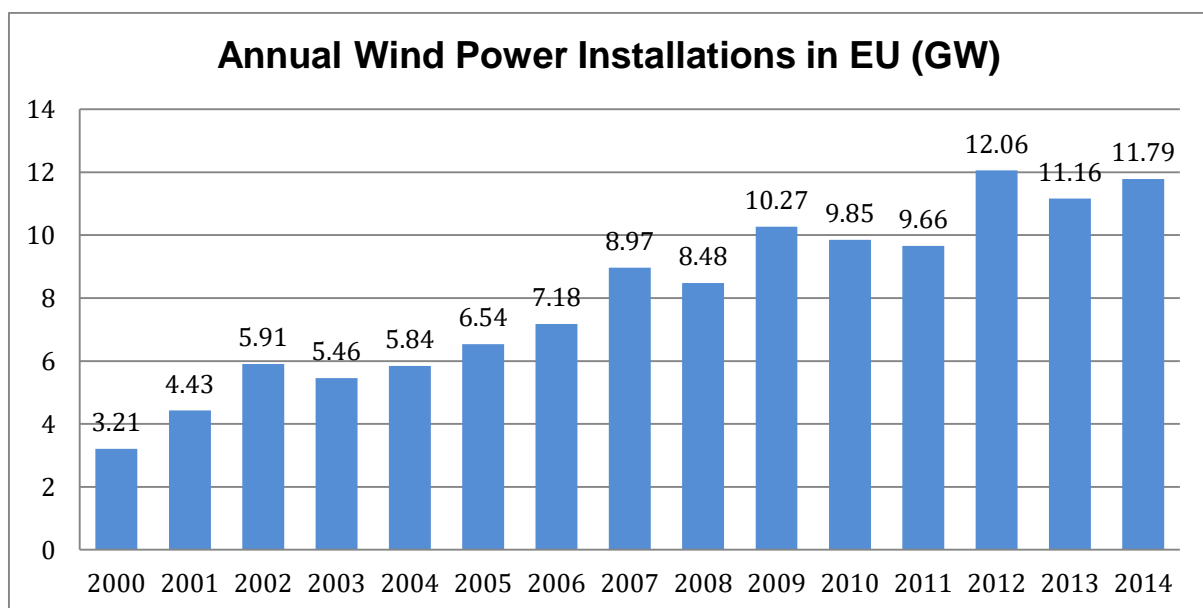
Graphic 1.2 – Annual Wind Power Installations in EU (GW); Total 128.8 GW (29,4% of 412.7 GW which represents the total power capacity installed in EU (Adapted from EWEA, 2014)

With regard to jobs employment growth, wind power has also had a huge impact in this sector. Since 2010, wind energy has contributed with € 32 Billion to the EU economy, which even by the year of 2012 only represented 37.6% of the global wind energy market. Between 2010 and 2012 there was an increase of 30% of jobs in wind energy in the EU. Moreover, in 2012 249,000 people were employed in EU Wind Energy field, and EWEA estimates that this number should increase up to 520,000 by the year of 2020.

Over the past 14 years, the EU power sector has generated wind and solar PV energy, while decommissioning fuel oil, coal, nuclear and gas. In 2012, wind energy allowed the saving of € 9.6 Billion of fossil fuel costs and it is estimated savings between € 22 to € 27 Billion per year by 2020, and € 47 to € 51 Billion by 2030. These results and estimations justify why wind

power can drive down wholesale electricity prices and, once again, the current investments in wind technologies. At this time, between €13.1 to € 18.7 Billion were already spent in EU wind farms.

Wind turbines that, as already stated, are used to generate energy from wind, produce 80 times more energy than what is used to build, install, operate, maintain and decommission them. Despite the increase of wind power capital, its associated low costs of operation and maintenance and inexistence of fuel costs, the lack of EU renewable energy targets after 2020 and the instability of national support mechanisms for renewable increase the perception of risk and make financing more expensive. One wind turbine can power more than 1,202 households or can fuel 2,315 electric cars.

With regards to the differences between onshore and offshore installations it is worth noting that after the installation of the first offshore wind farm in Denmark in 1991, the offshore market has been growing and 2,488 turbines are now installed and grid connected, making a cumulative total of 8,045.3 MW in 74 wind farms in 11 European countries. In fact, it is currently known that the offshore wind is more frequent and more powerful than in land, which means that offshore wind farms can easily overtake onshore wind projects in terms of installed capacity. Aesthetically offshore wind farms have a less negative impact when compared to onshore wind farms, as they are not visible or only barely visible from shore. Offshore wind power installations represent 12.6% of the annual EU wind energy market, down from 14% in 2013 (

EWEA, 2014). Graphic 1.3 shows the annual installations of wind energy since 2000, and makes a comparison between onshore and offshore installations.
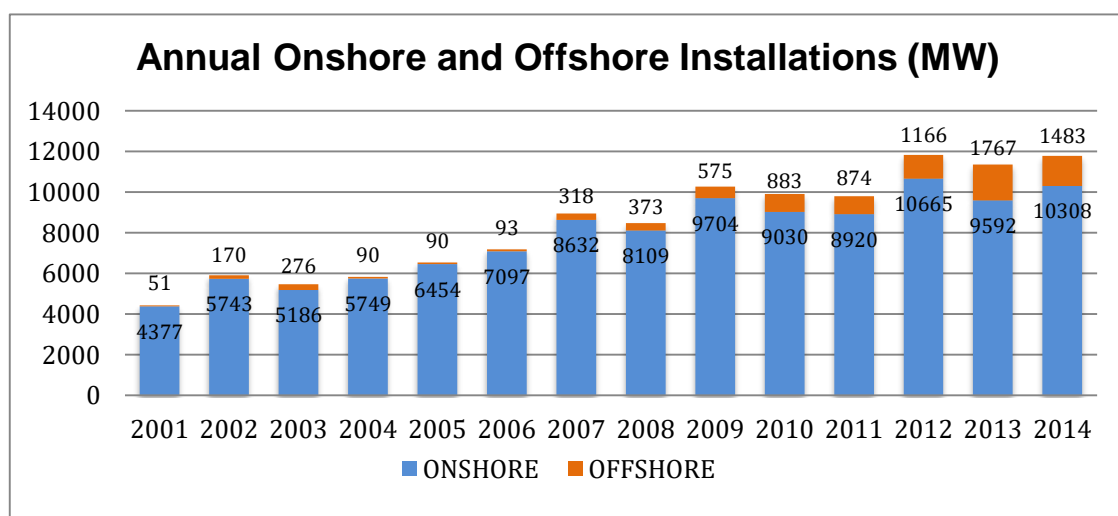
Graphic 1.3 – Annual Onshore and Offshore Installations (MW) (Adapted from EWEA, 2014)

Even so, the biggest disadvantage of offshore installations is that is that they involve higher costs, as more robust structures are needed to cope with the rough weather conditions. In spite of this fact, offshore wind power has a higher capacity factor, which in terms of energy production is much higher than onshore. Table 1.1 shows the major differences between the two different types of wind power.

Furthermore, and concerning, specifically, onshore wind energy market, it is important to mention that it is becoming highly competitive, even against the burning of fossil fuels. When taking into account fuel and CO_2 associated costs, which are constantly increasing, wind energy is less expensive than the energy generated by coal and gas and is even substantially cheaper than the nuclear one. Additionally, an increase of offshore market could only enhance its competitive status among other sources of energy.

According with GWEC, Global Wind Energy Council, at the end of 2014 throughout the European Union 128.8 GW of wind power were installed, out of which approximately 120.6 GW are onshore (Figure 1.A) and just over 8.2 GW offshore (Figure 1.B). Graphic 1.4 indicates the cumulative wind power installations in the EU since 2000. Europe has a total of 134 GW wind power capacity installed. A growth of 9.8% over 2013 was recorded, not surpassing the record of 12% registered in 2012, this shows the negative impact of market across Europe.

Table 1.1 – Onshore/Offshore wind turbines characteristics (Adapted from EWEA, 2014)

Average European Onshore/Offshore Wind Turbine		
EWEA	Onshore	Offshore
Capacity (MW)	2.2	3.6
Capacity Factor	24%	41%
Average Annual Energy Production (MWh)	4,702	12,961
CO_2 Emissions Avoided (t)	3,202	8,827
Installation Cost (€)	2 to 2,25 mn	5 mn

Figure 1.2 – A) Onshore wind energy B) Offshore wind energy
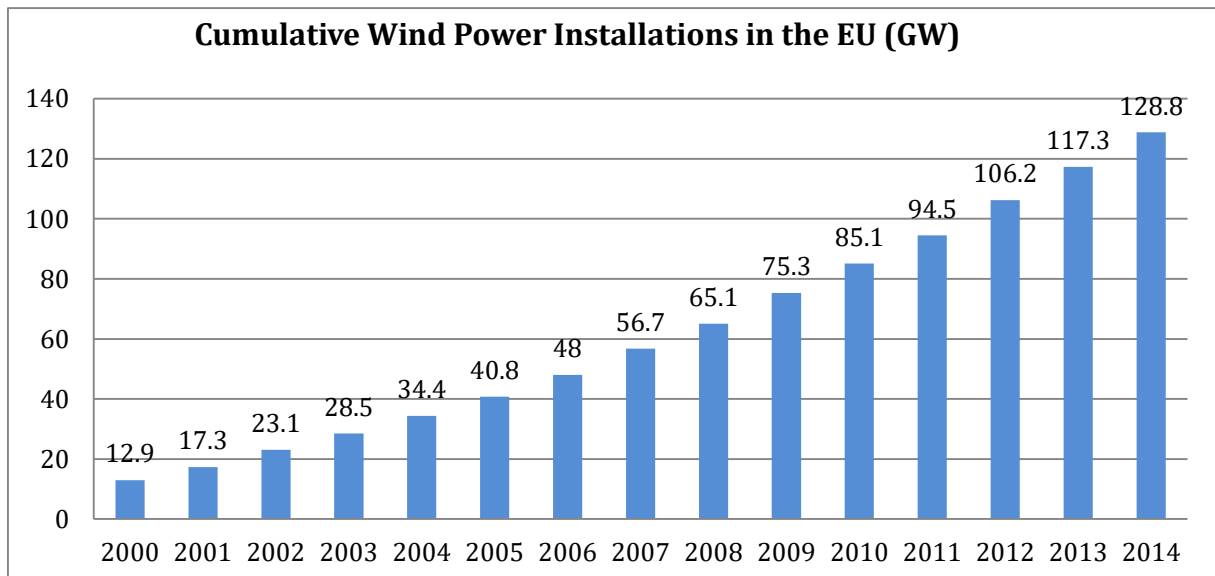
Graphic 1.4 – Cumulative Wind Power Installations in the EU (GW); Total 128,8 GW in the EU (Adapted from EWEA, 2014)

Among all EU countries, Germany was the one that presented the largest wind energy market in 2014, with a total of 5,279.2 MW of new capacity installed, where 528.9 MW are offshore wind energy, more than 10% of total capacity installed in Germany. Furthermore, with 39.2 GW Germany is also the EU country with more wind power installed, followed by Spain, the UK, France and Italy. It is also notable the fact that, nowadays, there are 7 other countries which have more than 1 GW installed. Portugal, Sweden and Denmark have now more than 4 GW installed. Graphic 1.5 shows the total wind power capacity installed in EU.

Total Wind Power Capacity Installed in EU (GW)

Germany; 39.2; 30%

Spain; 23; 18%

UK; 12.4; 10%

France; 9.3; 7%

Italy; 8.7; 7%

Sweden; 5.4; 4%

Portugal; 4.9; 4%

Denmark; 4.8; 4%

Poland; 3.8; 3%

Luxemburg; 0.1; 0%
Latvia; 0.1; 0%
Cyprus; 0.1; 0%
Czech Republic; 0.3; 0%
Croatia; 0.3; 0%
Estonia; 0.3; 0%
Lithuania; 0.3; 0%
Hungary; 0.3; 0%
Finland; 0.6; 0%
Bulgaria; 0.7; 1%
Belgium; 2; 2%
Greece; 2; 2%
Austria; 2.1; 2%
Ireland; 2.3; 2%
Netherlands, 2,8, 2%
Romania; 3; 2%
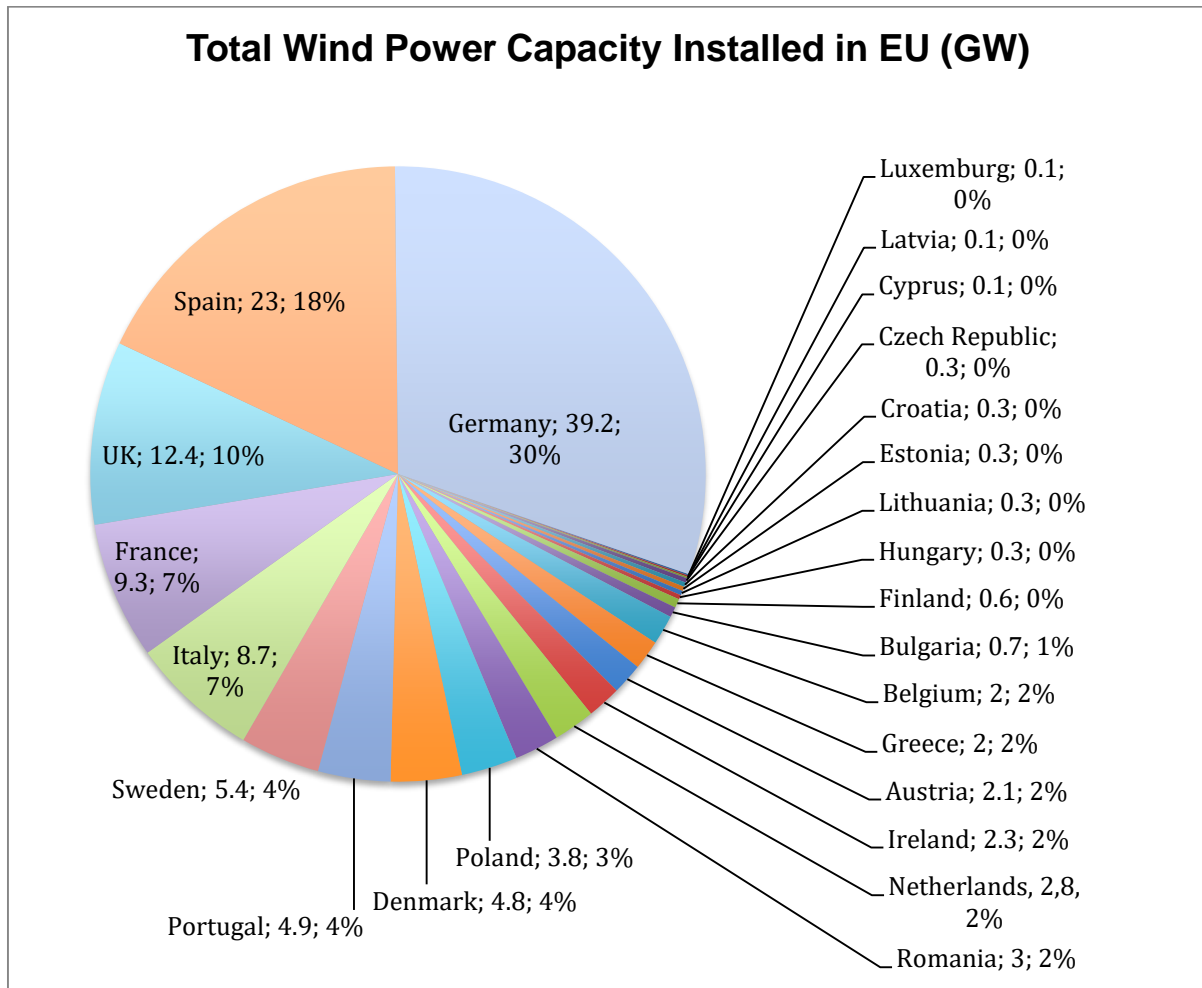
Graphic 1.5 – Total Wind Power Capacity Installed in EU, (Adapted from EWEA, 2014)

In the European Union the total electricity consumption rate is 2798 TWh of electricity. Since the total capacity of wind power installed is 128.8 GW, in a normal wind year the EU would produce 284 TWh from wind power technologies. This value is enough to cover more than 10 % of the previously stated consumption of electricity. As a matter of fact, this percentage could even be increased if the power grid is reinforced and better interconnected, and, consequently, improving its security and supply. This way it would be possible to increase the competition in the energy market, which would bring down prices. For an efficient integration of wind and other renewables, intraday and balancing power markets are needed, with demand-side management. Reinforcing key parts of the grid will provide massive savings between € 1 to 2 Billion per year.

The world needs the development of wind energy among other renewable energies, because when the resources of fossil fuels run out, humanity will need electricity and renewable energy

will be the only alternative. There is one forecast of which you can already be sure: someday renewable energy will be the only way for people to satisfy their energy needs. Because of the physical, ecological and (therefore) social limits to nuclear and fossil energy use, ultimately nobody will be able to circumvent renewable energy as the solution, even if it turns out to be everybody's last remaining choice. The question keeping everyone in suspense, however, is whether we shall succeed in making this radical change of energy platforms happen early enough to spare the world irreversible ecological mutilation and political and economic catastrophe (Scheer, 2006).

1.2   Objectives

The overall goal of this work was to improve cost-effective wind technologies. In order to achieve it, it was necessary to develop higher and more resistant towers, so it could be possible to withstand stronger winds, which are located at high heights and when there is less turbulence, and to take the advantage of more powerful turbines. When increasing the hub height, the diameter of the tubular portion turns out to exceed the maximum allowed for a current transport. Therefore, the industry is demanding the development (1) of a hybrid solution that corresponds in the design of a lattice segment, which should support the tubular part.

Initially it was intended a tower holding a total height of 150 meters, whose assembly would require the use of large cranes. As this could turn out to be a disadvantage for the use/assembly of the tower, it was then proposed the development (2) of a unique solution for the transition segment as well as ensuring the proper transmission of efforts that could allow a new type of erection system for the tubular section by a slide procedure. Although in this project, only the final stage of the transition segment was analysed. Construction phase and erection procedure were not objects of study during this project.

1.3   Thesis structure

This project is divided in ten chapters.

Chapter 1 provides the statistical information as well as the impacts of wind power in the EU economy. The summary, objectives and software used are also included in this chapter.

Chapter 2 contains general background information about previous wind towers together with the existing transition segments used in offshore installation with jacket foundations and also in hybrid lattice-steel wind towers.

Structural requirements and design load values for the design of the lattice structure are described on chapter 3. The lattice structural model is defined on chapter 4. Not only the element types as well the boundary conditions are present in the same chapter. Chapter 5 gives an overview of the design of the hybrid solution, which includes the global stability of tower as well as the local stability of elements in lattice structure and dynamic problems. Ultimate limit state is also given in the presented chapter.

An innovative conceptual model of the transition segment is explored in chapter 6. Finite element modelling, finite element analysis and the design of the transition segment is given on chapter 7.

Chapter 8 summarizes all the conclusions made throughout this work, moreover chapter 9 gives an outlook about further possible developments of wind towers.

Cited references are also presented in chapter 10 while relevant appendices are included in the appendix.

1.4 Used software

In this study the following computer programs were used:

- EXCEL, spreadsheet program, Microsoft Inc.
- ROBOT, advanced structural analysis software, Autodesk Inc.
- ABAQUS, general purpose finite element program, Abaqus Inc.
- AUTOCAD, computer aided design, Autodesk Inc.
- NX, product lifecycle management software, Siemens.

2   STATE OF ART

2.1   Wind power turbine tower structures

Windmills were first used to mill grain, pump water, or both. At the end of the 19th century the first wind turbines were built in Scotland and they revolutionized the field of wind energy and, consequently, renewable energy. In fact, their impact has even increased in the 21th century with the rising concern about Global Warming. Wind turbines evolved from windmills. The need for larger turbines has led to the development of different tower concepts: steel tower, lattice/truss tower, concrete tower, hybrid concrete-tubular steel towers and hybrid lattice-tubular steel towers.

2.1.1   Steel Tower

Steel tubular wind towers are by far the most used in the onshore market of wind power. These towers are composed by 3-4 segments, which are individually transported and assembled on site using bolted connections. In order to reduce the used material and achieve a greater efficiency the towers are conical: the diameter has its maximum value at the base decreases towards to the top. Furthermore, increased wind power, i.e. turbine power, increases the loads, bending and torsional moments acting on the structure. In order to withstand the increased loadings, the dimensions of the tower must be increased, i.e. both diameter of the tube and the thickness of the plate, tube wall, must be increased, which lead to further implications. (Elforsk, 2012).

The bolted connection is achieved with a flange, which is welded to the top and bottom of the tubular segments and bolted traditionally (Figure 2.1a). However, a High-strength tower in steel for wind turbines (HISTWIN) is developing an innovative solution of assembling joints using friction connection with opened slotted holes (HISTWIN, 2012) (Figure 2.1b).

Due to transportation limitations the diameter may not exceed 4.5 m since it is the practical limit for the diameter of complete ring sections that can be transported along the public highway. Apart from that in terms of production, is difficult to have plates thicker than 50 mm, although steel tubular wind towers with 150 m of hub height have already been produced.
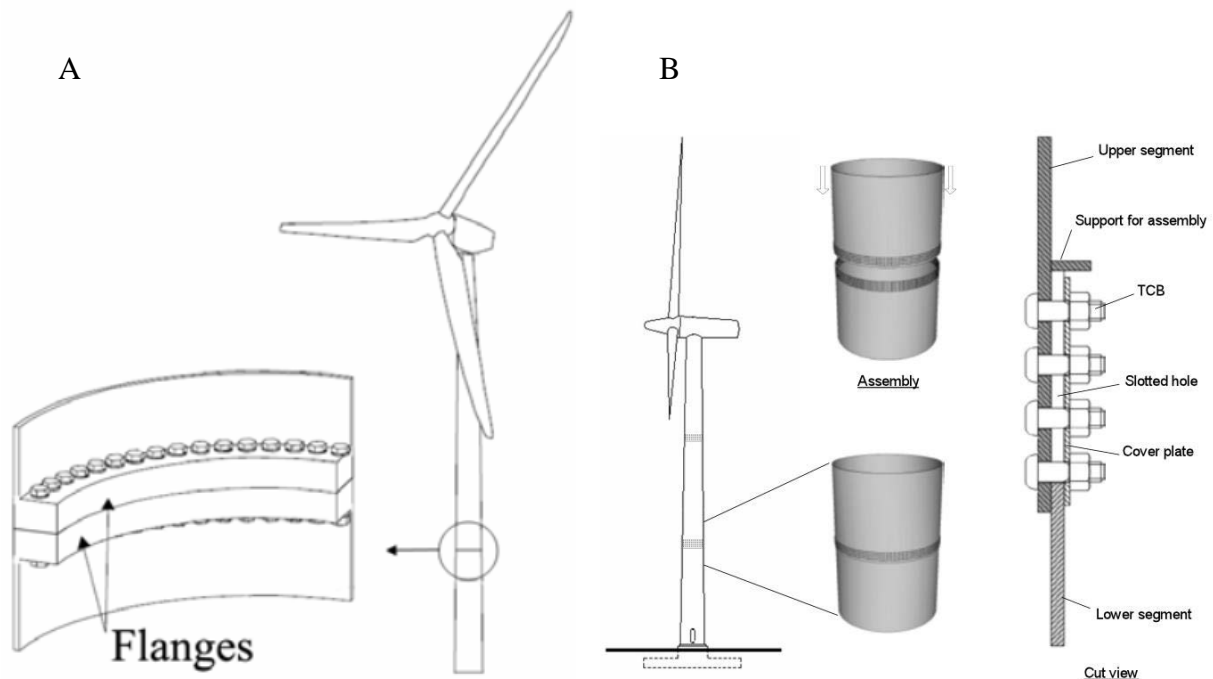
Figure 2.1 – Different methods for the assembly of the tubular segments A) traditional welded flange bolted connection (Heisterman, 2011) B) Friction connection (Histwin, 2012)

According to a periodical published by (Elforsk, 2012), the advantages of tubular towers are the following:

- A tubular steel structure is relatively light and due to its circular cross section has the same bending stiffness in all directions;
- Tubular towers have a good torsional stiffness;
- The required natural frequency can be easily achieved for certain types of turbines and hub heights;
- These towers can be relatively easy to install and has low maintenance costs;
- The tower can be climbed from the inside and is equipped with working platforms and a ladder with a fall protection system.

As a result of all advantages mentioned above, steel tubular towers are the most used in onshore wind farms. The Gansu Wind Farm Project (Figure 2.2) is the biggest wind farm in the world with almost 8 GW installed, there are plans to be increase up to 20 GW. It has an annual generation of 90 GW/h and it is located in Gansu, China.

Figure 2.2 – Gansu Wind Farm

Wind towers are exposed to an extremely aggressive environment, especially those who are in coastal areas. To prevent corrosion a special sandblasting procedure is usually applied which consists of placing an epoxy resin coating to the tower surface.

With regard to the tower foundation, it must comply with local rules and regulations; The foundation must be designed according to the local soil properties.

2.1.2 Lattice/Truss Tower

During the first years of commercial wind energy utilization, lattice towers were widely used in small turbines. As their sizes increased, steel tubular towers increasingly displaced the lattice towers. Recently, the interest in lattice towers has been rekindled, particularly in connection with large turbines with a hub height of 100m and more (Hau, 2006). Steel lattice structure is a very well-known method that is used to build a wide range of tower types, such as energy transmission lines, and they were even used to support wind turbines in the beginning of wind energy exploitation.

Lattice towers are made of an assembling of chords and braces, which are the main and secondary members respectively. The assembly has a specific order to reduce the amount of material used whilst ensuring a structural strength and stiffness. Truss towers are manufactured using welded steel profiles, notwithstanding that connecting members may be made using bolts. The main advantage of lattice towers when compared to steel tubular towers is that they only require half of the amount of material to achieve a similar resistance. Furthermore, since the towers can be easily assembled on site, transportation is not an issue.

Besides their associated low cost and easy transportation and assembly, below are presented other advantages regarding lattice towers:

- Straightforward design and detailing;
- Good dynamic behaviour;
- Economy of transportation;
- Simpler erection procedures.

Regarding the disadvantages, unlike tubular towers, due to the problem of fatigue in welded joints, maintenance is an important factor to be taken in consideration. Additionally, the enormous time spent on assembly and their visual appearances represent the major drawbacks of their use.

Lattice towers, in forested areas represent a great solution, since the turbine for a better efficiency needs to be above of the tree line, due truss towers are proving to be a pronounced solution for very tall towers. The highest wind tower installed so far is a steel lattice tower, whose installation was completed in 2003, and it holds 160 m of hub height and is known as Fuhrländer Wind Turbine Laasow (Figure 2.3).
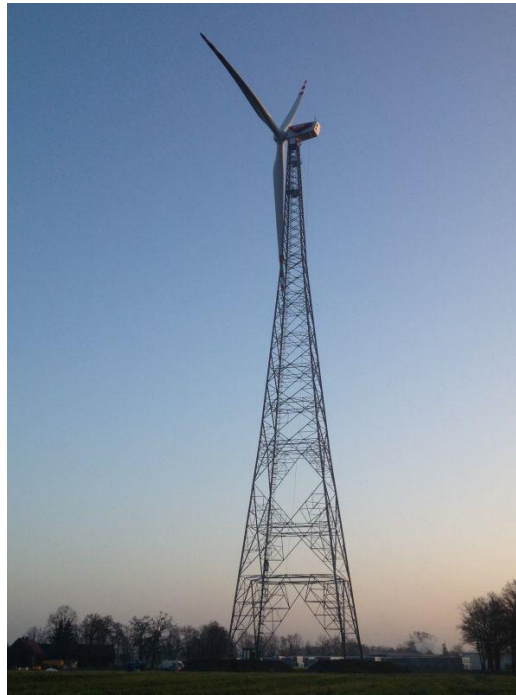
Figure 2.3 – 160 m Fuhrländer Wind Turbine Laasow

Nowadays, the lattice tower has again become an alternative to the tubular-steel tower in the case of the very high towers required for large turbines sited in inland regions (Hau, 2006).

2.1.3 Concrete tower

Wind towers can also be made of reinforced concrete. Despite the fact that concrete towers are not widely used, this type represents a good solution when towers need to be 100 m tall or more. Moreover, the increased steel price together with the development of new efficient production techniques have led to an increased number of concrete towers. Concrete towers, like all other concrete structures, have reinforced steel and make use of bridge technology. Post-tensioned reinforcement can also be achieved and implemented in concrete wind towers. It is worth noting that concrete towers can be made in the following ways:

- Site-mixed concrete
- Prefabricated concrete towers

With the traditional reinforced-concrete type of construction, the concrete is either mixed in liquid form on site or delivered in special vehicles as is done in most cases today. The concrete is poured into a timber form into which the steel reinforcement has first been inserted in the form of a steel wire mat. In this formwork, the concrete hardens so that the required shape emerges when the boarding is removed (Hau, 2006).

A great stiffness and robustness associated with the low maintenance that is required by these towers represent the great advantages of this type of towers. The long construction period is doubtlessly the main disadvantage of these towers. Nevertheless, with the development of prefabricated parts it can be shortened. Combining a proper design and production in accordance with the today's rules/legislation, these towers do not need maintenance during their expected life cycle.

As previously mentioned these towers can be reinforced concrete or post-tensioned reinforced concrete. Nevertheless, the disadvantage of building concrete towers with site-mixed concrete is that it requires a very long construction time since the lowest part should always be set before introducing a new stage. Furthermore, the construction process relies on the production and delivery of concrete not mentioning that a corresponding building infrastructure is also required. For these reasons site-mixed constructions are economically viable only in the construction of wind parks, not in the construction of isolated towers. However, a prototype of the Enercon E-112 with a total height of 120 m has already been built using this method, (Figure 2.4)

As regards site-mixed concrete towers made of post-tensioned concrete, they hold a high load bearing capacity and vary the pre-stressing which may influence the stiffness. Introducing a

pre-stressing on the concrete increases significantly the cost, and for this reason for commercial wind towers this method is not viable.

Figure 2.4 – Concrete tower prototype Enercon E-112

The most common prefabricated method is the use of centrifugally cast concrete towers, being used for small and medium sized towers. A very dense concrete state is achieved during the spinning procedures and has a high performance absorbing dynamic loads. As steel tubular towers, concrete towers can also be transported to the site in segments and assembled on top of one another.

The method most commonly used to build very high towers consists in prefabricating tower segments that are assembled with a concrete/resin mixture on site. Each segment has a length of 3,8 m and are produced with a usual formwork. In order to post tension and fix all segments, during the construction tensioning ropes are inserted into tubes throughout the length of the circumference. For the time being, particularly the prefabricated concrete construction is a preferred solution for high towers (Hau, 2006).

2.1.4   Hybrid concrete-tubular steel towers

With the new developments in pre-stressed concrete towers, together with the need for higher towers, hybrid concrete-steel towers started to be used. The typology of this tower consists in a lower part made of concrete, which is mounted directly on site and then pre-stressed and supports an upper part made of a set of steel tubular segments. The main advantage of this type of tower is that the concrete segment is produced on site so there is no limit concerning the diameter of the bottom part and size limits of transportations should no longer be obstacles. The tower also has high stiffness which also increases the natural frequency and decreases the resonance problems. Another consequence of the fact that the concrete part is built on site, the tower is free of joints and can then be pre-stressed over the entire height using external tendons. The transition of concrete to steel is ensured by means of anchor bolts. The connections of the steel tubular segments are the same as the ones used on steel tubular wind towers (described in section 2.1). Nordex developed a new turbine N90/2500 (LS) that is supported by a 120 m hybrid concrete-steel (Figure 2.5). The bottom part is 60 m tall and is composed by several concrete parts where the lowest part has 8 m diameter and supports all steel tubular segments. The main disadvantage is the long construction time and the need for large cranes to assemble the towers.

Figure 2.5 – Nordex turbine N90/2500 supported by 120 m hybrid concrete-steel tower

As previously mentioned, in section 2.1.3, concrete towers can be of site-mixed concrete or prefabricated concrete as can be hybrid concrete and steel towers. GRI (Global Reporting Initiative) Hybrid Towers provide the wind industry with innovative solutions that address the

challenges posed by new generations of turbines, based on proven reliability of steel and the capacity of precast concrete to solve the weaknesses that steel alone is unable to do (GRI, 2000). The precast concrete segments are transported individually, and when the foundation is completed they are assembled on site (Figure 2.6a). The steel tubular segments are assembled when the concrete part is completed. According to GRI between 2010 and 2015 all built hybrid towers were 100 m high with a turbine with 3.0 MW (Figure 2.6b). Over the next five years there are plans to achieve 125 m of height with 5.0 MW, and 150 m height supporting a 10 MW turbine later.
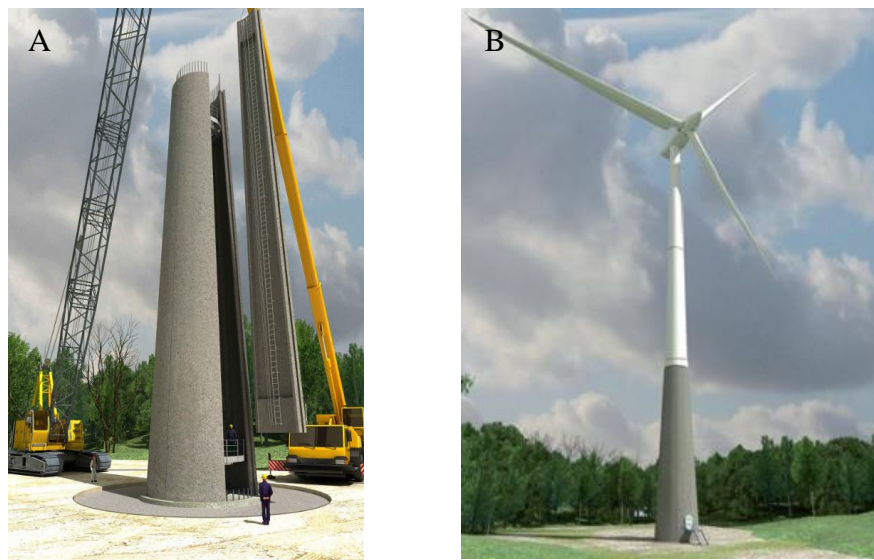
Figure 2.6 – A) Cranes assembling the precast concrete parts B) GRI hybrid concrete-steel wind tower

2.1.5   Hybrid Lattice-Steel Tower

In order to increase the annual production of electricity, bigger wind energy turbines and higher towers are being developed. Hybrid lattice-steel towers allow greater hub heights. The tower consists of three components: a (1) bottom part (lattice), which supports the (2) steel tubular segments and they are connected by a (3) transition piece. The tubular segments, as well as the steel tubular towers, are individually transported and assembled on site with bolted connections, as described in section 2.1.1. Regarding size limits for road transportation, on public highways 4.5 m is the maximum. Once all parts of the lattice are assembled on site a bigger diameter can be achieved and consequently a higher hub height. Suzlon Energy installed the highest hybrid wind tower with 120 m (Figure 2.7). It should be noted that this solution is very recent and is still under development. Through technology innovation these towers will be able to support bigger turbines and reach the 150 m of hub height. This solution with eight supporting chords

leads to a cheaper foundation design, due to the low bending moment on the base, when compared to the steel tubular towers concept.

Figure 2.7 – Suzlon Energy 120 m hybrid lattice-steel tower

2.2 Transition Segments

The main goal of this project is to develop a conceptual design in order to achieve a unique solution for the transition segment for hybrid lattice-steel tubular towers. Offshore wind towers, using jacket foundations make use of a transition piece. This will be the basis for the design of an innovative solution that will allow the erection of tubular towers by slipping and, for this reason, avoiding the need for large cranes.

2.2.1 Jacket Foundations

Offshore wind turbines are constituted by an upper part, which is a tubular steel tower, and a bottom part that supports the upper part, the two segments are connected by a transition piece. The structure of the bottom part can be:

- Monopile (Figure 2.8D)
- Tripod (Figure 2.8B)
- Space frame or jacket foundations (Figure 2.8C)
- Gravity base (Figure 2.8D)
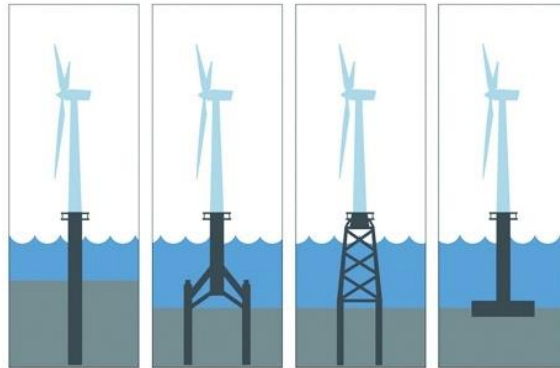
Figure 2.8 – Different base structures for the support of offshore towers A) Monopile; B) Tripod; C) Jacket; D) Gravity base

A jacket foundation is similar to a lattice tower. All its members have small diameter steel circular hollow sections in a "X" configuration, which ensures a high stiffness and robustness that, in turn, withstands rough weather conditions. According with DTU (Technical University of Denmark) department of wind energy, jacket foundations can be applicable at large depths, between 60 and 70 meters. The components of a standard jacket foundation are presented in figure 2.9.

Figure 2.9 – Standard jacket foundations components and transition piece detail

2.2.2 Hybrid Lattice-Steel tubular tower

As mentioned in the section 2.1.5, hybrid lattice-steel tubular towers are relatively new and under development. Nevertheless, there were already some developments regarding the transition piece. In (Figueiredo, 2013) a transition segment (Figure 2.10) with a diameter of 4500 mm, total height of 9120 mm (by overlapping two segments of 4560 mm) and whose connection with the chords members (legs of the lattice) was provided by a gusset plate was presented. The two overlapped pieces are divided in 8 parts and connected by flanges and the same gusset plate that connects the chords members of the lattice.

The 120 m hybrid lattice-steel tower installed by Suzlon Energy (see section 2.1.5) also has a transition piece, which also constitutes the basis for the design of innovative transition piece. In this particularly case, the transition piece has a cabinet, working platforms, ladder with fall protection system and a service lift.
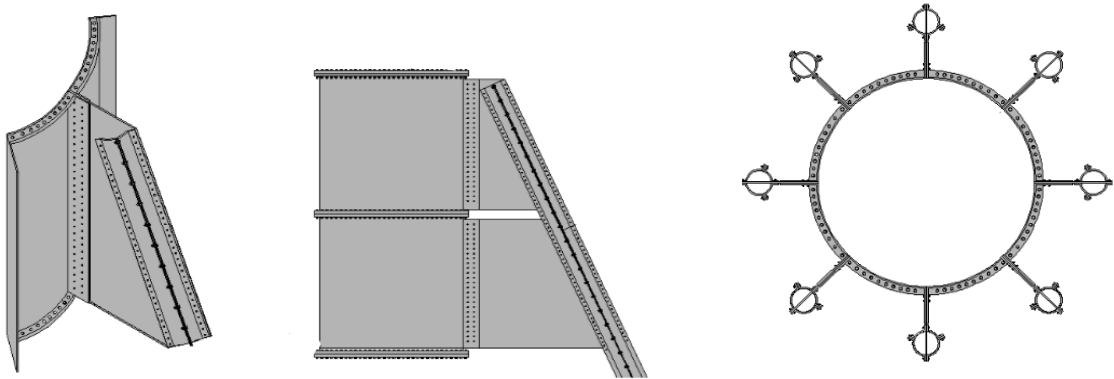
Figure 2.10 – Transition piece (adapted from Figueiredo, 2013)

Moreover, with recent advances in wind technology offshore structures new and different concepts were idealized (Figure 2.11 and 2.12). The conceptual model presented on chapter 6 (Figure 6.1) was conceived through the different concepts presented.
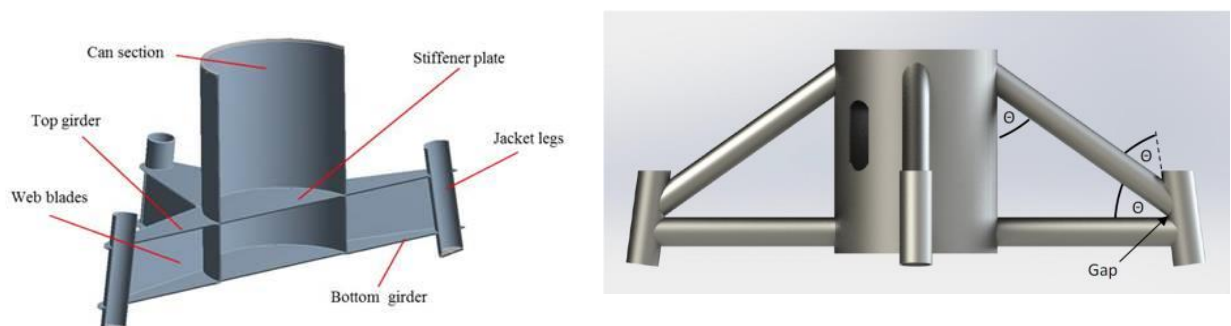
Figure 2.11 – Concepts of transition pieces

3 STRUCTURAL REQUIREMENTS AND DESIGN LOADS FOR LATTICE STRUCTURE

3.1 STRUCTURAL REQUIREMENTS

International Standards (ISO/IEC) and the European Committee for Standardization (CEN) are international organizations responsible for designing codes and guidelines for wind energy equipment. IEC 61400-1 (2005) outlines minimum design requirements for wind turbines and specifies essential design requirements to ensure the engineering integrity of onshore wind turbines. EN 1993 Eurocode 3 and EN 1997 Eurocode 7 are respectively guidance documents for the design of the steel tower and foundations (Geotechnical Design). The structural design of the wind tower must provide adequate strength and stiffness to withstand extreme loads from the highest wind speeds which may occur, ensuring this way a fatigue safety and providing a proper dynamic behavior, of the turbine during its intended life, by avoiding resonance issues. In this document it is presented a developed research on wind class II-A turbines, the most common wind class turbine in use. Such research took into account on wind loads acting directly on the tower as well as the effects of wind acting on the rotor during operation, represented by concentrated loads on the top of the tower.

3.2 ULTIMATE LIMIT STATE DESIGN LOADS

The wind action and fatigue are the variabilities that control the design of the tower. The loads for the design of the tower were obtained from the study (Carlos Rebelo, 2014) which, in turn, is based on EN 1991-1-4 and ISO 4354. Tower loading is bound to the type and power of the turbine and to the dynamic characteristics of the tower (Carlos Rebelo, 2014). In this project two different loads situations were analyzed: (i) extreme wind load in non-operating condition (EW), (ii) extreme wind load in operating condition (EO). These loads will be further applied in the mechanical model of the superstructure as concentrated loads acting on the top of the tower. Such load situations are used for ultimate limit state checks related to resistance and stability.

3.2.1 Extreme wind load in non-operating condition (EW)

The load combination called extreme wind load in non-operating condition (EW) includes loads on top of tower and wind load distributed along the height of the tower. In this condition the turbine is in parked position and the steady wind speed at hub height measured at every 10 min is Vref = 42.5 m/s, according to the definition of turbine class II. The wind loads for this

combination for top cross sections of the tower are shown in Table 3.1. This load table was prepared based on (Lanier, M W) plus the effect of the wind along the tower obtained from EN1991 using a base velocity Vb = 33 m/s.

Table 3.1 – Extreme Operation Condition Loads (ULS)

Case 2 - Extreme Operation Condition (EO)				
Top	Fx (kN)	1065	Mx (kN.m)	14987
	Fy (kN)	1065	My (kN.m)	14987
	Fz (kN)	-4879	Mz (kN.m)	3966

3.2.2 Extreme wind load in operating condition (EO)

This combination called extreme wind loading in operating condition (EO) includes loads on top of tower adapted from (Lanier, M W) which may contain effects of faults in the operation of the turbine and wind load distributed along the tower height. The maximum operating gust at hub height is Vhub = 33 m/s corresponding to the base velocity vb = 20.8 m/s for a height of 10 m as stated in EN1991. The wind loads for top cross sections of the tower for this combination are presented in Table 3.2.

Table 3.2 – Extreme Non-Operation Conditions Loads (ULS)

Case 3 - Extreme Non-Operation Conditions (EW)				
Top	Fx (kN)	578	Mx (kN.m)	28568
	Fy (kN)	578	My (kN.m)	28569
	Fz (kN)	-5000	Mz (kN.m)	5834

3.3 DYNAMIC PERFORMANCE OF THE WIND TOWER

The most important design requirement concerning the dynamic performance of the turbine on the whole is to prevent the exciting rotor forces from resonating with the natural tower bending frequencies. The natural frequencies of the tower must include tower head mass and soil structure interaction. Therefore, it was initially considered a Repower 5MW turbine, whose characteristics are presented in Table 3.3. A load of 4512.2 kN was applied on the model to simulate the mass of the turbine, before performing a modal analysis in order to obtain the Eigen frequencies of the tower.

Table 3.3 – Characteristics of Repower 5MW WT (adapted from Jonkman et al, 2009)

REpower 5MW Wind Turbine	
Rated Power	5 MW
Rotor Diameter	126 m
Hub Heights	150 m
Power Control	Variable Speed , Collective Pitch
Rotor Speed	6.9 rpm, 12.1 rpm
Cut-In Wind Speed	3 m/s
Cut-Out Wind Speed	25 m/s
Rated Wind Speed	11.4 m/s
Total Mass	460 ton
	4512.2 kN

The exciting forces of the rotor have basically two sources: (i) Mass imbalances of the moving parts, mainly the rotor and the blades, (ii) Aerodynamic imbalances that result from the asymmetrical air flow acting on the rotor, the tower shadow effect and the vertical wind shear. Of note the fact that type ii forces are the critical ones, since they cannot be avoided. The first frequencies of excitation are usually called 1P (per revolution) and corresponds to the rotor angular speed. They are the only ones that present in one-bladed turbines and they are the basic frequency of excitation for all other turbines. Higher harmonics appear for multi-bladed turbines as 2P, 3P, etc. The first natural bending frequency of the tower must not under any circumstances coincide with the critical exciting forces. The dynamic definition "Stiff" or "soft" tower corresponds to the position of the tower's first natural frequency relative to the dominant excitation frequency of the rotor (graphic 3.1).
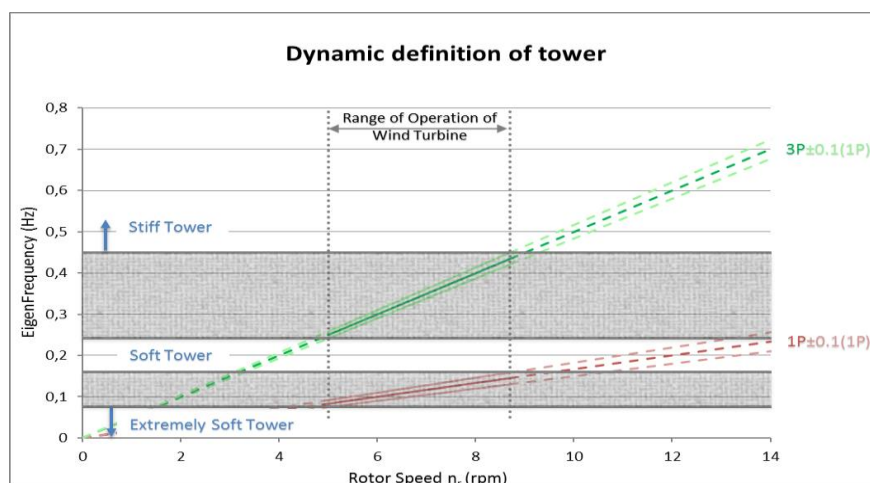
Graphic 3.1 – Dynamic definition of tower relative to wind
turbine (adapted from Baniotopoulos et al, 2015)

4   CONCEPTUAL MODEL OF LATTICE STRUCTURE

A structural analysis of the lattice structure can only be possible after understanding all the requirements that this structure should meet are clearly understood. After obtaining an outcome for a conceptual design model, through the use of specific software a mechanical model of the tower can be simplified for engineering modeling and structural analysis in order to ensure every detailed requirement.

4.1   GEOMETRY

After a literature review of different types of wind towers, the present study was dedicated to give an integrated view on the feasibility of optimizing the performance of onshore hybrid steel wind tower with 150m high hub (Figure 4.1b). As mentioned previously, the hybrid wind tower is composed of 60m of lattice structure (superstructure), which will support the main steel tubular tower structure with 90 m height and a 5 MW wind turbine on the top.

The lattice tower has been designed to provide stiffness and robustness. The truss action and larger base dimensions of the tower with 30 m as the base radius, help resisting the applied loads more effectively while leading to a lighter structural design.

The superstructure consists of eight chords, which are connected by bracing members forming a vertical plane frame or truss, type X (Figure 4.1a). The chords are inclined 65° from the ground and they are positioned in a circle. In order to provide more stiffness in the top of the tower, the distance among the truss braces should decrease, allowing the lattice tower holding a stable structure. The layout of the truss leads to welded K-joint angle for the whole structure.
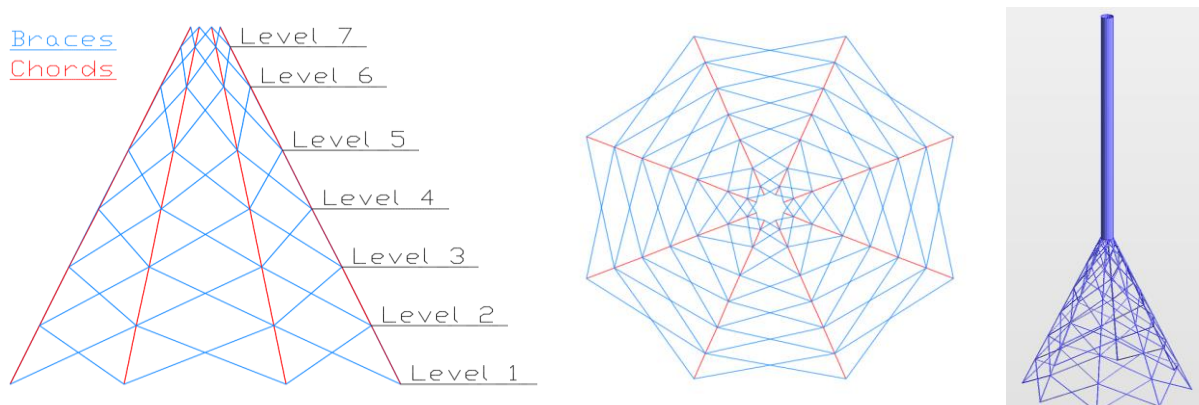
Figure 4.1- a) Profile and top view of the superestructure; b) Conceptual model of Hybrid Lattice-Tubular Steel Tower

For further structural design of the elements of the superstructure and for better overview of the optimization process, the elements of the superstructure were divided into eight groups based on their location and dimensions (see Table 4.1).

Table 4.1- Groups and dimensions of the structural elements

LATTICE GEOMETRY			
Level	Height (m)	Chords L (m)	Braces L (m)
1	9.82	10.82	23.76
2	19.64	10.82	20.71
3	29.46	9.82	17.83
4	39.28	11.82	15.19
5	50	10.82	13.69
6	56.67	8.35	8.32
7	60	3.67	4.30

4.2 MATERIAL PROPERTIES

The properties of the steel used on the structural design, S355H, fulfill all ductility and strength requirements established by the EC3 Part 1-1, section 3 (CEN, 2005a). The nominal values of yield strength "f_y" and ultimate strength "f_u" steel are defined according to standard EN 10210-1 (CEN, 1994). Overall, as characteristic values were obtained, as presented on table 4.2.

Table 4.2- Material properties for superstructure

S355H - EN 10210-1	
f_y (N/mm^2)	355
f_u (N/mm^2)	510
E (N/mm^2)	210000
G (N/mm^2)	81000
ν	0.3
α (/K)	12×10^{-6}
ρ (kg/m^3)	7850

4.3   ELEMENT TYPE, BOUNDARY COUNDITIONS AND RIGID LINK

Being a lattice superstructure, the final conceptual model must ensure that the behavior of the supporting structure is the closest to a truss structure. Therefore, the brace elements were modeled as *truss elements*. However, due to the high bending moment transmission level coming from the steel tubular tower, chord elements were modeled as *column elements* (Figure 4.2a)*. It is worth mentioning, the steel tubular tower is an element-column with 4500mm of diameter and 30mm of thickness.

The transmission of efforts should be performed by the transition piece, which is represented in the model by "rigid link", with a high level of stiffness as demonstrated in Figure 4.2b. A detailed numerical study of the transition piece presented on further chapters. Internal forces obtained on this rigid link will be for the design of the conceptual model of the transition piece.

The lower boundary condition was conceived to allow the tower to rotate consequently avoiding the bending moments in the base (Figure 4.2c). In order to achieve such behavior, *pinned* supports were considered in the base of each chord.
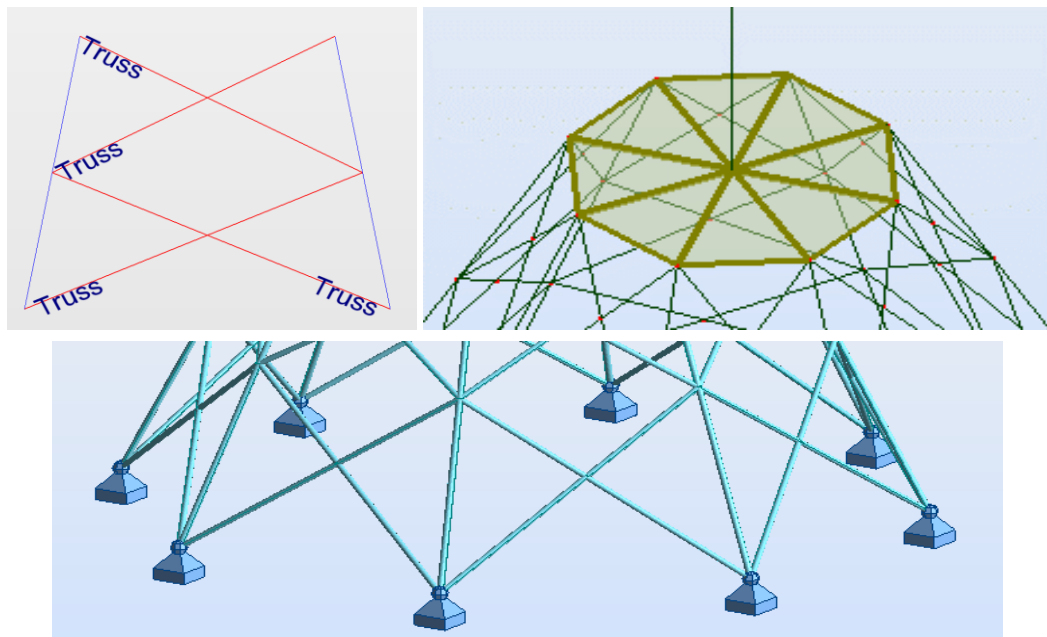
Figure 4.2 – a) Element type truss/column; b) Rigid Link; c) Boundary Condition

5 DESIGN OF THE LATTICE STRUCTURE

This project was developed according with the general requirements of EN1990 and EN1993 part 1-1 (CEN, 2005a). "EN 1990 establishes principles and requirements for the safety, serviceability and durability of structures, describes the basis for their design and verification and gives guidelines for related aspects of structural reliability." (CEN, 2009).

Standard EN 1990 establishes that structural safety is ensured by use of a safety class methodology. The structure to be designed is classified into a safety class based on the failure consequences. The classification is normally determined by the purpose of the structure. As the structural design is according to EN1993 (CEN, 2005a), it can be adopted a reliability differentiation class RC2, established in (CEN, 2001).

5.1 STRUCTURAL ANALYSIS

The capacity of the resistant elements of the structure is not relevant if the design efforts are not adequately evaluated. The overall analysis of efforts and displacements of the structure essentially depends on the characteristics of deformability and stiffness. However, the global stability and the local stabilities of each element, the behavior of the cross sections and of joints, the imperfections and deformability of support also depends on deformability and stiffness. Thus, the definition of the type of analysis to adopt it is an important decision that should be taken into account all the aforementioned aspects. Structural analysis was performed during the design and optimization process using the software "Autodesk Robot Structural Analysis Professional 2015"

The design of steel structures normally leads to optimized and consequently quite slender structures. Eventually, the phenomena of instability increases as the slenderness of the elements increases, and it is normally necessary to check the global stability of the structure. Furthermore, this concept shows to have a high level of ductility and flexibility, ultimately leading to large deformations.

Performing a non-linear analysis takes account of the high second-order effects, such as the change of bending rigidity depending on the longitudinal forces. Considering geometric non-linearity takes the second order effects into consideration and often improves the convergence of the calculation process for the superstructure. In addition, *truss elements* were used, causing a structural non-linearity. Moreover, in order to take maximum advantage of the plasticity resistant capacities of the steel, only elements with a cross section classification 1 or 2, according to EN 1993-1-1 5.5 were used.

5.2   Iterative Design Procedure

In order to meet the objective established in chapter 1, while fulfilling the cited structural requirements in chapter 3, a light resistant lattice structure is requested. This way, all the member should have a high ratio of utilization.

In chapter 3, design loads to check the Ultimate Limit State are presented. However, these loads only consider the wind acting in one direction, but during the lifetime of the hybrid tower the wind will can act in all directions. The members that are located on the opposite side of the considered wind direction will be the critical ones. In order to consider all wind directions, all the members of each level will have the same cross section of the most critical member of the same level. Consequently, the design of the members will be made per level. The definition of the levels is presented on the previous chapter.

Furthermore, the lattice structure has two types of elements, where the chords are *column* type and the braces are *truss* type. The detailed design of one element type will be presented. Regardless of existing members in high level of tension, the design of members in compression is more severe due to the buckling.

5.2.1   Design of a Brace Member

As, the brace members are *truss* elements, these members only have axial forces, and the design is governed by the buckling resistance in uniform compression. The buckling length of these elements was consider as Lcr=1.0xL according to EN1993-1-1 Annex BB.1.3. In Figure 5.2 a flowchart is presented to describe the iterative design procedure for the brace members. The main goal was to achieve the higher ratio of utilization. The detailed design for the brace member corresponds to the level 1, which is the most slender element, and its location is marked in red on figure 5.1.
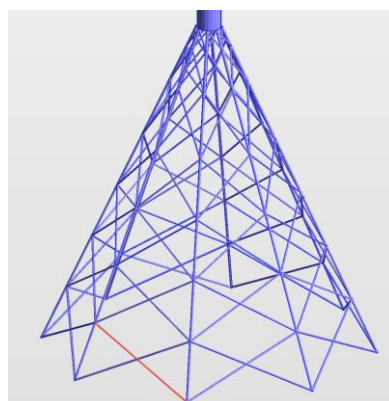

Figure 5.1 – Brace member level 1
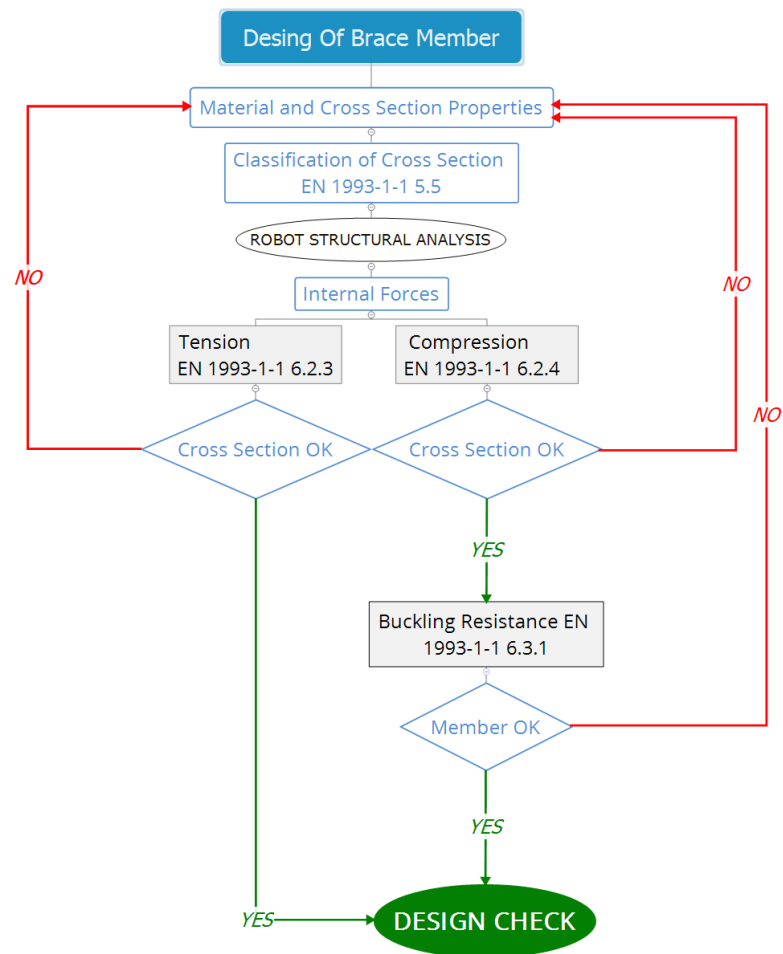
Figure 5.2 – Design of Brace Member Procedure (Flowchart)

i)   Geometry Properties
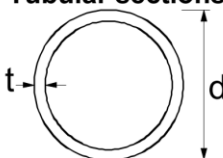
Table 5.1 – Geometry properties brace member

CHS 355,6 x 8		
Outside Diameter	D (mm)	355.60
Inside Diameter	Di (mm)	339.60
Thickness	t (mm)	8.00
Mass	M (Kg/m)	68.67
Sectional Area	A (cm^2)	87.36
Moment of Inertia	I (cm^4)	13201.37
Radius of Gyration	i (cm)	12.29
Elastic Modulus	W_{el} (cm^3)	742.48
Plastic Modulus	W_{pl} (cm^3)	966.78
Torsional Constant	I_t (cm^4)	26402.75

ii)   *Cross Section Classification EN1993-1-1 5.5.2 T5.2*

$$\frac{d}{t} = \frac{355.6}{8} \cong 44.45 \le 70\varepsilon^2 \cong 70 \times 0.66 = 46.34 \ (Class\ 2) \qquad (Eq\ 5.1)$$

Table 5.2 – Cross section classification for tubular section EN1993-1-1 5.5.2 T5.2

Tubular sections
t → ⬤ d

Class	Section in bending and/or compression				
1	$d/t \le 50\varepsilon^2$				
2	$d/t \le 70\varepsilon^2$				
3	$d/t \le 90\varepsilon^2$				
	NOTE For $d/t > 90\varepsilon^2$ see EN 1993-1-6.				
$\varepsilon = \sqrt{235/f_y}$	f_y	235	275	355	420	460
	ε	1,00	0,92	0,81	0,75	0,71
	ε^2	1,00	0,85	0,66	0,56	0,51

iii)   Internal Forces

$$N_{Ed} = 352.45\ kN\ (Compression) \qquad (Eq\ 5.2)$$

iv)   *Compression EN1993-1-1 6.2.4*

$$\frac{N_{Ed}}{N_{c,Rd}} = \frac{352.45}{3101.33} = 0.11 \le 1.0 \qquad (Eq\ 5.3)$$

$$N_{c,Rd} = \frac{Af_y}{Y_{M0}} = \frac{87.36 \times 355.0}{1.0} = 3101.33\ kN \qquad (Eq\ 5.4)$$

v)   Buckling Resistance – Uniform Members in Compression *EN1993-1-1 6.3.1*

$$\frac{N_{Ed}}{N_{b,Rd}} = \frac{352.45}{444.95} = 0.79 \le 1.0 \qquad (Eq\ 5.5)$$

$$N_{b,Rd} = \frac{\chi A f_y}{\Upsilon_{M1}} = \frac{0.14 \times 87.36 \times 355.0}{1.0} = 444.95 \, kN \qquad \text{(Eq 5.6)}$$

$$\chi = \frac{1}{\Phi + \sqrt{\Phi^2 - \lambda^2}} = \frac{1}{3.94 + \sqrt{3.94^2 - 2.53^2}} = 0.14 \qquad \text{(Eq 5.7)}$$

$$\Phi = 0.5[1 + \alpha(\lambda - 0.2) + \lambda^2] = 0.5[1 + 0.21(2.53 - 0.2) + 2.53^2] = 3.94 \quad \text{(Eq 5.8)}$$

$$Circular \; Hollow \; Section, S355, Hot \; Finnished \rightarrow Buckling \; Curve = a \rightarrow \alpha = 0,21$$

$$\lambda = \sqrt{\frac{A f_y}{N_{cr}}} = \sqrt{\frac{87.36 \times 355}{484.67}} = 2.53 \qquad \text{(Eq 5.9)}$$

$$N_{cr} = \frac{\pi E I}{L_{cr}^2} = \frac{\pi \times 210 \times 13201.37}{23.76^2} = 484.67 \qquad \text{(Eq 5.10)}$$

5.2.2 Design of a Chord Member

As, the chords members are *column* elements, these members have not only axial and shear forces as bending and torsional moments. The design is governed by the buckling resistance in bending and axial compression. The buckling length of these elements was considered as Lcr=0.9xL according to EN1993-1-1 Annex BB.1.3. The flowchart present in (Figure 5.3) describes the iterative design procedure for the chord members, where the main goal was to achieve the higher ratio of utilization. The detailed design for the chord member corresponds to the level 7, which is the most loaded element, and its location is marked in red.
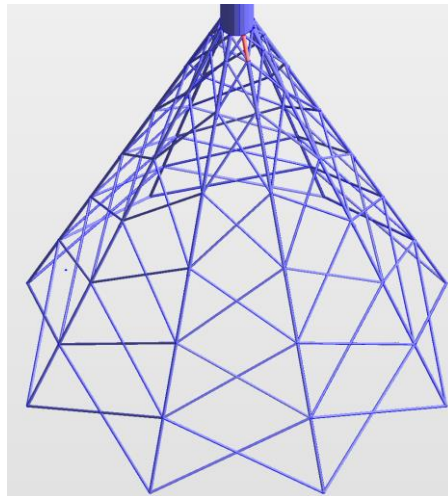
Figure 5.3 – Chord member level 7
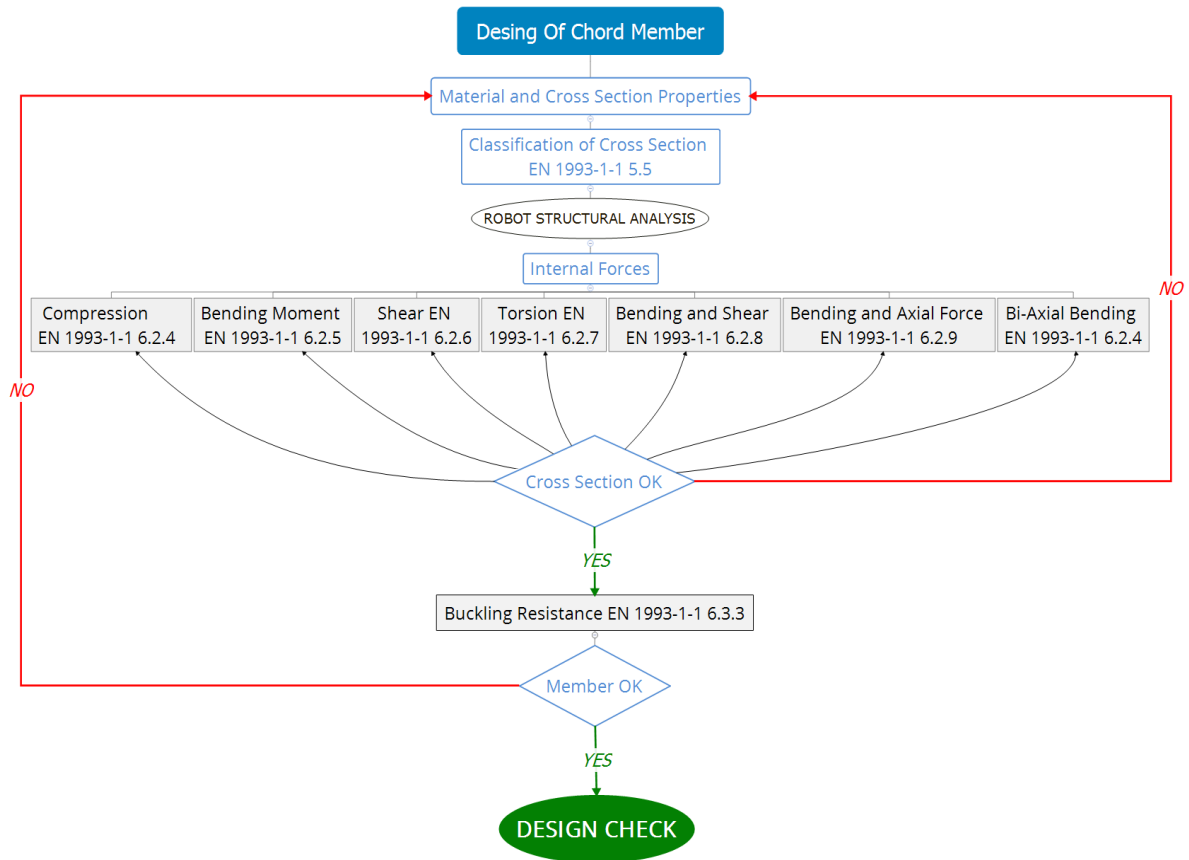
Figure 5.3 – Design of Chord Member Procedure (Flowchart)

i)   Geometry Properties

Table 5.3 – Geometry properties chord member

CHS 559 x 25		
Outside Diameter	D (mm)	559.00
Inside Diameter	Di (mm)	509.00
Thickness	t (mm)	25.00
Mass	M (Kg/m)	329.65
Sectional Area	A (cm^2)	419.40
Moment of Inertia	I (cm^4)	149821.62
Radius of Gyration	i (cm)	18.90
Elastic Modulus	W_{el} (cm^3)	5360.34
Plastic Modulus	W_{pl} (cm^3)	7134.11
Torsional Constant	I_t (cm^4)	299643.25

ii)   *Cross Section Classification EN1993-1-1 5.5.2 T5.2*

$$\frac{d}{t} = \frac{559}{25} \cong 22.36 \; \leq 50\varepsilon^2 \cong 50 \times 0.66 = 33 \; (Class\; 1) \qquad (Eq\; 5.11)$$

iii)   Internal Forces

Table 5.4 – Internal forces for chord member

Ned (kN)	VEd,y (kN)	VEd,z (kN)	MEd,y (kN.m)	MEd,z (kN.m)	MEd,T (kN.m)
13428.54	-7.44	35.46	126.45	56.00	0.00

iv)   *Compression EN1993-1-1 6.2.4*

$$\frac{N_{Ed}}{N_{c,Rd}} = \frac{13428.54}{14888.79} = 0.90 \; \leq 1.0 \qquad (Eq\; 5.12)$$

$$N_{c,Rd} = \frac{Af_y}{\gamma_{M0}} = \frac{419.40 \times 355.0}{1.0} = 14888.79 \qquad (Eq\; 5.13)$$

i)   *Bending Moment EN1993-1-1 6.2.5*

$$\frac{M_{Ed}}{M_{c,Rd}} = \frac{126.45}{2532.61} = 0.05 \leq 1.0 \qquad (Eq\; 5.14)$$

$$M_{c,Rd} = M_{pl,Rd} = \frac{W_{pl}f_y}{\gamma_{M0}} = \frac{7134.11 \times 355.0}{1.0} = 2532.61 \qquad (Eq\; 5.15)$$

v)   Shear *EN1993-1-1 6.2.6*

$$\frac{V_{Ed}}{V_{c,Rd}} = \frac{35.46}{5472.41} = 0.11 \leq 1.0 \qquad (Eq\; 5.16)$$

$$V_{c,Rd} = V_{pl,Rd} = \frac{A_v\left(f_y/\sqrt{3}\right)}{\gamma_{M0}} = \frac{267.0 \times \left(355.0/\sqrt{3}\right)}{1.0} = 5472.41 \qquad (Eq\; 5.17)$$

vi)   Torsion *EN1993-1-1 6.2.7*

$$\frac{T_{Ed}}{T_{Rd}} = \frac{0}{3805.84} = 0 \leq 1.0 \qquad (Eq\ 5.18)$$

$T_{Ed} = T_{t,Ed} + T_{w,Ed}$; For Circular Hollow Sections $T_{w,Ed} \cong 0 \rightarrow T_{Ed} = T_{t,Ed}$

vii)   Combined Shear force with Torsion EN1993-1-1 6.2.7 (9)

$$\frac{V_{Ed}}{V_{pl,T,Rd}} = \frac{35.46}{5472.41} = 0.01 \leq 1.0 \qquad (Eq\ 5.19)$$

$$V_{pl,T,Rd} = \left[1 - \frac{\tau_{t,Ed}}{(f_y/\sqrt{3})/\gamma_{M0}}\right] \times V_{pl,Rd} = 5472.41 \qquad (Eq\ 5.20)$$

viii)   Bending combined with shear and Torsion EN1993-1-1 6.2.8

According to EN1993-1-1 6.2.8 (2), when the shear force is less than half of the plastic shear resistance ($V_{pl,Rd}$), its effect on the moment resistance may be neglected. Nevertheless, when torsion is present but its value combined with shear represents half of the plastic shear resistance ($V_{pl,T,Rd}$), the value of moment resistance may not be reduced.

ix)   Bending and Axial Force EN1993-1-1 6.2.9

$$\frac{M_{Ed}}{M_{N,Rd}} = \frac{126.45}{407.62} = 0.05 \leq 1.0 \qquad (Eq\ 5.21)$$

$$M_{N,Rd} = M_{N,y,Rd} = M_{N,z,Rd} = M_{pl,Rd}(1 - n^{1.7}) = 2532.61(1 - 0.90^{1.7}) = 407.6 \ (Eq\ 5.22)$$

$$n = \frac{N_{Ed}}{N_{pl,Rd}} = \frac{13428.54}{14888.79} = 0.90 \qquad (Eq\ 5.23)$$

x)   Bi-axial Bending EN1993-1-1 6.2.9

$$\left[\frac{M_{y,Ed}}{M_{N,y,Rd}}\right]^{\alpha} + \left[\frac{M_{z,Ed}}{M_{N,z,Rd}}\right]^{\beta} = \left[\frac{126.45}{407.62}\right]^2 + \left[\frac{56.00}{407.62}\right]^2 = 0.12 \leq 1.0 \quad \text{(Eq 5.24)}$$

For Circular Hollow Sections $\rightarrow \alpha = 2 ; \beta = 2$ $\rightarrow$ EN1993-1-1 6.2.9 (6)

xi)   Buckling Resistance – Uniform Members in Bending and Axial Compression *EN1993-1-1 6.3.1*

Not only using cross sections of the class 1 or 2, but also Circular Hollow Sections, the effects of shifting moment and torsion may be neglected, therefore the expressions given on EN1993-1-1 6.3.1 may be simplified as presented.

$$\frac{N_{Ed}}{\frac{\chi_y N_{Rk}}{Y_{M1}}} + k_{yy}\frac{M_{y,Ed}}{\frac{M_{y,Rk}}{Y_{M1}}} + k_{yz}\frac{M_{z,Ed}}{\frac{M_{z,Rk}}{Y_{M1}}} \leq 1.0 \qquad \text{(Eq 5.25)}$$

$$\frac{13428.54}{\frac{0.99 \times 14888.79}{1.0}} + 0.94\frac{126.45}{\frac{2532.61}{1.0}} + 0.57\frac{56.00}{\frac{2532.61}{1.0}} = 0.97 \leq 1.0 \quad \text{(Eq 5.26)}$$

$$\frac{N_{Ed}}{\frac{\chi_z N_{Rk}}{Y_{M1}}} + k_{zy}\frac{M_{y,Ed}}{\frac{M_{y,Rk}}{Y_{M1}}} + k_{zz}\frac{M_{z,Ed}}{\frac{M_{z,Rk}}{Y_{M1}}} \leq 1.0 \qquad \text{(Eq 5.27)}$$

$$\frac{13428.54}{\frac{0.99 \times 14888.79}{1.0}} + 0.57\frac{126.45}{\frac{2532.61}{1.0}} + 0.9\frac{56.00}{\frac{2532.61}{1.0}} = 0.96 \leq 1.0 \quad \text{(Eq 5.28)}$$
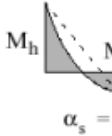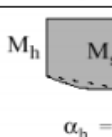
As a section not susceptible to torsional deformations, the interaction factors are obtained as demonstrates on table 5.5 (EN1993-1-1, Annex B, T B.1):

Table 5.5 - Interaction factors k_{ij} for members not susceptible to torsional deformations

K_{yy}	$C_{my}\left(1 + (\lambda_y - 0.2)\dfrac{N_{Ed}}{\dfrac{\chi_y N_{Rk}}{\gamma_{M1}}}\right) \leq C_{my}\left(1 + 0.8\dfrac{N_{Ed}}{\dfrac{\chi_y N_{Rk}}{\gamma_{M1}}}\right)$	(Eq 5. 29)
k_{yz}	$0.6 \times k_{zz}$	(Eq 5. 30)
k_{zy}	$0.6 \times k_{yy}$	(Eq 5. 31)
K_{zz}	$C_{mz}\left(1 + (\lambda_z - 0.2)\dfrac{N_{Ed}}{\dfrac{\chi_z N_{Rk}}{\gamma_{M1}}}\right) \leq C_{mz}\left(1 + 0.8\dfrac{N_{Ed}}{\dfrac{\chi_z N_{Rk}}{\gamma_{M1}}}\right)$	(Eq 5. 32)

Where the equivalent uniform moment factor C_{mij} are obtained according table 5.5:

Table 5.6 - Equivalent uniform moment factors Cmij; source: EN1993-1-1 T B.3.

Moment diagram	range		C_{my} and C_{mz} and C_{mLT}	
			uniform loading	concentrated load
M ⬛ ψM	$-1 \leq \psi \leq 1$		$0,6 + 0,4\psi \geq 0,4$	
M_h M_s ψM_h $\alpha_s = M_s/M_h$	$0 \leq \alpha_s \leq 1$	$-1 \leq \psi \leq 1$	$0,2 + 0,8\alpha_s \geq 0,4$	$0,2 + 0,8\alpha_s \geq 0,4$
	$-1 \leq \alpha_s < 0$	$0 \leq \psi \leq 1$	$0,1 - 0,8\alpha_s \geq 0,4$	$-0,8\alpha_s \geq 0,4$
		$-1 \leq \psi < 0$	$0,1(1-\psi) - 0,8\alpha_s \geq 0,4$	$0,2(-\psi) - 0,8\alpha_s \geq 0,4$
M_h M_s ψM_h $\alpha_h = M_h/M_s$	$0 \leq \alpha_h \leq 1$	$-1 \leq \psi \leq 1$	$0,95 + 0,05\alpha_h$	$0,90 + 0,10\alpha_h$
	$-1 \leq \alpha_h < 0$	$0 \leq \psi \leq 1$	$0,95 + 0,05\alpha_h$	$0,90 + 0,10\alpha_h$
		$-1 \leq \psi < 0$	$0,95 + 0,05\alpha_h(1+2\psi)$	$0,90 - 0,10\alpha_h(1+2\psi)$
For members with sway buckling mode the equivalent uniform moment factor should be taken $C_{my} = 0,9$ or $C_{Mz} = 0,9$ respectively.				

$C_{my} = 0.9$ (elements with sway buckling mode on direction z)   (Eq 5.33)

$C_{mz} = 0.9$ (elements with sway buckling mode on direction y)   (Eq 5.34)

$$k_{yy} = \min\left\{ \begin{array}{c} 0.9\left(1 + (0.25 - 0.2)\dfrac{13428.54}{\dfrac{0.99 \times 14888.79}{1.0}}\right) = 0.94 \\[4mm] 0.9\left(1 + 0.8 \times \dfrac{13428.54}{\dfrac{0.99 \times 14888.79}{1.0}}\right) = 1.56 \end{array} \right\} = 0.94 \quad \text{(Eq 5.35)}$$

$$k_{yz} = 0.6 \times k_{zz} = 0.57 \tag{Eq 5.36}$$

$$k_{zy} = 0.6 \times k_{yy} = 0.57 \tag{Eq 5.37}$$

$$k_{zz} = \min \left\{ \begin{array}{l} \dfrac{0.9\left(1 + (0.25 - 0.2)\dfrac{13428.54}{0.99 \times 14888.79}\right) = 0.94}{1.0} \\[4ex] 0.9\left(1 + 0.8 \times \dfrac{13428.54}{0.99 \times 14888.79}\right) = 1.56 \\[2ex] \hline 1.0 \end{array} \right\} = 0.94 \tag{Eq 5.38}$$

5.2.3 Lattice Structural Design

In the previous sections 5.2.1 and 5.2.2, an analysis of structural static behavior for ultimate limit state was performed. Due to the high flexibility of the hybrid concept, a global non-linear analysis was considered. The lattice tower is a rigid structure, with a top rigid segment to ensure the high level transmission of efforts from the steel tubular tower. The study of the first mode of shape, which is the bending of the tower, allowed understanding the behavior of the structure members. An iterative design procedure was performed and the critical members were designed by hand calculations per level, the final cross sections for the members, the governing design case and their utilization ratio are present on Table 5.6 and 5.7. In annex I and II it is shown the final results of a detailed numerical analysis of each critical member per lever. Annex I corresponds to chord members and annex II is relatesd to brace members. Nevertheless, the design of all elements were verified on *Robot Structural Analysis* and it can be checked on annex III.

Table 5.7 – Chords design per level

LATTICE DESIGN					
Level	Chords				
	Bar	Profile	L (m)	Ratio	Design Case
1	25	CHS 406.4x10	10.82	0.92	2 EO
2	24	CHS 406.4x12	10.82	0.88	2 EO
3	14	CHS 406.4x12	9.82	0.88	2 EO
4	9	CHS 457x16	11.82	0.81	2 EO
5	21	CHS 457x16	10.82	0.93	2 EO
6	254	CHS 559x25	8.35	0.86	2 EO
7	169	CHS 559x25	3.67	0.97	2 EO

Table 5.8 – Braces design per level

LATTICE DESIGN					
Level	Braces				
	Bar	Profile	L (m)	Ratio	Design Case
1	304	CHS 355.6x8	23.76	0.79	2 EO
2	333	CHS 323.9x8	20.71	0.98	2 EO
3	321	CHS 323.9x10	17.83	0.82	2 EO
4	331	CHS 323.9x10	15.19	0.91	2 EO
5	371	CHS 355.6x16	13.69	0.82	2 EO
6	215	CHS 323.9x16	8.32	0.97	2 EO
7	204	CHS 355.6x16	4.30	0.97	2 EO

Once the structural design is done, it is necessary to estimate the amount of steel used to obtain the total mass of the structure. This may allow (i) having an estimation of total cost and (ii) performing a close comparison between the several towers concepts to determine if this solution is feasible. If so may be a competitive concept in the market for wind towers that support multi megawatt large turbines.

The features of the software *Robot Structural Analysis*, obtained the map of steel quantities for the circular hollow sections profiles of the lattice structure, as presented in the table below (Table 5.9). The weight of the lattice structure is estimated to be approximately 233.5 tons.

Table 5.9 – Map of quantities for lattice structure

Total per sections	Number	Length	Unit Weight	Bar Weight	Total Weight
S 355	n	m	KG/m	KG	KG
CHS 323.9x8	16	331.52	62.35	20670.77	20671
CHS 323.9x10	32	528.32	77.43	40907.26	40907
CHS 323.9x16	16	133.28	121.72	16222.7	16223
CHS 355.6x8	16	380.16	68.63	26091.82	26092
CHS 355.6x16	32	287.86	134.28	38654.84	38655
CHS 406.4x10	8	86.56	98.16	8496.77	8497
CHS 406.4x12	16	165.12	116.7	19269.65	19270
CHS 457x16	16	181.12	174.33	31575.18	31575
CHS 559x25	16	96.25	329.18	31683.86	31684
Total	168				233 574
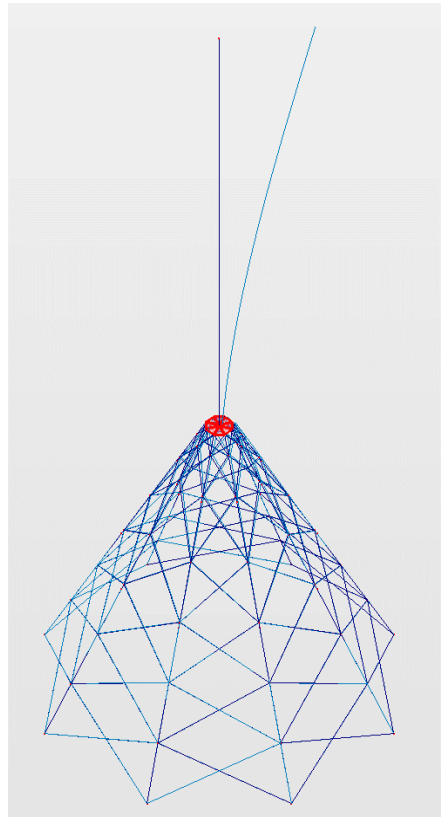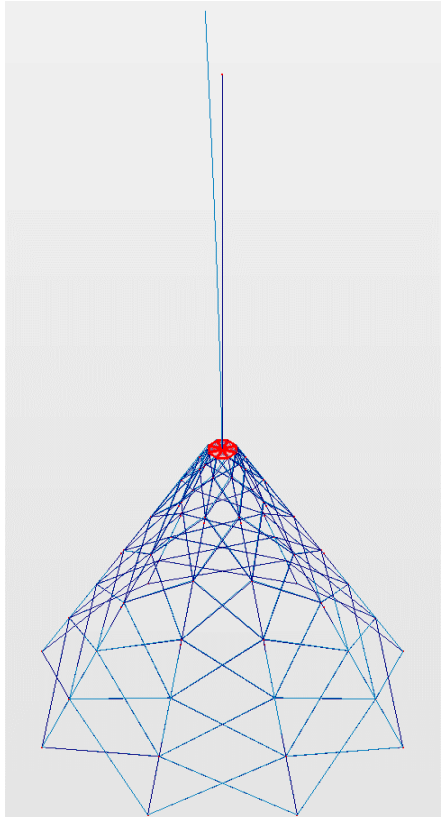
Attached is presented a table (Table E.1) with information about the various quantities of the various concepts of current wind towers.

5.3 DYNAMIC ANALYSIS

As mentioned previously in section 3.3, the dynamic performance of the tower is highly important. Furthermore, it is mandatory to prevent that the first natural bending frequency of the tower coincides with the critical exciting forces from the wind turbine which would cause resonating problems, leading to a possible collapse of the tower.

Initially was considered a 5MW turbine from Repower, where the characteristics can be seen on Table 3.3. A modal analysis was performed to verify if the resonating problem would exist or not. Table 5.10 shows the first two bending modes and the corresponding bending natural frequencies.

Table 5.10 – Domaining bending natural frequencies/modes

| Mode | 1 | Frequency (Hz) | 0,15 | Mode | 2 | Frequency (Hz) | 0,15 |

Once obtained the domain natural bending frequencies, it is required to assess if the exciting rotor forces coincide with them causing resonating. Graphic 5.1 shows that for this wind turbine the tower may not satisfy the dynamic performance criteria.
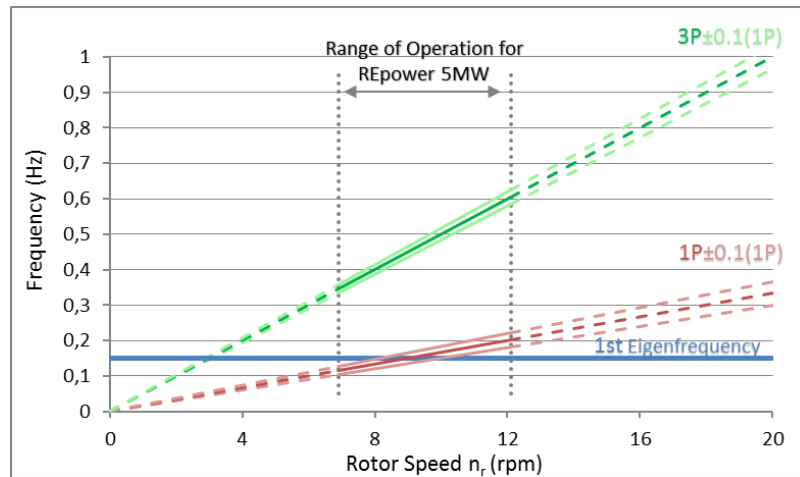
Graphic 5.1 – Dynamic performance for WT Repower 5MW

According to (Hau, 2006) if the technical concept of the wind turbine is feasible, the vibrational coupling between the rotor and tower will not be as drastic as originally feared. In turn, if so, the tower design must be modified. However, if considering a different wind turbine where the vibrational coupling is achieved the solution may be considered. Three more wind turbines were additionally analyzed: (i) Siemens Wind Turbine SWT-3.0-113; (ii) Siemens Wind Turbine SWT-6.0-154; (iii) Siemens Wind Turbine SWT-7.0-154; in all of the dynamic performance criteria were met, causing no resonating problems. The tables below represent the main characteristics of the three wind turbines and the corresponding graphics show the dynamic performance of the tower.

Siemens Wind Turbine SWT-3.0-113	
Rated Power	3 MW
Rotor Diameter	113 m
Hub Heights	127,5 m
Power Control	Pitch regulation with variable speed
Rotor Speed	6.5 rpm, 14,7 rpm
Rotor Speed*	6.5 rpm, 12 rpm
Cut-In Wind Speed	3 - 5 m/s
Cut-Out Wind Speed	25 m/s
Rated Wind Speed	12 - 13 m/s
Total Mass	145 ton
1st Eigenfrequency	**0,22 Hz**
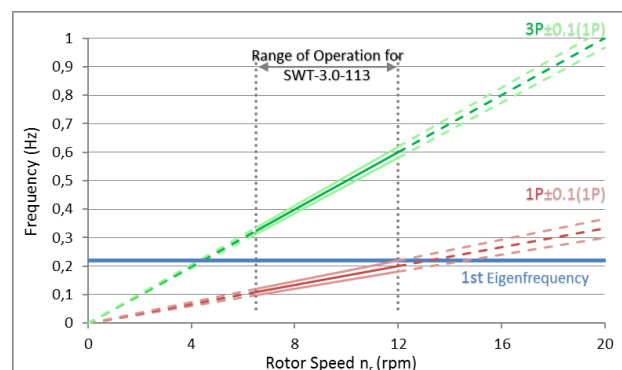
Graphic 5.2 – Dynamic performance for WT SWT-3.0-113

Siemens Wind Turbine SWT-6.0-154	
Rated Power	6 MW
Rotor Diameter	154 m
Hub Heights	Site Specific
Power Control	Pitch regulation with variable speed
Rotor Speed	5 rpm, 11 rpm
Rotor Speed*	5 rpm, 8.7 rpm
Cut-In Wind Speed	3 - 5 m/s
Cut-Out Wind Speed	25 m/s
Rated Wind Speed	12 - 14 m/s
Total Mass	360 ton
1st Eigenfrequency	0,16 Hz

Graphic 5.3 – Dynamic performance for WT SWT-6.0-154

Siemens Wind Turbine SWT-7.0-154	
Rated Power	7 MW
Rotor Diameter	154 m
Hub Heights	Site Specific
Power Control	Pitch regulation with variable speed
Rotor Speed	5 rpm, 11 rpm
Rotor Speed*	5 rpm, 8.7 rpm
Cut-In Wind Speed	3 - 5 m/s
Cut-Out Wind Speed	25 m/s
Rated Wind Speed	12 - 14 m/s
Total Mass	360 ton
1st Eigenfrequency	0,16 Hz

Graphic 5.4 – Dynamic performance for WT SWT-7.0-154

For all three wind turbines the dynamic performance criteria is met and the tower may be considered as a *soft tower*, according what was previously stated in chapter 3.3. The Siemens Wind Turbine SWT-7.0-154 is shown below as an example. Attached is a table (table D.1) with the full dynamic analysis results for the wind tower with the Siemens wind turbine SWT-7.0-154.
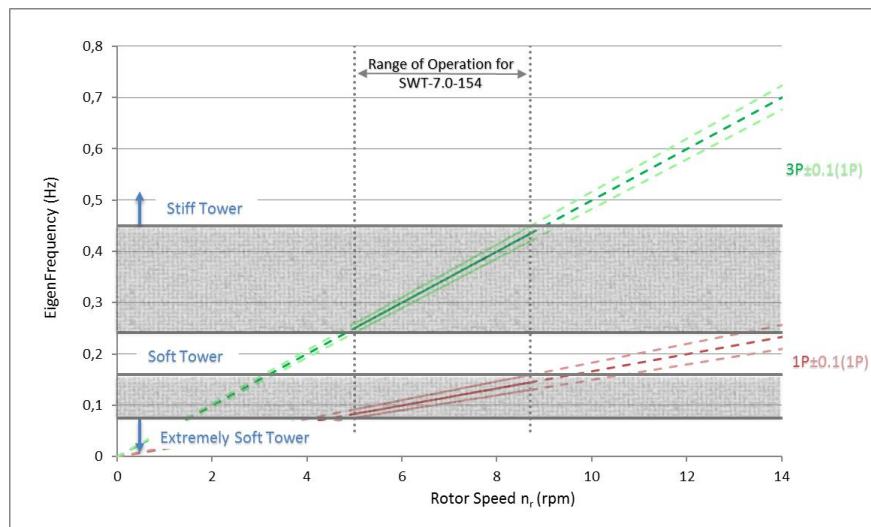
Graphic 5.5 – Dynamic definition of soft tower

6   CONCEPTUAL MODEL OF TRANSITON SEGMENT

In order to ensure good behavior of the hybrid tower, the transition segment has to ensure the correct transmission of the internal forces from the tubular tower to the lattice support structure. Due to the high level of bending moment, torsional moment and axial compression, the transition segment needs to have a high level of stiffness. A conceptual model is suggested in this work, which has 5 main parts: (i) Chord, (ii) Outer Ring, (iii) Elliptical tube, (iv) Inner ring and (v) Flange connection. The inner ring set is composed by the inner ring and the eight elliptical tubes. The conceptual model was developed using the software NX and can be seen in the figure 6.1.
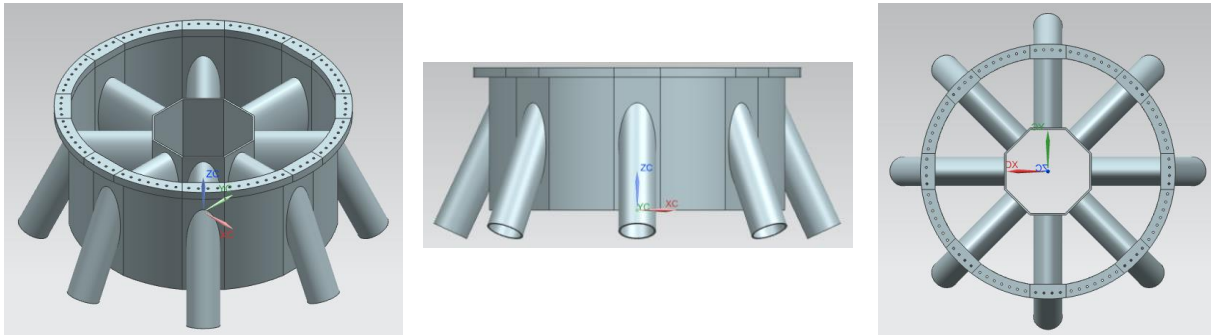
Figure 6.1 – Conceptual model of transition segment

The outer ring is composted by 2 pieces, a plate and an arc plate, which are repeated 8 times each other. This reduces the complexity of the welding where the chords meet the outer ring. The dimensions can be seen in Table 6.1. The two parts are welded together making a nearly perfect cylinder 2 m high and with a corresponding diameter to the bottom part of the tubular tower of 4.5 m. The chords members that have a cross section of 559x32 are welded to the plates making with the vertical an angle of 25º. Furthermore, the chords are separated by an angle of 45° from top the view.

Table 6.1 – Geometric properties for outer ring

Outer Ring			
Plates		Arc Plates	
b (mm)	700	L (mm)	1064.3
h (mm)	2000	r (mm)	2250
t (mm)	36	t (mm)	36
n	8	n	8

Once the circular hollow section is cut with an angle of 25º, it will take the form of an ellipse. The elliptical tube will then connect the outer ring to the inner ring, making a proper transmission of the forces and thereby creating a double-ring that increases significantly the stiffness of the segment. The inner ring is a polygon composed of eight plates, the angle between each plate is 135 ° and the dimensions can be seen in table 6.2.

Table 6.2 – Geometric properties for polygon plates

Polygon Plates	
b (mm)	700
h (mm)	1500
t (mm)	36
n	8

The connection between the tubular tower and the transition piece is made through a welded flange connection (WFC) (figure 2.1a)). It is important to mention that the WFC was not object of study in this project. And for that reason in Figures 6.1 and 6.2 it is merely representative. Moreover, the introduction of holes for the bolts on the model have a significant increase of computation effort. Thus the bolts will not be considered (Figure 7.2). The same type of connection will be used to link the lattice structure to the transition segment, once again this connection was not object of study, so the figure 6.2 it is also merely representative. Furthermore, the transition segment has a total weight of 28.5 tons, which can be easily assembled using a crane. The same crane has to be capable to assemble the hub of the wind turbine which corresponds to 60-70% of the total wind turbine mass. Therefore, the same crane it is suitable to assemble the transition segment. Concerning road transportation issues, once the transmission segment is fully welded, it can be transported in two parts and then finally assembled on site.
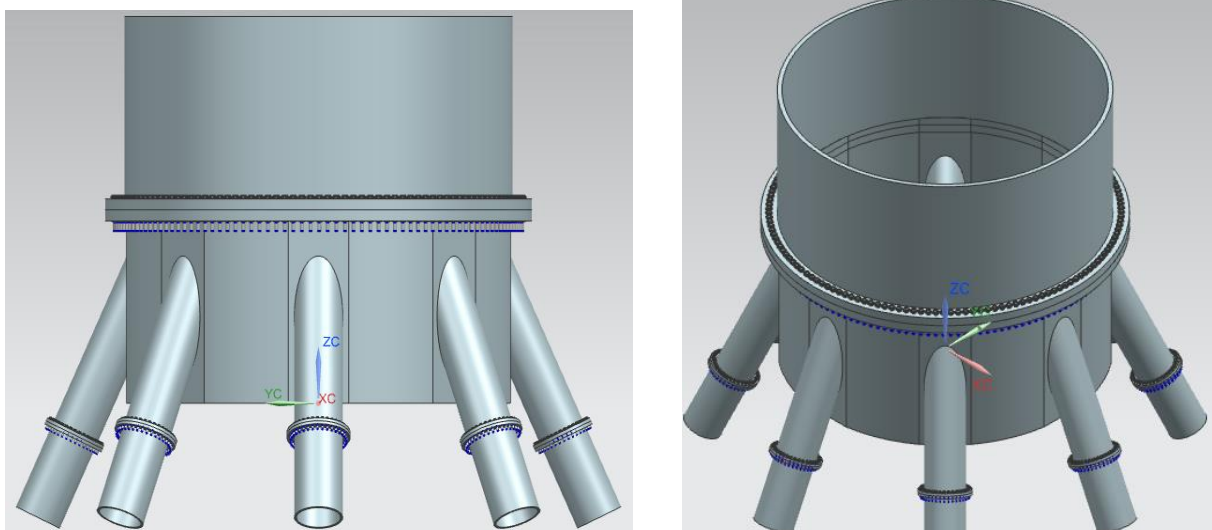
Figure 6.2 – Insertion of the transition segment on the hybrid tower

7 FINITE ELEMENT ANALYSIS OF THE TRANSITON SEGMENT

In the previous chapter it was presented the conceptual model of the transition segment and since, it was determined that it was a feasible solution, a finite element analysis (FEA) on *ABAQUS* has to be performed according to EN1993-1-6 standard. Such standard takes into account the requirements for the design against the ultimate limit state of: (i) Plastic limit, (ii) Cyclic plasticity; (iii) buckling and (iv) fatigue. Only the plastic and buckling limit state were analyzed on this project. It is important to mention that since the model was created on a different software, a file *.step* was created on software NX and then imported to *ABAQUS*. The assembly, iteration properties, boundary conditions, elements mesh were developed on *ABAQUS*.

7.1 FINITE ELEMENT MODELING

7.1.1 Assembly and Iteration Properties

Initially, to create the model, all the five parts had to be assembled on module assembly. The figure (figure 7.1) bellow shows the model geometry, where all the part instances are assembled generating the transition segment.
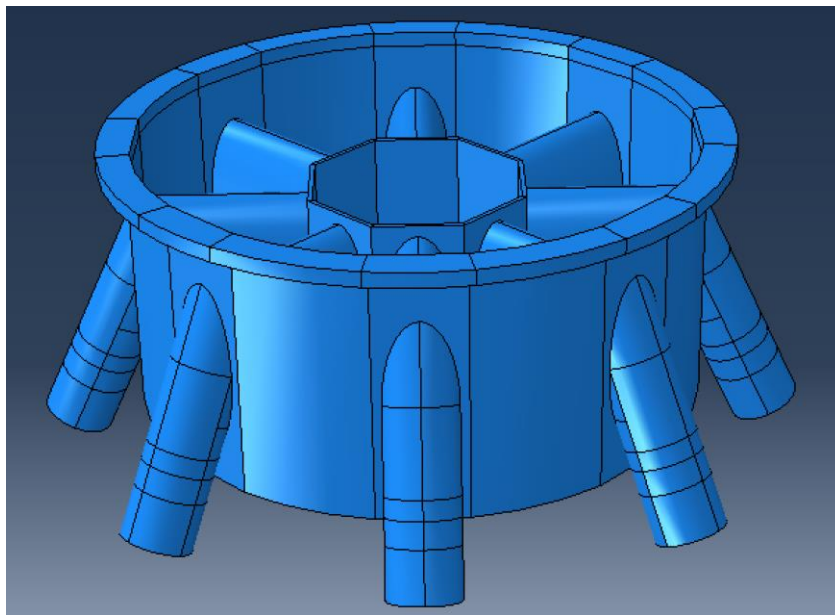
Figure 7.1 – Assembly of the transition segment

Although all the part instances are in the correct position on the assembly it is necessary to model the interaction between all the elements, for *ABAQUS* to recognize the model as one segment. Four *tie* constrains had to be created to simulate the interaction of the assembly: (i) interaction between chord and outer ring; (ii) interaction between outer ring and elliptical tube; (iii) interaction between elliptical tube and inner ring and (iv) interaction between outer ring and the welded flange. Figure 7.2 shows all four interactions.
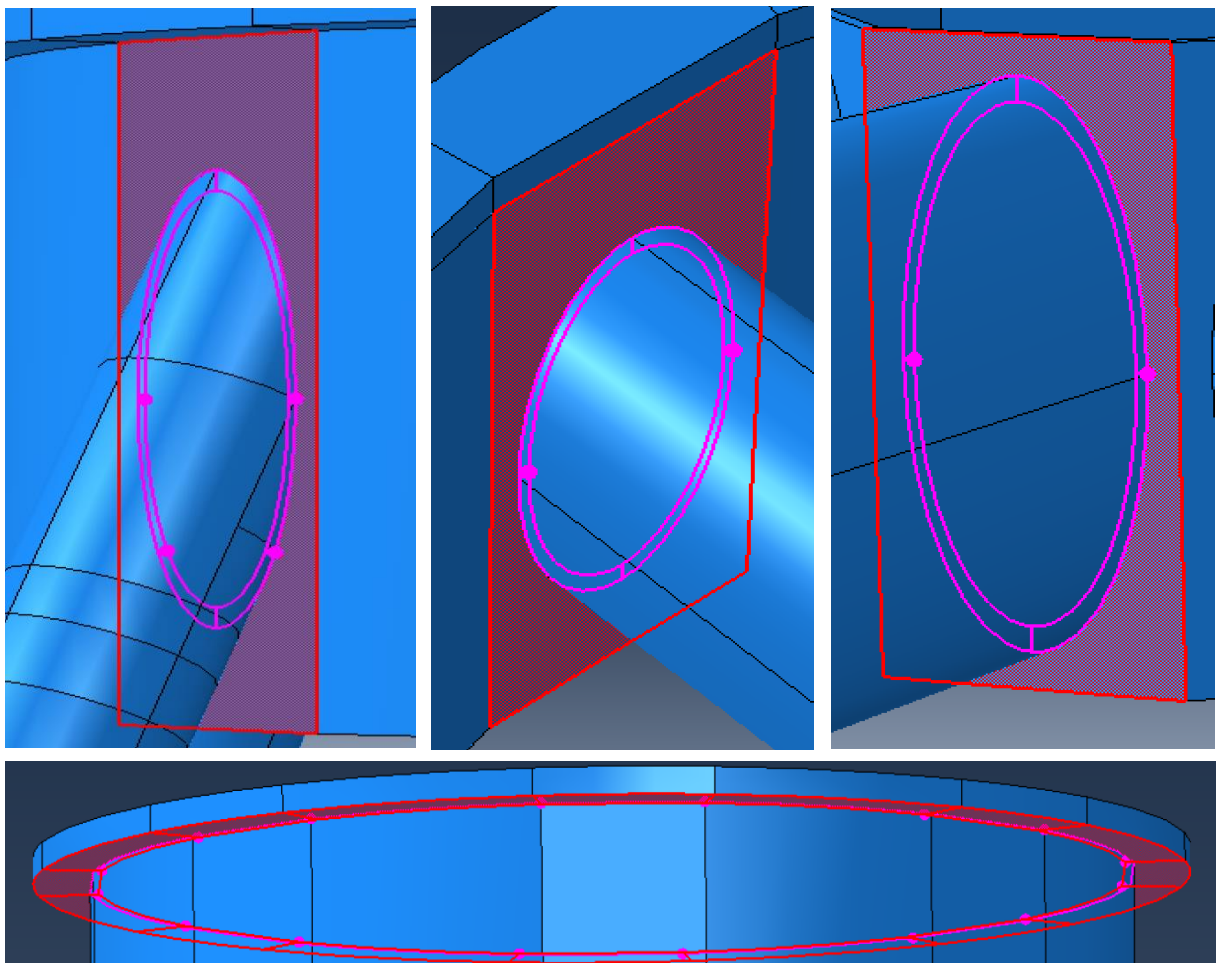
Figure 7.2 – Tie constraint interactions

7.1.2 Boundary Conditions

In order to model accurately the transition piece, there was an attempt to replicate the boundary conditions on the real structure (figure 6.2), on the model. Therefore, it was created a reference point (RP) for each support. Furthermore, coupling constraint was created in order to have a

control point of that region. Then, all translations and rotations were restrained on the RP. This procedure can be seen on figure 7.3 and it was repeated 8 times, for the all supports.

Figure 7.3 – Boundary conditions for supports

7.1.3 Load Point

The same procedure that was done for the boundary conditions was repeated for the load application, since it is the same type of connection WFC. A reference point was created (RP-C), which was named as load point (LP), Figure 7.4, and then coupling constraint was created. As a result of obtaining the design loads actions on *Robot Structural Analysis*, the load values are given on the *rigid link*, and using this procedure it is the only way to apply the design load actions, see table 7.2.
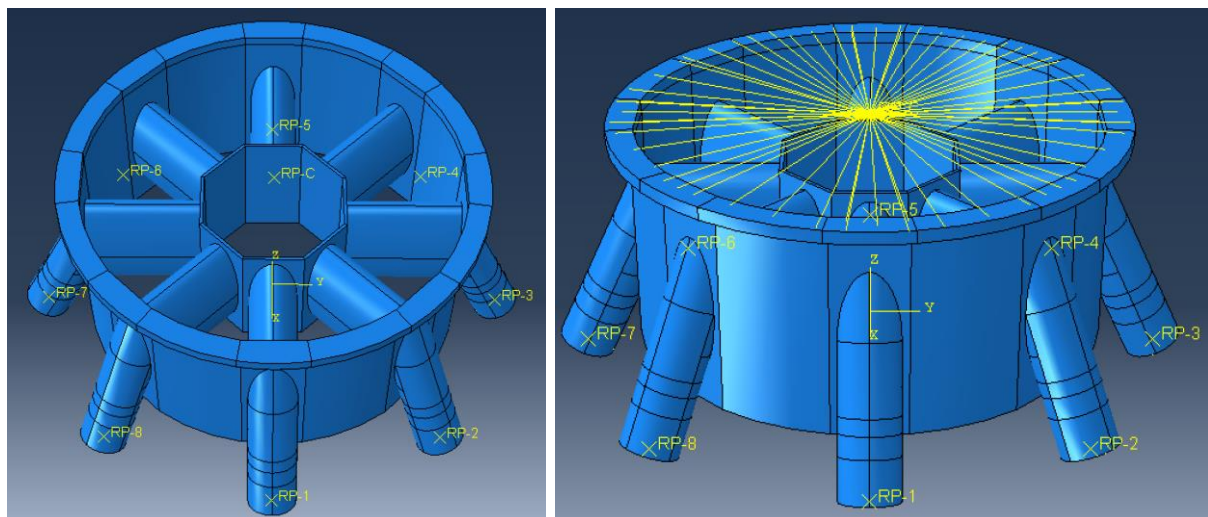
Figure 7.4 – Reference points and coupling constraint

ABAQUS has no inbuilt unit system. Caution is highly recommended when using consistent units as SI-system. In this project, the SI-mm system was used (table 7.1). The axis from *Robot Structural Analysis* do not coincide with the axis from *ABAQUS*. Therefore, it was considered when applied the loads (table 7.1).

Table 7.1 - a) Units SI system mm b) Corresponding axis

ABAQUS		
Quantity	SI (m)	SI (mm)
Length	m	mm
Force	N	N
Mass	kg	tonne (10^3 kg)
Time	s	s
Stress	Pa (N/mm^2)	MPa (N/mm^2)
Energy	J	mJ (10^{-3} J)
Density of Steel	7850 kg/m^3	7,85E-09 tonne/mm^3
Acceleration of Gravity	9,81 m/s^2	9810 mm/s^2
Young's Modulus of Steel	210E9 Pa	210E3 MPa

AXIS		
Robot	Abaqus	
x	z	3
y	y	2
z	x	1

Table 7.2 – Design loads values

LOADS Robot		
Fx	-4879	kN
Fy	1065	kN
Fz	1065	kN
Mx	-3966	kN*m
My	-123278	kN*m
Mz	-89126	kN*m

LOADS Abaqus		
Fx	1,0650E+06	N
Fy	1,0650E+06	N
Fz	-4,8790E+06	N
Mx	8,9126E+10	N*mm
My	1,2328E+11	N*mm
Mz	3,9660E+09	N*mm

7.1.4 Mesh and Element Type

The finite element mesh is exclusively constituted by tridimensional solid elements. The element type of C3D8R was adopted, due to the high dimension of the model. A different type of solid element such as C3D8, C3D20 or C3D20R would increase exponentially the computation effort. Since the model has a complex shape, given by a lot of partitions (see figure 7.1) in all part instances were created in order to have a structured mesh technique. Table 7.3 summarizes the important data relative to the mesh, including the number of finite elements.

Table 7.3 – Meshing information

Part	Element Type	Element Shape	Mesh Techinque	Number of Finite Elements	Number of Nodes
Chord	C3D8R	Hexahedral	Structured	6060	8336
Outer Ring	C3D8R	Hexahedral	Structured	156000	210080
Elliptical Tube	C3D8R	Hexahedral	Structured	4860	6720
Inner Ring	C3D8R	Hexahedral	Structured	19200	26240
Flange	C3D8R	Hexahedral	Structured	7056	10290
All Model	C3D8R	Hexahedral	Structured	269616	367058

In order to ensure adequate results from *ABAQUS* simulation a refined and good quality mesh should be used. However, the computer resources required to perform the finite element analysis increase with the level of the mesh refinement. Since the outer ring is the most critical part a mesh convergence study was done for this part. A linear analysis was performed using a standard general procedure. An axial load of 1 000 000 N was applied at the load point. A vertical *path* was created through the entire height of the plate where one of the chords meets the outer ring. The criteria to stop the mesh refinement was that the difference should be lower than 1% when compared to the previous mesh size. The graphic 7.1 shows the stress distribution through the *path*. Moreover, table 7.4 reviews the mesh convergence study and held not only the different mesh sizes but also the criteria used to stop the mesh refinement.

Table 7.4 – Mesh convergence study

Mesh_#	n_x	n_z	Max Stress(Mpa)	Erro (%)
Mesh_1	40	100	3,71934	-0,90%
Mesh_2	35	88	3,75283	1,28%
Mesh_3	30	75	3,70467	2,28%
Mesh_4	25	63	3,62022	-1,84%
Mesh_5	20	50	3,68697	3,18%
Mesh_6	15	38	3,56960	9,61%
Mesh_7	10	25	3,22650	-
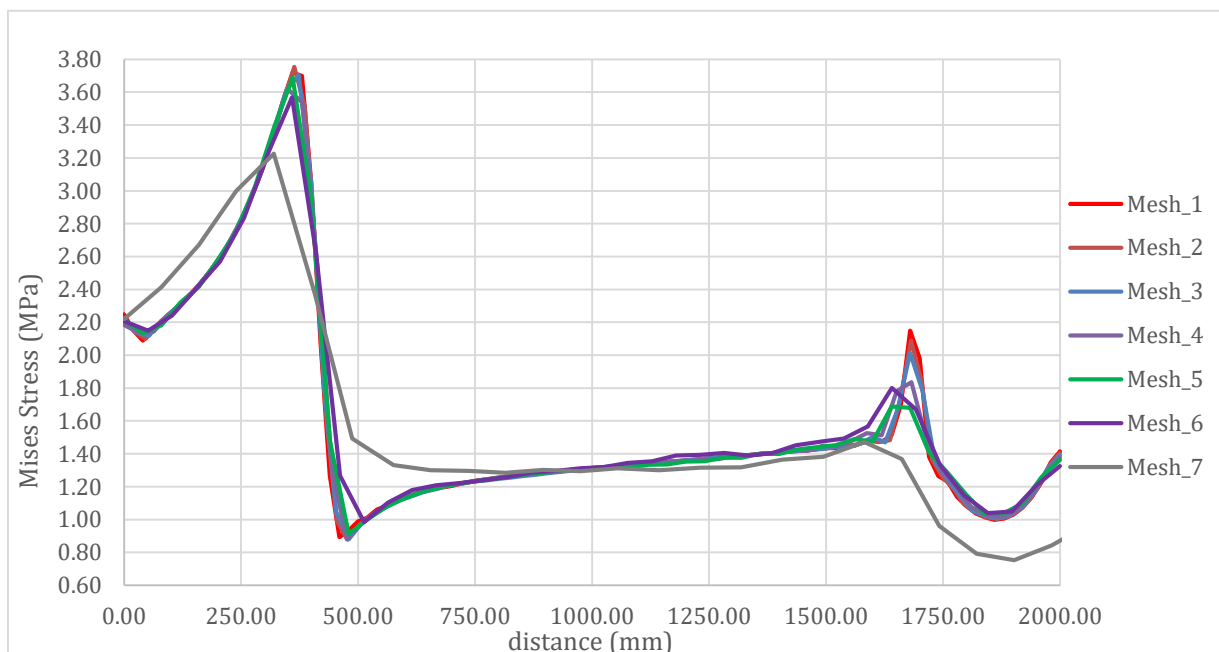
Graphic 7.1 – Mesh convergence study

7.1.5 Type of analysis

For assessing not only plastic limit state but also buckling limit state, several types of analysis had to be performed. The table 7.5 presented below summarizes all completed analysis. Addionally, it is also presented a general description of each type of analysis.

Table 7.5 – Types of analysis performed (addapted from EN1993-1-6, 2007)

Type of Analysis	Description
Linear Elastic Shell Analysis (LA)	An analysis that predicts the behavior of a thin-walled shell structure on the basis of the small deflection linear elastic shell bending theory, related to the perfect geometry of the middle surface of the shell.
Linear Elastic Bifurcation Analysis (LBA)	An analysis that evaluates the linear bifurcation eigenvalue for a thin-walled shell structure on the basis of the small deflection linear elastic shell bending theory, related to the perfect geometry of the middle surface of the shell. It should be noted that, where an eigenvalue is mentioned, this does not relate to vibration modes.
Geometrically Nonlinear Analysis (GNA)	An analysis based on the principles of shell bending theory applied to the perfect structure, using a linear elastic material law but including nonlinear large deflection theory for the displacements that accounts full for any change in geometry due to the actions on the shell. A bifurcation eigenvalue check is included at each load level.
Materially Nonlinear Analysis (MNA)	An analysis based on shell bending theory applied to the perfect structure, using the assumption of small deflections, but adopting a nonlinear elasto-plastic material law.
Geometrically and Materially Nonlinear Analysis (GNMA)	An analysis based on shell bending theory applied to the perfect structure, using the assumptions of nonlinear large deflection theory for the displacements and a nonlinear elasto-plastic material law. A bifurcation eigenvalue check is included at each load level.
Geometrically and Materially Nonlinear Analysis with Imperfections included (GNMIA)	An analysis with imperfections explicitly included, based on the principles of shell bending theory applied to the imperfect structure (i.e. the geometry of the middle surface includes unintended deviations from the ideal shape), including nonlinear large deflection theory for the displacements that accounts full for any change in geometry due to the actions on the shell and a nonlinear elastoplastic material law. The imperfections may also include imperfections in boundary conditions and residual stresses. A bifurcation eigenvalue check is included at each load level.

7.2   STRESS DISTRIBUTION

As a result of being a unique conceptual model, and considering the magnitude of the design load values, firstly a linear analysis (LA) was performed in order to obtain the stress distribution on the transition segment (Figure 7.5). It is important to mention that the welded flange connection and the supports were not object of study. Therefore, only the outer ring and the inner ring set were analyzed. A standard general procedure was performed.
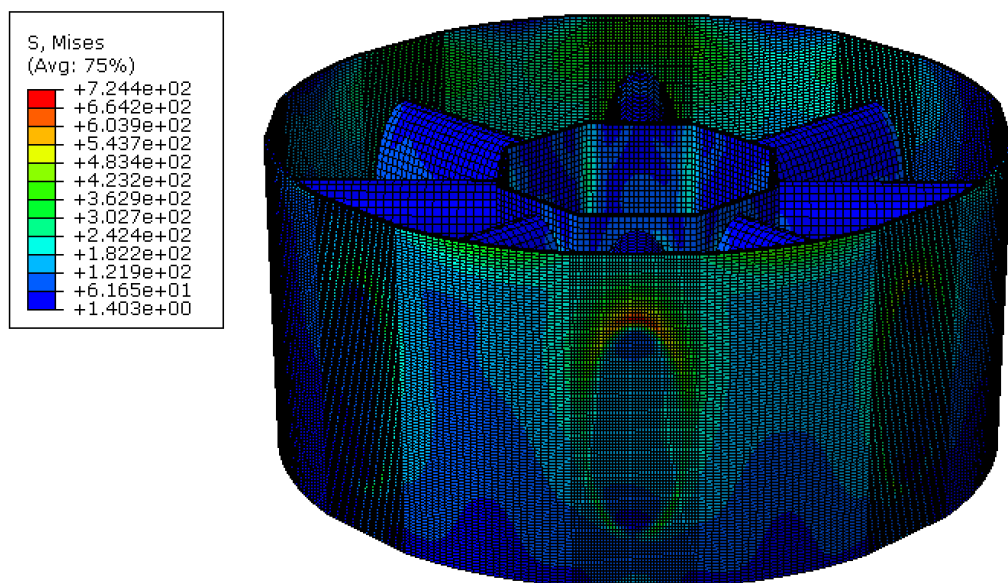
Figure 7.5 – Stress distribution on transition segment (LA)
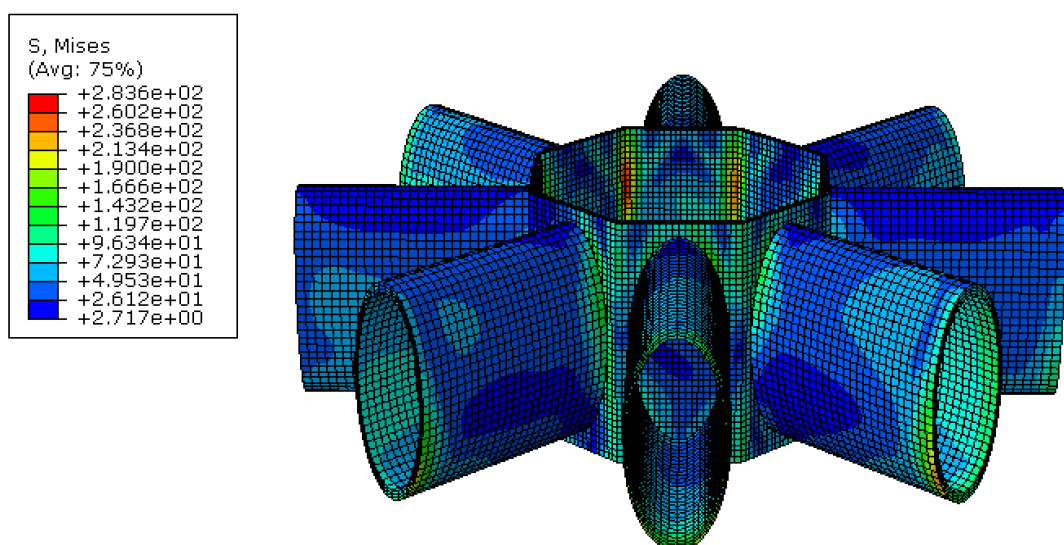
Figure 7.6 – Stress distribution on inner ring set (LA)
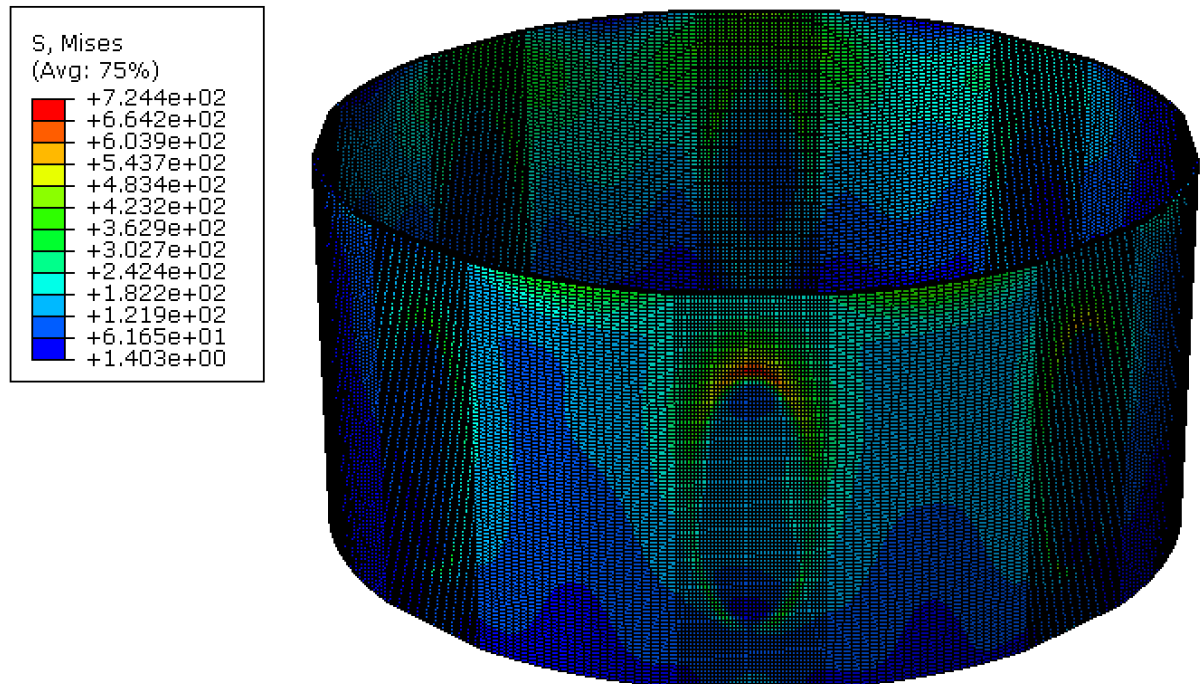
Figure 7.7 – Stress distribution on outer ring (LA)

Both outer ring and inner ring set were design taking into account the Von Mises Stress distribution. The outer ring should be composed by high-strength structural steel Strenx 900 (SSAB), that certifies a minimum yield strength of 900 MPa. It provides high impact toughness, where low weight is required and affords good resistance to fractures. SSAB also ensures not only a superior bendability but also a surface quality. Since, all the pieces are going to be welded, SSAB guarantees weldability with excellent heat-affected-zone (HAZ) strength and toughness. For the inner ring set, steel S355 was used that has a minimum yield strength of 355 MPa.

7.3 INFLUENCE OF THE INNER RING

Once the design of the of the outer ring is done, it is important to estimate the contribution of the inner ring set. Considering the complexity of the geometry of the transition segment, a geometrically non-linear analysis was performed with the load design values, not only for the model with the inner ring set but also for the model without the inner ring set reinforcement (figure 7.8 and figure 7.9).
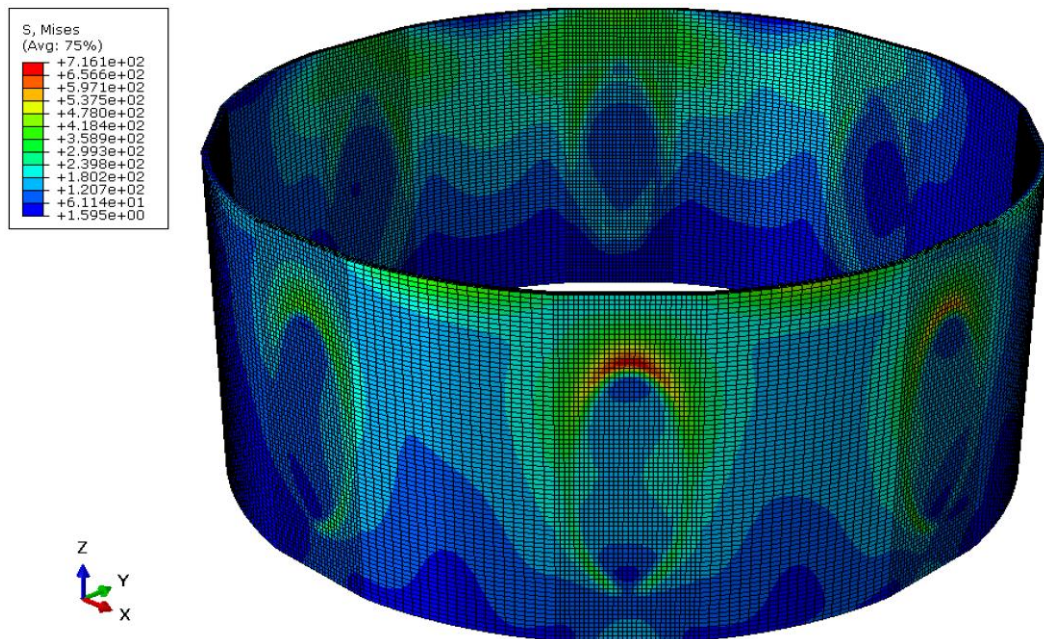
Figure 7.8 – Stress distribution on outer ring with inner ring set σ_{Ed} =716 MPa (GNA)
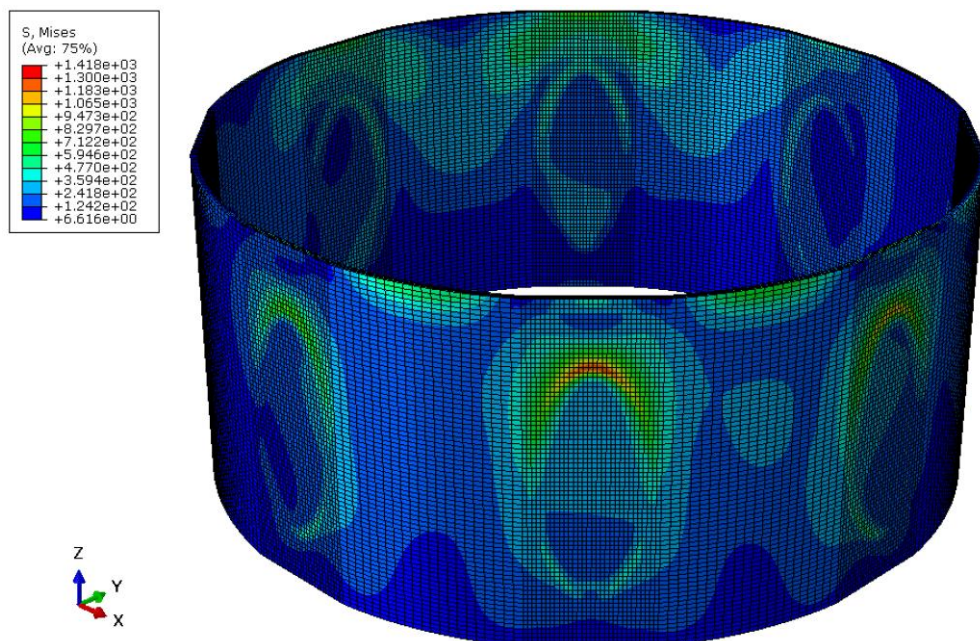
Figure 7.9 – Stress distribution on outer ring without inner ring set σ_{Ed} =1418 MPa (GNA)

The Von Mises stress distribution was compared for the two models. Although the stress distribution on the inner ring set is significantly lower than the outer ring, its presence causes a reduction of 50% on the stress distribution on the outer ring. Therefore, it was concluded that the inner ring set has a key impact on the resistance of the transition segment.

7.4 PLASTIC LIMIT STATE (LS1)

The plastic limit state (LS1) was verified according to the standard EN1993-1-6 6.3. The ultimate limit state where the structure develops zones of yielding a pattern such that its ability to resist increased loading is deemed to be exhausted by yielding of the material. The resistance offered by the structure at the plastic limit state is closely related to a small deflection theory plastic limit load or plastic collapse mechanism. Tensile rupture phenomenon may occur when the shell wall experiences gross section tensile failure, leading to a possible separation of the shell parts. Since the transition segment, has no fastener holes, verification at the limit state of tensile rupture covers the check for the plastic limit state.

For design by global numerical analysis, according to EN1993-1-6 4.1.1 (6), either a MNA or GMNA should be performed when checking LS1. Considering the high complexity of the geometry as achieving accurate and realistic results, a GMNA was performed. In order to verify LS1, Von Mises design strength has to be higher than the Von Mises stress distribution on the transition segment parts.

7.4.1 Material laws

To take into account, the material non-linearity, the plasticity of the steel had to be introduced on the finite element model through property module. Simple plasticity material model was used. Graphic 7.2 shows the material law for the high strength steel S900 and for the steel S355.
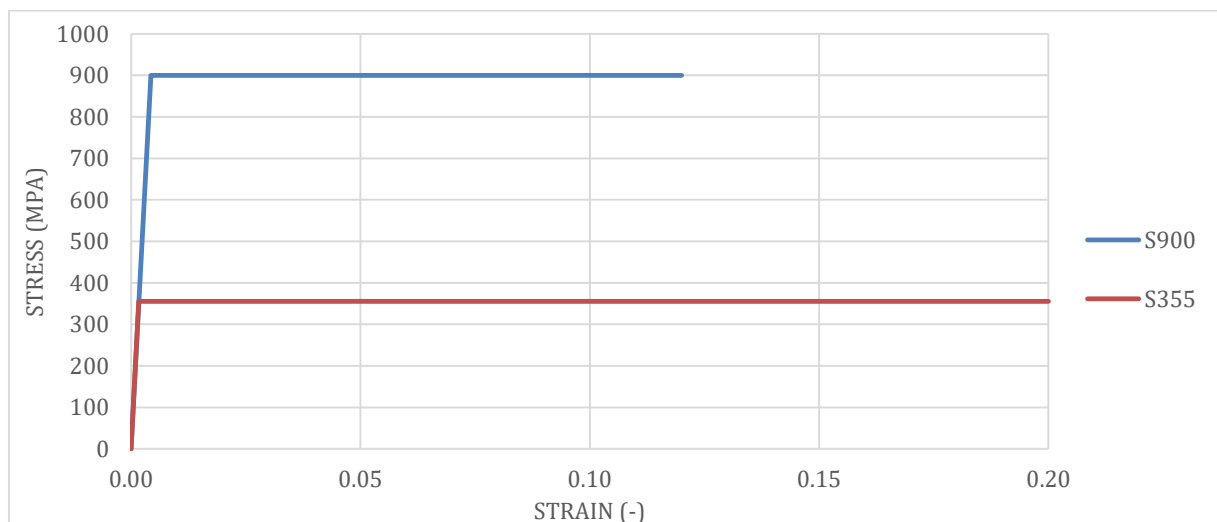
Graphic 7.2 – Steel curve stress-strain for S900 and S355

7.4.2 Outer Ring

The outer ring is composed by S900, which has at least a yield strength of 900 MPa.
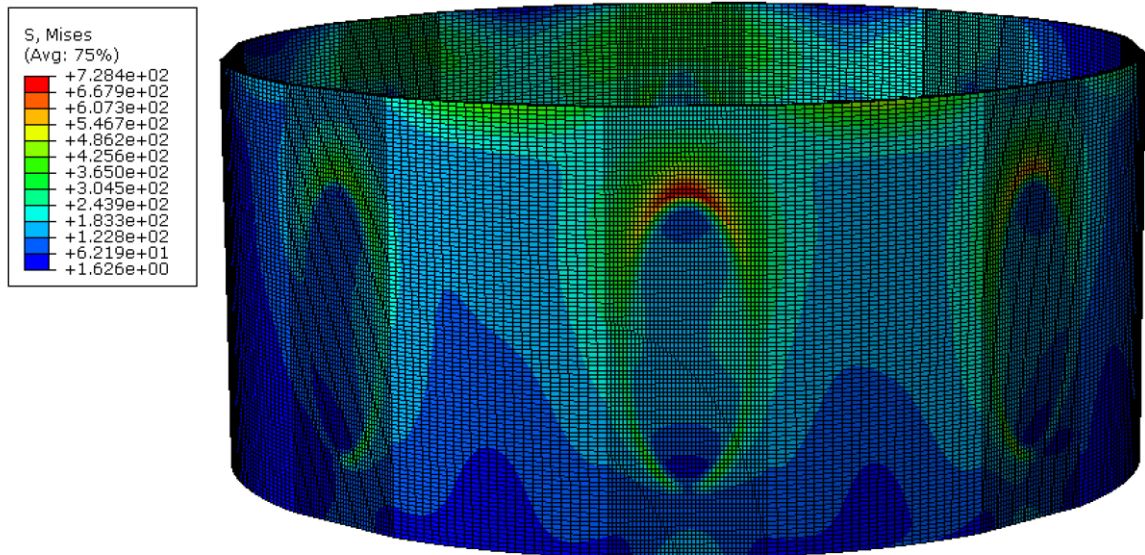
Figure 7.10 – Stress distribution for outer ring (GMNA)

$$\sigma_{MISES,Ed} = 728.4 \le f_{yd} = 900 \; MPa \;\rightarrow\; \text{LS1 verified for outer ring}$$

7.4.3 Inner ring set
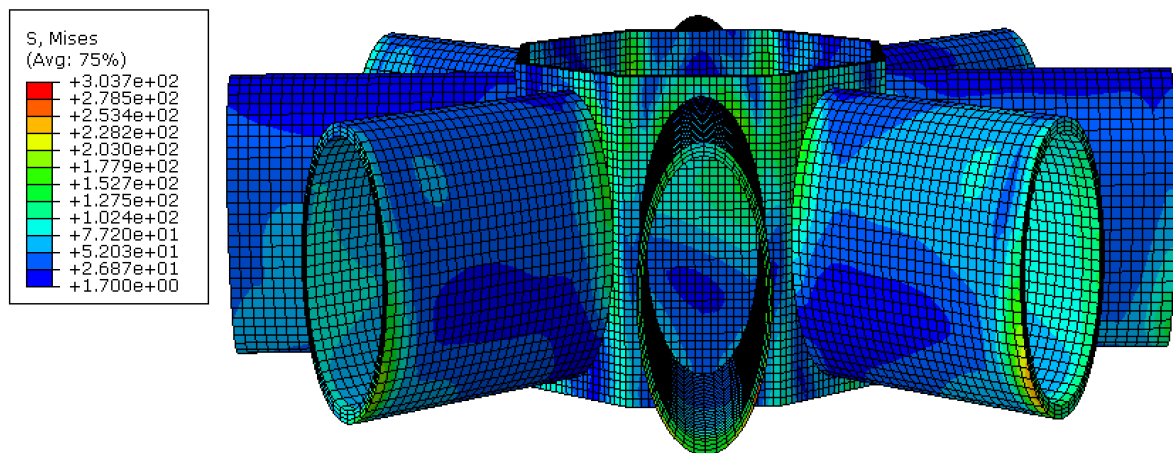
Figure 7.11 - Stress distribution for inner ring set (GMNA)

$$\sigma_{MISES,Ed} = 303.7 \le f_{yd} = 355 \; MPa \rightarrow \text{LS1 verified for inner ring set}$$

Plastic limit state is verified for the transition segment, according to EN1993-1-6 6.3.

7.5 BUCKLING LIMIT STATE (LS3)

The buckling limit state (LS3) was verified according to the standard EN1993-1-6 8.7. According to the same standard, LS3 is the ultimate limit state where the structure suddenly loses its stability whether under membrane compression or shear. It leads either to large displacements or to the structure being unable to carry the applied loads.

Three different situations were considered to verify LS3: (i) Axial compression load; (ii) Bending moment around the x-axis and (iii) Bending moment around the xy-axis, where the angle from top view is 67.5º, to consider the direction in which there are no direct support, that turned to be the critical one, see figure 7.12.
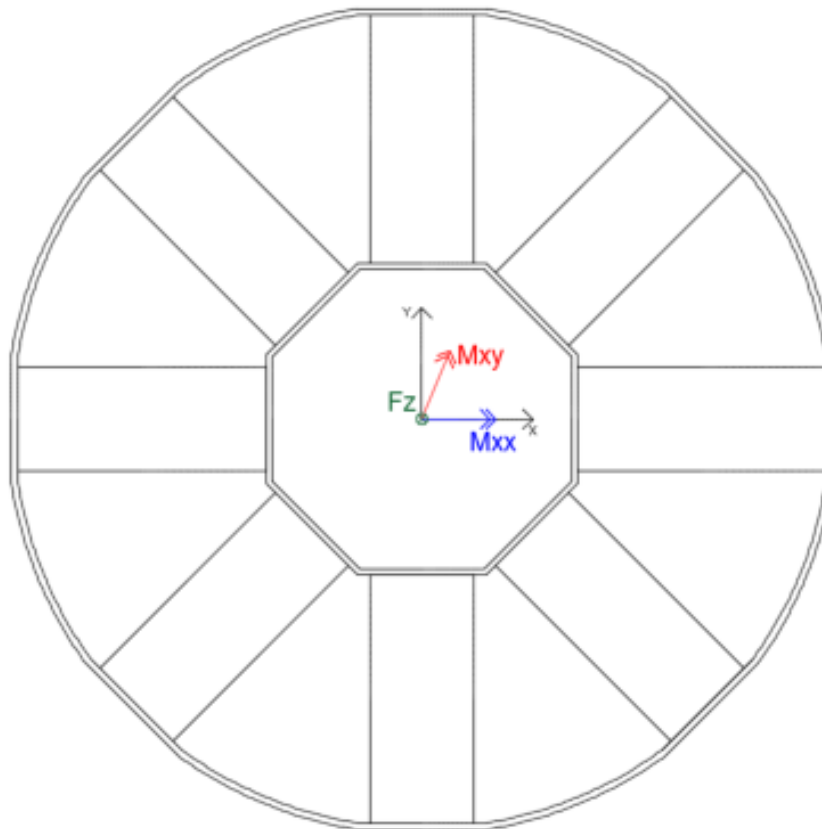
Figure 7.12 – Buckling limit state considered situations

According to EN1993-1-6 8.7, for the design by global numerical analysis a Geometrically and Materially non-linear analysis with imperfections included (GMNIA) has to be performed.

7.5.1   GMNIA approach in EN1993-1-6 8.7

Firstly, an LBA is needed to obtain eigen mode-affine shapes of imperfections. Furthermore, imperfections are applied to the succeeding model using shape from LBA and amplitudes calculated in EN1993-1-6 8.7.2(18). Moreover, simple plasticity material model should be used for the design (no strain hardening), as used for verifying LS1 (see chapter 7.4.1). Thus the ultimate load amplification factor ($r_{R,GMNIA}$) may be obtained using a numerical solver for post-buckling finite element analysis on the design load values.

Nonlinear buckling analysis with effect of the steel plastification was used to investigate the post buckling behavior and find if the yield transforms the stable post buckling behavior into unstable, since, after the yield, an increase in the deformation causes a decrease of the corresponding load.

Since the post buckling behavior may become unstable when the elasto-plastic deformations occur, it is very important to investigate the influence of imperfections on the structure loading capacity. A numerical study shall consider buckling and post buckling problems with the influence of imperfections in engineering structures in order to find out the most accurate, reliable and realistic numerical method for complex structures, such as this novel conceptual model of transition segment for hybrid lattice-tubular steel wind towers.

For post buckling analysis two different methods were used: (i) standard solver Newton-Rapson and (ii) standard static RIKS solver. To verify the buckling limit state for the axial load the Newton-Raphson method was used, however, due to convergence issues standard static RIKS solver was used to assess LS3 for the two bending moment cases.

The Newton-Raphson method is a powerful technique for solving equations numerically, it is based on linear approximation using tangent lines. Although having a devastating efficiency on solving numerical problems, Newton-Rapson method experience convergence issues and stops at limit load.

Standard static RIKS solver based on arc-length method, the load proportionality factor at each iteration is modified so that the solution follows some specified path until convergence is achieved. The arc-length is kept fixed for current increment, whereas in the latter case, new arc-length is evaluated at the beginning of each load step to ensure the achievement of the solution procedure. For further increments the load-factor is computed according to the rate of convergence of the solution process. In case of divergence from the solution path, the arc-length is reduced and computations are performed once again. Moreover, RIKS method is able to find solution during unloading process.

7.5.2   Axial compression load

In order to obtain the eigen mode-affine shapes, a linear elastic bifurcation analysis was performed to the model with a vertical compression load of 1N, see figure 7.13. The critical buckling load of the ideal structure (Eigenvalue) for the first mode is 1.4668E9 N.
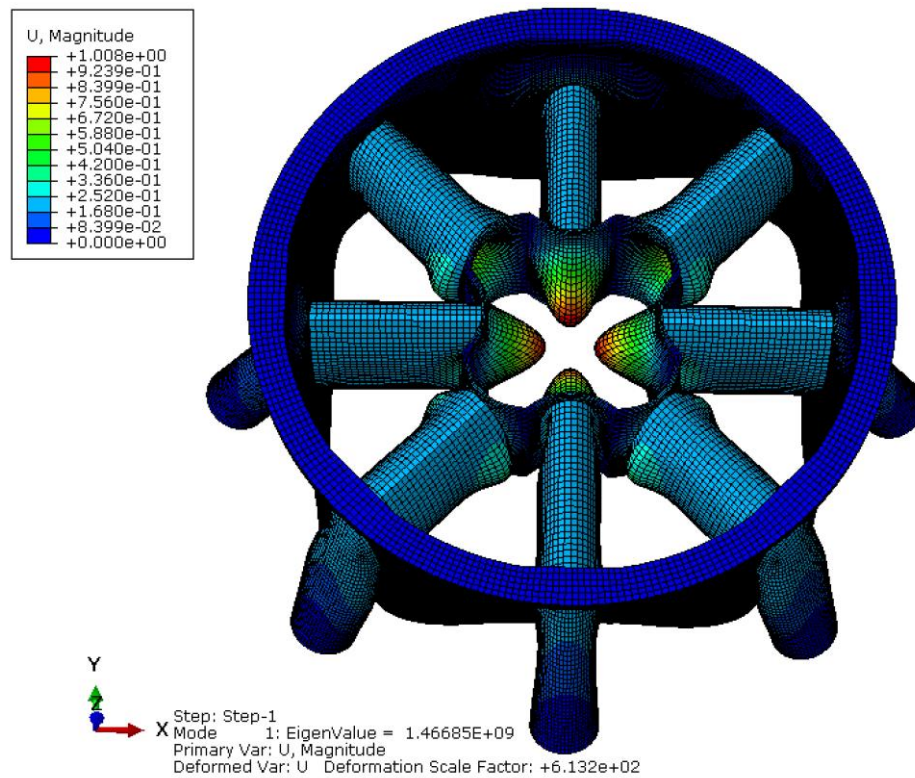
Figure 7.13 – Eigen mode shape for axial load compression (LBA)

The second step consists in calculating the magnitude of the imperfection for the post-buckling analysis. According to the EN1993-1-6 8.7 (18) the amplitude of the adopted equivalent geometric imperfection form should be taken as dependent on the fabrication tolerance class. For both different steels it was considered a fabrication tolerance quality class B. The maximum deviation, $\Delta w_{0,eq}$, of the imperfection from the perfect structure shape should be estimated by the following formula:

$$\Delta w_{0,eq} = max \left\{ \begin{array}{c} \Delta w_{0,eq,1} = l_g \times U_{n1} \\ \hline \Delta w_{0,eq,2} = n_i \times t \times U_{n2} \end{array} \right\} = max \left\{ \begin{array}{c} \Delta w_{0,eq,1} = 0 \\ \hline \Delta w_{0,eq,2} = 25 \times 36 \times 0.016 \end{array} \right\}$$
$$= 14.4 \ mm \tag{Eq 7.1}$$

Since the local buckling had its greatest amplitude in the inner ring set which is composed by plates, so the $\Delta w_{0,eq,1}$ is not aplicable for this case. Nevertheless, the amplitudes can be estimated according EN1993-1-5, where for local buckling on panels the imperfection magnitude should be taken as the following formula:

$$e_{0w} = min\left\{\begin{matrix} a/200 \\ b/200 \end{matrix}\right\} = min\left\{\begin{matrix} 7000/200 \\ 1500/200 \end{matrix}\right\} = min\left\{\begin{matrix} 3.5 \\ 7.5 \end{matrix}\right\} = 3.5 \ mm \qquad (Eq \ 7.2)$$

Therefore, it was considered a magnitude of 14.4 mm for the imperfections to analyze the most unfavorable situation. In order to introduce the imperfections on the succeeding model for the post-buckling analysis, the keywords had to be changed. The procedure was done according to ABAQUS documentation for post-buckling analysis.

As mentioned previously, the ultimate load amplification factor ($r_{R,GMNIA}$) was calculated using the Newton-Rapson method. A vertical displacement of 200 mm was applied at the load point. To obtain the imperfect elastic-plastic buckling load with more precision it was specified on module step the following values presented on table 7.6.

Table 7.6 – Definition of step parameters

Step Time	Minimum Increment	Initial Increment	Maximum Increment
200	0,001	0,1	0,5

Due to the maximum increment being only 0.5 mm, the maximum load can be estimated with high precision. The load-displacement curve is shown on the graphic below, where the load is the sum of reaction forces in z-direction of all eight supports and the displacement corresponds to the displacement which was applied at the load point. The maximum load obtained was 252 030 000 N.
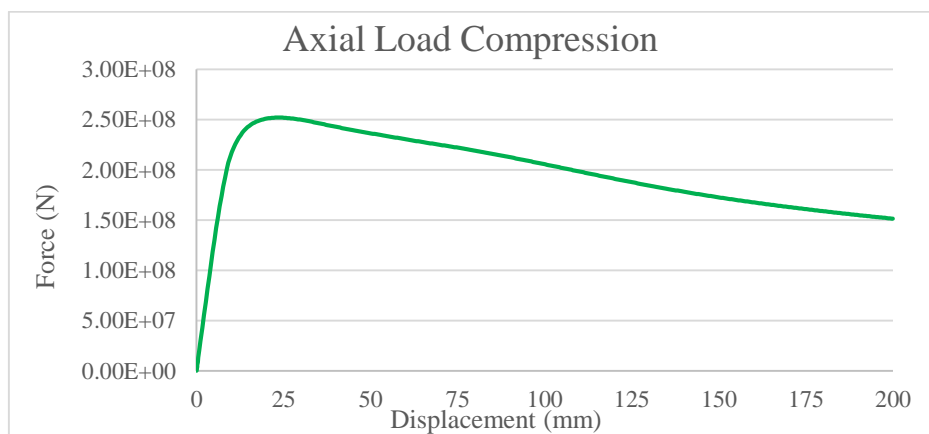
Graphic 7.3 – Force-displacement curve for checking LS3

7.5.3   Bending moment around the xx-axis

The procedure to assess the stability limit state for bending moment about the x-axis, is similar to that described in sub previous chapter. A unit bending moment about the x-axis was applied and then a linear elastic bifurcation analysis was performed. The critical buckling load of the ideal structure (Eigenvalue) for the first mode is 1.8120E12 N.mm.
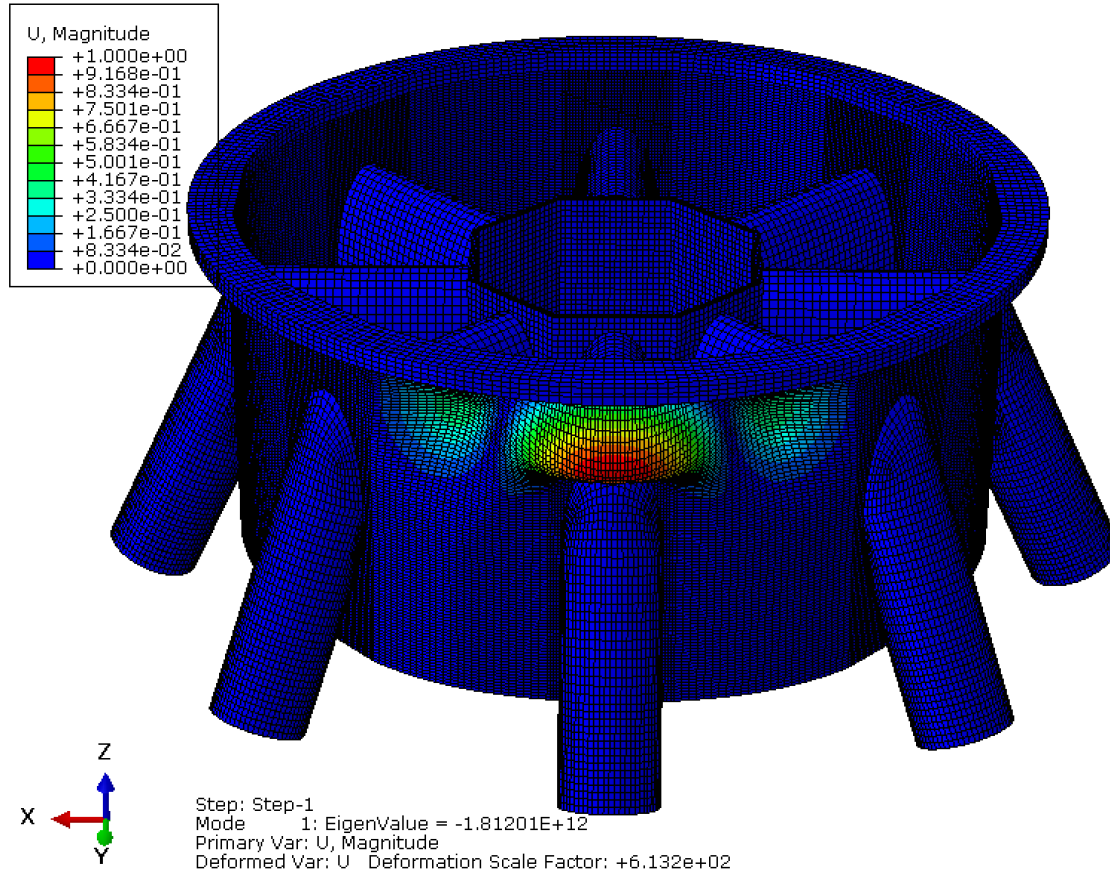
Figure 7.14 – Eigen mode shape for bending moment in turn of x-axis (LBA)

Once obtained the eigen mode shape for the critical mode, it is then necessary to estimate the magnitude of the imperfections to apply for the following model to determine the imperfect elastic-plastic buckling load. Similar to 7.5.2 the local buckling occurs on a plate. However it happens on the outer ring and not on the inner ring. The imperfections are estimated on the following expressions below.

$$\Delta w_{0,eq} = max\left\{\frac{\Delta w_{0,eq,1} = l_g \times U_{n1}}{\Delta w_{0,eq,2} = n_i \times t \times U_{n2}}\right\} = max\left\{\frac{\Delta w_{0,eq,1} = 0}{\Delta w_{0,eq,2} = 25 \times 36 \times 0.016}\right\}$$

$$= 14.4 \text{ mm} \tag{Eq 7.3}$$

$$e_{0w} = min\left\{\begin{matrix}a/200\\b/200\end{matrix}\right\} = min\left\{\begin{matrix}7000/200\\2000/200\end{matrix}\right\} = min\left\{\begin{matrix}3.5\\10\end{matrix}\right\} = 3.5 \; mm \qquad \text{(Eq 7.4)}$$

Similar to the axial load compression case, the magnitude of the imperfections calculated on EN1993-1-6 are more unfavorable than the ones estimated according to EN1993-1-5. Therefore, a magnitude of 14.4 mm was consider and applied on the following model. The same procedure was performed to include the imperfections on the calculations.

Due to convergence issues, the numerical problem was solved using standard static RIKS procedure. As mentioned previously, this method increases the load until obtaining the maximum load amplification factor. A curve bending moment-rotation, where the maximum bending moment obtained was 5.2485E11 N.mm, is shown on the graphic below.
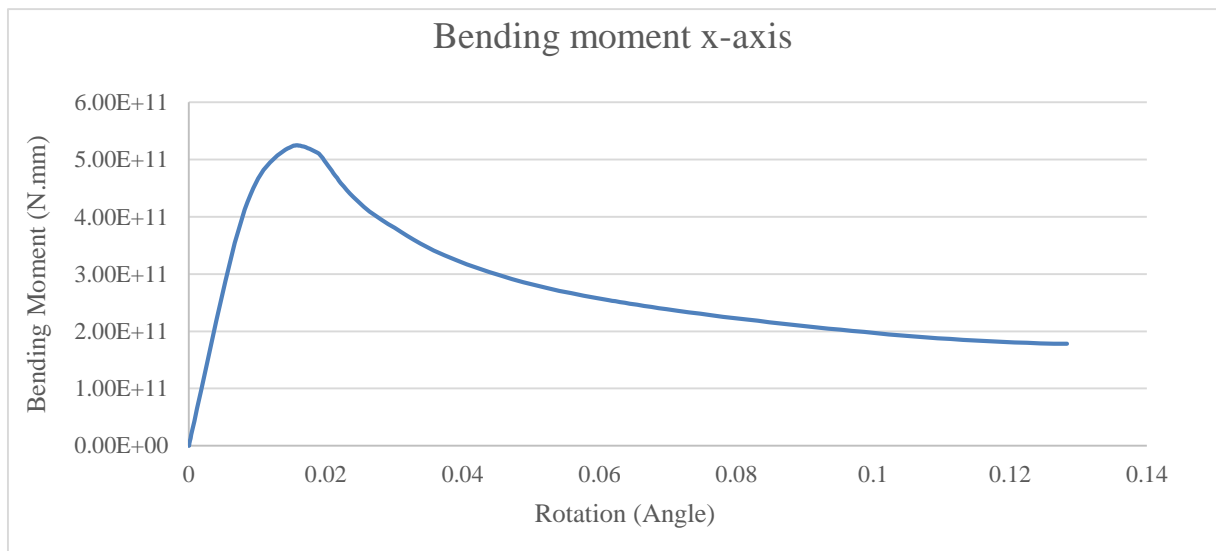
Graphic 7.4 - Bending moment-rotation for checking LS3 (Mxx)

7.5.4 Bending moment around the xy-axis

In order to assess the buckling limit state, for the bending moment in turn of the xy-axis, the same procedure done on 7.5.3 was performed once again. However, for this time it was necessary to apply the bending moment with the angle of 67.5°. The following table shows the calculations to determine the percentage of moment to apply in each direction to have a resultant unit bending moment direction with the angle of 67.5°.

Table 7.7 – Unit bending moment resultant

M	M1 (xx)	M2 (yy)	α (°)	α (rad)
1,00	0,38	0,92	67,5	1,18

Furthermore, the elastic critical buckling load of the ideal structure (Eigenvalue) for the second mode was obtained 1.8279420E12 N.mm through a linear elastic bifurcation analysis (figure 7.15).
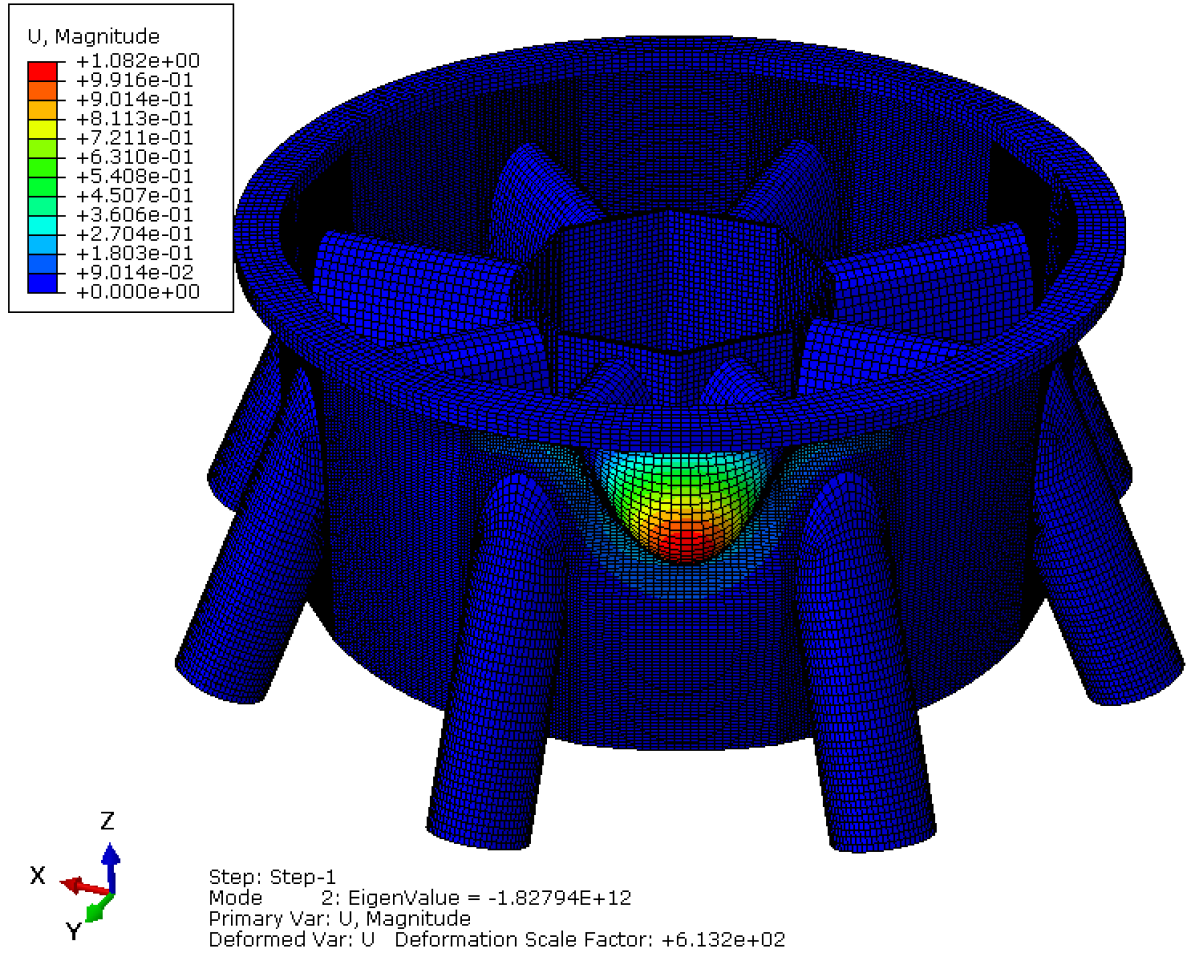
Figure 7.15 – Eigen mode shape for bending moment in turn of x-axis (LBA)

Since the eigen mode shapes are determined, the next step was to estimate the magnitude of the imperfections, the following expressions below were used.

$$\Delta w_{0,eq} = max \left\{ \frac{\Delta w_{0,eq,1} = l_g \times U_{n1}}{\Delta w_{0,eq,2} = n_i \times t \times U_{n2}} \right\} = max \left\{ \frac{\Delta w_{0,eq,1} = 1266 \times 0.016}{\Delta w_{0,eq,2} = 25 \times 36 \times 0.016} \right\}$$

$$= max \left\{ \frac{\Delta w_{0,eq,1} = 20.2}{\Delta w_{0,eq,2} = 14.4} \right\} = 20.2 \; mm \hspace{2cm} (Eq \; 7.5)$$

$$l_g = l_{g\theta} = 2.3(l^2 \times r \times t)^{0.25} = 2.3(1064^2 \times 2250 \times 36)^{0.25} = 1266 \; mm \hspace{1cm} Eq \; (7.6)$$

Therefore the magnitude considered was 20.2 mm. Nevertheless both magnitudes were considered in two diferent models, to evaluate the influence of the magnitude on the load amplification factor. With the intention to do a close comparision between the results from the two bending moment cases, the same static RIKS procedure was performed. In order to compare the results of the imperfect structure with the perfect structure, a geometrically and materially non-linear analysis (GMNA) was performed to the structure with no imperfections. Graphic 7.5 shows the results of the three performed analysis.
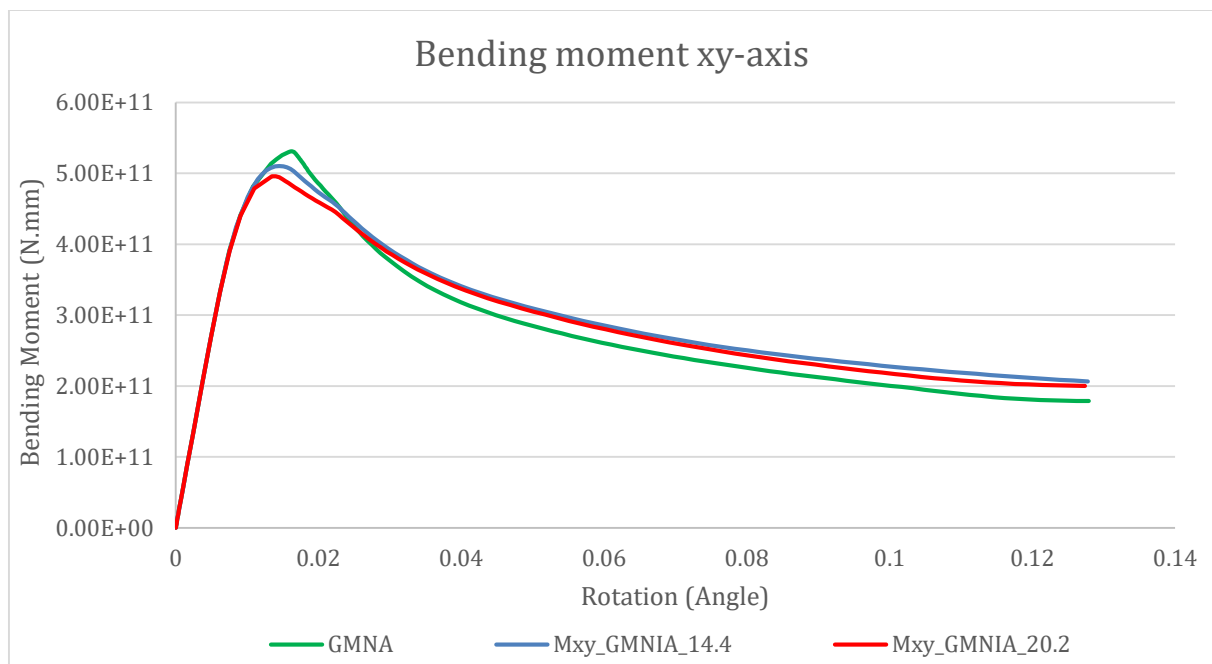
Graphic 7.5 - Bending moment-rotation for checking LS3 (Mxy)

The ultimate bending moment achieved was 4.9585E11 N.mm. Thus this case is the most unfavorable of all the three analyzed cases. According to EN1993-1-6 8.7.2 (4) a materially non-linear analysis (MNA) has to be performed to establish the overall relative slenderness − λov for the complete shell structure according to the following formula:

$$\lambda_{OV} = \sqrt{\frac{r_{Rpl}}{r_{Rcr}}} = \sqrt{\frac{1.8279420E12}{1.16770E12}} = 0.80$$

Where, r_{Rpl} stands for the critical buckling load of the ideal structure (LBA) and r_{Rcr} is the load amplification factor for a materially non-linear analysis (MNA). It is important to mention that the overall relative slenderness was only estimated for the most critical case.

7.5.5   Buckling strength verification

The buckling strength verification was verified according to EN1993-1-6 8.7.3. Once the results of the post buckling analysis are obtained for the three considered cases, the imperfect elastic-plastic buckling resistance ratio $r_{R,GMNIA}$ was established. The characteristic buckling resistance ratio r_{Rk} should be found from the imperfect elastic-plastic buckling resistance ratio $r_{R,GMNIA}$, adjusted by the calibration factor k_{GMNIA}. The design buckling resistance ratio r_{Rd} should then be assessed using the partial factor γ_{M1}, according with the following equations:

$$r_{Rk} = K_{GMNIA} \times r_{R,GMNIA}$$
$$r_{Rd} = \frac{r_{Rd}}{\gamma_{M1}}$$

A calibration factor was used to verify the buckling strength. However, to estimate its value a close comparison against test results on a shell structure with appropriately similar features has to done. Since this is a novel conceptual model, there are no similar test results, therefore this calibration requirement is very challenging. Nevertheless, the values of calibration factor are within the range $0.8 \leq K_{GMNIA} \leq 1.2$. Therefore, to consider the most unfavorable case, it was assumed a calibration factor of 0.8. The summary of the buckling strength verification is shown on the table presented below.

Table 7.8 – Buckling stregth verification (LS3)

Design by global numerical analysis using GMNIA EC3-1-6 8.7				
GMNIA	Axial Compression Load	Bending Moment XX	Bending Moment XY	Bending Moment XY
Rd	2.5203E+08	5.2485E+11	5.1028E+11	4.9585E+11
Ed	4.8790E+06	1.5212E+11	1.5212E+11	1.5212E+11
Eigenvalue	1.4669E+09	1.8120E+12	1.8279E+12	1.8279E+12
Imp. Mag.	14.4	14.4	14.4	20.2
$r_{R,GMNIA}$	51.66	3.45	3.35	3.26
k_{GMNIA}	0.8	0.8	0.8	0.8
r_{Rk}	41.32	2.76	2.68	2.61
γ_{M1}	1.1	1.1	1.1	1.1
r_{Rd}	**37.57**	**2.51**	**2.44**	**2.37**

The case with the bending moment acting in turn of the xy-axis, with the angle of 67.5º, with the imperfection magnitude of 20.2 mm, was the most unfavorable situation. Yet, a design buckling resistance ratio of 2.37 was obtained. Therefore, the buckling limit state is verified. Further research where some optimization of the transition segment should be performed. The following graphics shows the curve for imperfect elastic-plastic buckling resistance ratio-deformation and the design buckling resistance ratio-deformation.
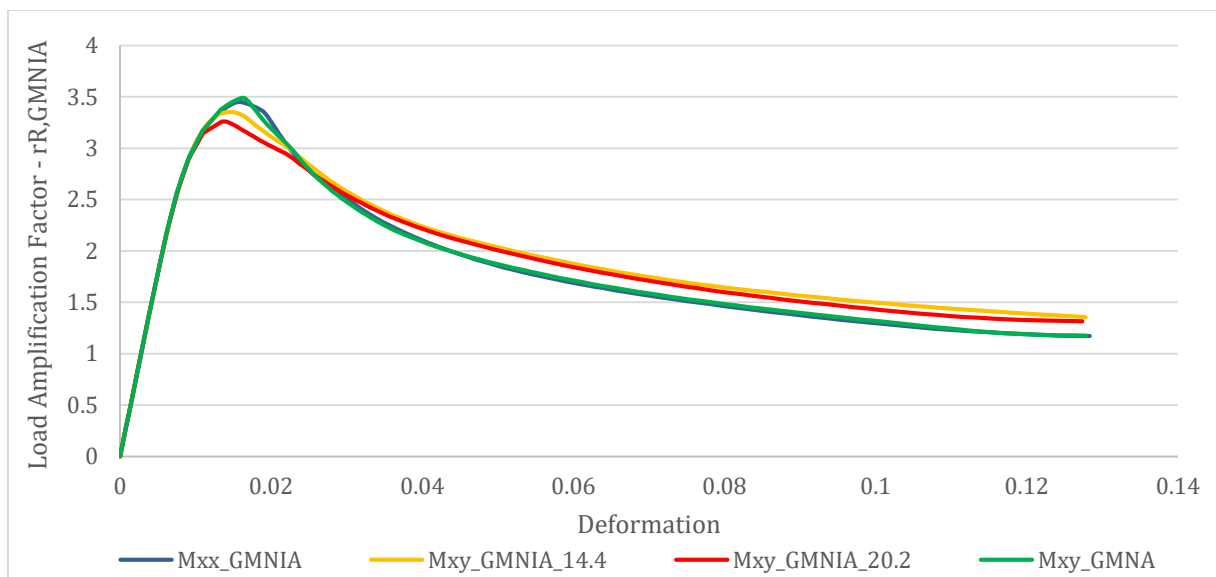
Graphic 7.6 – Imperfect elastic-plastic buckling resistance ratio-deformation curve (LS3)
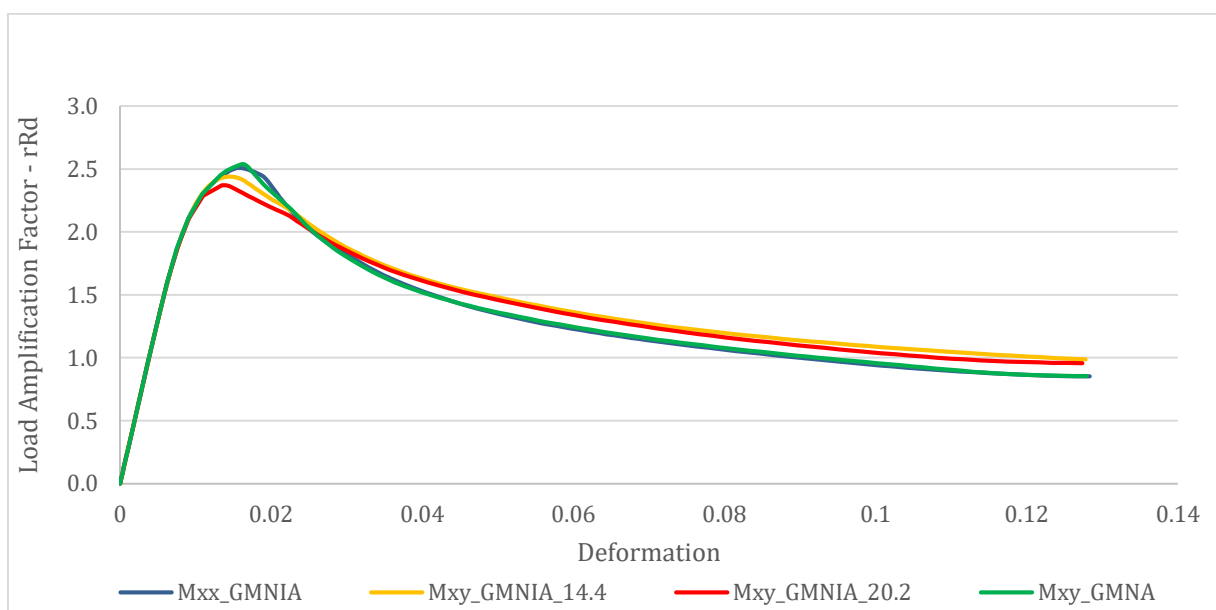
Graphic 7.7 - Design buckling resistance ratio-deformation curve (LS3)

8 CONCLUSIONS

This study, aimed to develop the technology wind energy. Nowadays renewable energy, specifically wind energy, has a huge impact on global energy production. Recently Portugal run for four days straight on renewable energy alone and according to Wind Europe trade association wind energy could meet a quarter of Europe's power needs in the next 15 years.

In this document, it was initially presented a literature review of the various concepts of wind towers and the basics of the wind energy and wind towers. This should allow any reader to get an idea of how the wind technology works.

The first aim of this study was fully accomplished. It consisted in designing a light weight strong lattice structure, by assembling an excellent hybrid lattice-tubular steel solution for the wind towers market. The hybrid solution design fulfils not only for the ultimate limit state but also for the dynamic performance of the tower. This concept supports a 7 MW wind turbine, which, at the present time is the biggest wind turbine for wind energy converters.

Through a short analysis with reference to the table E.1, it can be seen that the hybrid lattice-tubular steel tower presents a lower structural steel quantity than the steel tubular towers. Another advantage of this tower is its transportation and assembly, since the maximum length of the structural elements of the lattice is 12 m and the maximum diameter of the tubular tower is 4.5 m both satisfy the maximum requirements for road transportation. The assembly of the lattice elements is fully welded, however a new type of elements is proposed on (Figueiredo, 2013) where its assembly is fully bolted (Figure 8.1).
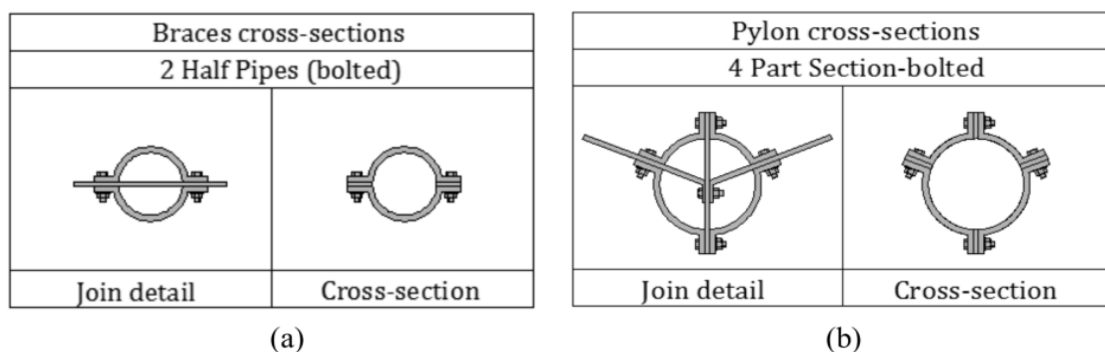
Figure 8.1 – Bolted circular hollow section a) Braces Section b) Chords Section (Figueiredo, 2013)

The new tubular cross-section consists of bolted separate parts, with different layout and dimensions, easily transported and assembled in-site. The main priorities of new tubular cross-section are: the reduction of connections costs, fatigue design limitations and use of "almost" maintenance-free fasteners. The design and manufacturing of bolted connections are developed for the effective in-site assembling of lattice tower part while considering the extensive use of maintenance free pre-stressed bolts (Figueiredo, 2013).

To compare the steel towers concepts with the concrete hybrid concepts a more detailed budget analysis should be performed. An life cycle analysis (LCA) also should be performed when comparing the various concepts in order to have the complete information about all concepts.

The second aim of idealizing a conceptual model for an innovative transition segment was entirely accomplished. Furthermore, a finite element analysis was performed to level of the piece, providing a good behavior for the design load actions. It was also concluded, that the use of high strength structural steel (S900) on the outer ring part has a crucial impact on the transition segment, due to the high strength and toughness combined with its low weight. Moreover, the addition of the inner ring set on the transition segment provides a significant increase of the stiffness of transition segment where a better stress distribution is accomplished. Additionally, it can be easily assembled on site and with a few adaptations can support a novel erection procedure by slide procedure for the upper tubular steel parts of the hybrid concept.

Globally, the two proposed objectives were met.

9   FUTURE WORK

As a consequence of the global warming problem, the energy market has grown exponentially and its tendency is to keep on growing increasingly, until all the global energy needs are finally met. Obviously, this shall take several more years, and further research and the development for renewable energy it is demanding for acquiring green cities and consequently a green world with no pollution. The European Union proposed plans on renewable energy policies is that in 2020, 34% of the total consumption of energy should come from renewable sources, including about 500 TW h from wind energy representing 14% of the total consumption.

Within this context, a more detailed analysis should be performed on the hybrid tower to fully understand the behavior of the tower during its intended design life. Moreover, a seismic (Earthquake loading) analysis of the tower should be performed. Since, all the connections between of the braces to the chords are welded, a fatigue safety check must be carried out. Furthermore, the fatigue safety check is usually the governing design check.

Additionally, a life cycle analysis may also be performed, in order to compare the impacts due to the production of renewable energy with the production of conventional energy. Life-cycle analysis is a comprehensive methodology for the quantification of potential environmental impacts of a product or a system over its life cycle, from raw material acquisition, processing, manufacturing, use and disposal in the end-of-life stage (Gervásio et al, 2014). The LCA should have special attention with more detail the support structure emphasizing the importance of the end of-life stage of wind towers and the recycling and reusing of structural components. The life cycle analysis of a wind tower is represented on Figure 9.1.
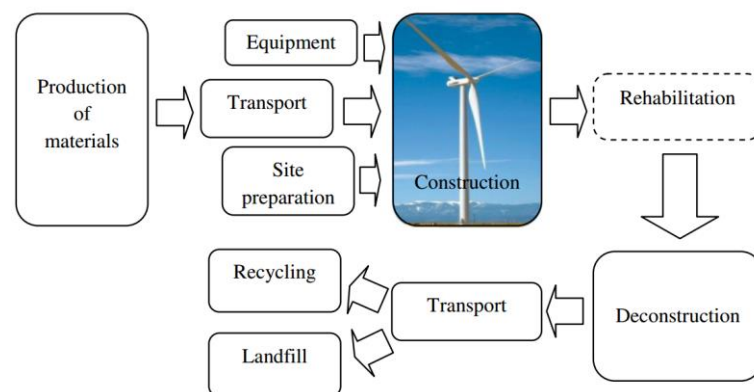
Figure 9.1 – Life cycle analysis of a wind tower (addapted from Gervásio et al, 2014)

Similar to the hybrid tower, the transition segment is fully welded. Therefore, the fatigue limit state (LS4) should be verified for the novel concept. Moreover, the cyclic plasticity limit state (LS2) should be verified as well, in order to have a complete study of the transition segment according to the standard EN1993-1-6. Once the novel concept checks for all limit states, an optimization process of the transition may be performed, in order to decrease its weight and consequently decrease the ratio cost/effectiveness. Increasing the inner ring diameter, thus decreasing the length of the elliptical tubes is one path that could lead to optimization.

In order to increase, the hybrid lattice-tubular steel tower, an even more competitive solution on the wind towers market, it is demanding to develop the erection procedure. First, some adaptations have to be made to the transition segment. The welded flange not only has to be interior and not exterior but also has to be bigger, using two rods of prestressed bolts and complemented with stiff plates. The figure below (Figure 9.2) shows in detail the transition from to connection for a concrete-tubular steel hybrid tower. A similar process can be adapted to the novel concept studied in this project. However, a detailed finite element analysis has to be done to simulate the transition and it has to be assessed if it is a feasible solution.
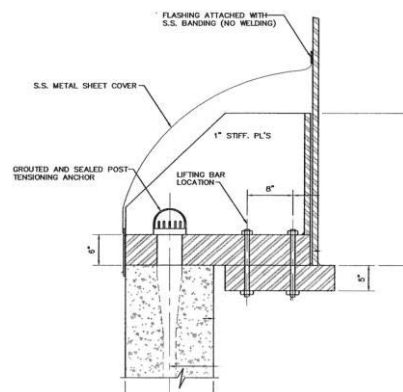
Figure 9.2 – Concrete tower to tubular steel tower conection (addapted from Hau, 2006)

Furthermore, the inner ring set is a key element on the transition segment and since it only can be assembled after the erection of the tubular parts, it has to be slightly adapted. Thus, to the end of each elliptical tube has to be welded an end plate. This plates will be further bolted to the outer ring, which will have also to be prepared and adapted to that. After prestressing the new inner ring set, it will be assembled with prestressed bolts to the outer ring. However, a construction phase study has to be performed to check whether the outer ring is stiff enough to withstand the erection procedure without collapsing.

It is worth to mention, that the present study was performed for onshore applications. Nevertheless, this hybrid concept can be easily adapted for offshore applications.

10 REFERENCES

Alves, Cristina. 2013. "Fatigue Behaviour of Wind Towers : Comparative Analysis of Flange Connections of Hybrid Steel- Concrete Wind Towers." University of Coimbra.

Ancona, Daniel et al. 2009. *WIND TURBINE TECHNOLOGY - FUNDAMENTAL CONCEPTS OF WIND TURBINE ENGINEERING*. Second. ed. David. Spera. ASME PRESS.

Baniotopoulos, C.C. et al. 2015. *Trends and Challenges for Wind Energy Harvesting*. Coimbra.

Baniotopoulos, Charalampos et al. 2015. *ADVANCES IN WIND ENERGY TECHNOLOGY*. Malta: Faculty for the built Environment, University of Malta.

BWEA. 2005. "Wind Turbine Technology." : 1–4.

Chen, Yang. 2014. "MSc Project Steel Structures : High Strength Steel Structures – FEM Validation Experiments."

EWEA. 2009a. *The Economics of Wind Energy*. 2009b. 3 International Journal of Energy Technology and Policy *The Economics of Wind Energy*. http://www.inderscience.com/link.php?id=6769.2015a. "The European Offshore Wind Industry - Key Trends and Statistics 2013." (January) 2015b. *Wind in Power*.

Figueiredo, Guilherme. 2013. "Structural Behavior of Hybrid Lattice – Tubular Steel Wind Tower." University of Coimbra.

Gervasio, H. et al. 2014. "Comparative Life Cycle Assessment of Tubular Wind Towers and Foundations - Part 2: Life Cycle Analysis." *Engineering Structures* 74: 292–99. http://dx.doi.org/10.1016/j.engstruct.2014.02.041.

GRI. 2015. "GRI Hybrid Towers." http://www.gri.com.es/en/business/gestamp-hybrid-towers.

GWEC. 2015. *Global Wind Statistics*. http://www.gwec.net/wp-content/uploads/2013/02/GWEC-PRstats-2012_english.pdf.

Haluzan, Ned. 2012. "Wind Energy Project." *Renewable Energie Articles*.

Hassanzadeh, Manouchehr. 2012. *Cracks in Onshore Wind Power Foundations Cracks in Onshore Wind Power Foundations-Causes and Consequences*.

Hau, Erich. 2013. *Wind Turbines Fundamentals, Technologies, Application, Economics*. Munich: Springer.

Heistermann, Christine. 2011. "Behaviour of Pretensioned Bolts in Friction Connections."

Hermann Scheer, *Energy Autonomy: The Economic, Social and Technological Case for Renewable Energy* (2006)

IRENA. 2013. *Renewable Power Generation Costs*.

Jonkman, Jm, S Butterfield, W Musial, and G Scott. 2009. "Definition of a 5-MW Reference Wind Turbine for Offshore System Development." *Contract* (February): 1–75. http://tethys-development.pnnl.gov/sites/default/files/publications/Jonkman_et_al_2009.pdf.

Júnior, Arafam. 2014. "Estruturas Metálicas Offshore Para Suporte de Turbinas Eólicas." University of Coimbra.

Lanier, M W. 2005. *LWST Phase I Project Conceptual Design Study : Evaluation of Design and Construction Approaches for Economical Hybrid Steel / Concrete Wind Turbine Towers LWST Phase I Project Conceptual Design Study : Evaluation of Design and*

Construction Approaches for.

Meseguer, Pablo. 2015. "MASTER THESIS REPORT Structures for Offshore Wind Turbines . Fatigue Analysis of a Jacket Support , Comparison between Welded and Cast."

NORDEX. 2013. "Turbines INSTALLED on 120 Meter High Hybrid Towers."

Novoselac, Stipica, Todor Ergić, and Pavo Baličević. 2012. "Linear and Nonlinear Buckling and Post Buckling Analysis of a Bar With the Influence of Imperfections." *Tehnički vjesnik* 19(3): 695–701.

Pires, Pedro. 2013. "Design of Concrete-Steel Transitions in a Hybrid Wind Turbine Tower." University of Coimbra.

Rebelo, C. 2013. "Design for Renewable Energy Systems."2014. "Comparative Life Cycle Assessment of Tubular Wind Towers and Foundations - Part 1: Structural Design." *Engineering Structures* 74: 283–91. http://dx.doi.org/10.1016/j.engstruct.2014.02.040.

Simões, Rui. 2014. *Manual de Dimensionamento de Estruturas Metálicas*. Coimbra: CMM.

Standard, Europeam. 2005. "Eurocode 3: Design of Steel Structures - Part 1-1: General Rules and Rules for Buildings."

Standard, European. 2006. "En 1993-1-5." : 1–53

Standard, European. 2007. "En 1993-1-6." : 1–94.

SUZLON. 2014. "Hybrid Lattice Tower." http://www.suzlon.de/index.php/54.html.

VAN DER TEMPEL, Jan. 2006. "Design of Support Structures for Offshore Wind Turbines." Technische Universiteit Delft.

Tirtawinata, Zelda. 2015. "FATIGUE AND SENSITIVITY ANALYSIS OF TIME DOMAIN SIMULATION OF STEEL WIND TOWER."

Veljkovic, M. et al. 2012. *HISTWIN - High-Strength Tower in Steel for Wind Turbines*.

Wiser, Ryan, and Mark Bolinger. 2013. "Wind Technologies Market Report Summary." (August): 1–39.

11 APPENDIX

Appendix I – Design of critical brace members per level

Appendix II – Design of critical chord members per level

Appendix III – Robot design for all members

Appendix IV – Modal analysis results

Appendix V – Towers concepts comparison

A. Appendix I – Design of critical brace members per level

Table A.1 – Utilization ratio for critical brace members per level

Braces								
Level	Bar	Element Type	Profile	Steel	Class	L (m)	Ratio Robot	Ratio Excell
1	304	Truss	CHS 355.6x8	S355	2	23.76	0.79	0.79
2	333	Truss	CHS 323.9x8	S355	2	20.71	0.98	0.98
3	321	Truss	CHS 323.9x10	S355	1	17.83	0.82	0.82
4	331	Truss	CHS 323.9x10	S355	1	15.19	0.91	0.91
5	371	Truss	CHS 355.6x16	S355	1	13.69	0.82	0.82
6	215	Truss	CHS 323.9x16	S355	1	8.32	0.97	0.97
7	204	Truss	CHS 355.6x16	S355	1	4.30	0.97	0.97

Table A.2 – Cross section for critical brace members

Outside Diameter	Inside Diameter	Thickness	Mass	Sectional Area	Moment of Inertia	Radius of Gyration	Elastic Modulus	Plastic Modulus	Torsional Constants
D	Di	t	M	A	I	i	W_{el}	W_{pl}	It
mm	mm	mm	Kg/m	cm^2	cm^4	cm	cm^3	cm^3	cm^4
323.9	307.9	8.0	62.4	79.4	9910.1	11.2	611.9	798.5	19820.2
323.9	303.9	10.0	77.5	98.6	12158.3	11.1	750.7	985.7	24316.7
323.9	291.9	16.0	121.6	154.8	18389.9	10.9	1135.5	1518.2	36779.9
355.6	339.6	8.0	68.7	87.4	13201.4	12.3	742.5	966.8	26402.7
355.6	323.6	16.0	134.2	170.7	24663.0	12.0	1387.1	1846.6	49326.0

Table A.3 – Definition of buckling curve

Cross Section		Buckling Curves	Imperfection Factor α
Hollow Section		a_0	0.13
Hot Finished		**a**	**0.21**
S355		b	0.34
		c	0.49
EN1993-1-1 6.3.1.2 T6.2		d	0.76

Table A.4 – Brace member verification

	Level 1	Level 2	Level 3	Level 4	Level 5	Level 6	Level 7	Units
Braces Verification - Cross Section and Member Verification according EN 1993-1-1								
α	0.21	0.21	0.21	0.21	0.21	0.21	0.21	-
L_{cr}	23.76	20.71	17.83	15.19	13.69	8.32	4.30	m
N_{cr}	484.7	478.9	792.7	1092.1	2727.5	5506.2	27645.7	kN
$\bar{\lambda}$	2.5	2.4	2.1	1.8	1.5	1.0	0.5	**Buckling Effects can't be ignored**
λ	0.0	185.4	160.6	136.8	113.9	76.3	35.8	**Verify**
Φ	3.9	3.7	2.9	2.3	1.7	1.1	0.6	-
χ	0.1	0.2	0.2	0.3	0.4	0.7	0.9	-
N_{Ed}	352.5	427.1	582.9	867.5	1879.2	3556.9	5480.9	kN
$N_{c,Rd}$	3101.3	2818.5	3500.8	3500.8	6059.9	5494.2	6059.9	kN
$N_{b,Rd}$	445.0	437.7	711.9	955.3	2281.2	3661.2	5659.2	kN
Ratio	0.79	0.98	0.82	0.91	0.82	0.97	0.97	**Verify**

B. Appendix II – Design of critical chord members per level
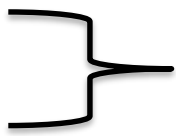
Table B.1 – Utilization ratio for critical chord members per level

Chords								
Level	Bar	Element Type	Profile	Steel	Class	L (m)	Ratio Robot	Ratio Excell
1	25	Beam	CHS 406.4x10	S355	2	10.82	0.92	0.92
2	24	Beam	CHS 406.4x12	S355	2	10.82	0.88	0.88
3	14	Beam	CHS 406.4x12	S355	2	9.82	0.88	0.88
4	9	Beam	CHS 457x16	S355	1	11.82	0.81	0.81
5	21	Beam	CHS 457x16	S355	1	10.82	0.93	0.93
6	254	Beam	CHS 559x25	S355	1	8.35	0.86	0.86
7	169	Beam	CHS 559x25	S355	1	3.67	0.97	0.97

Table B.2 – Cross section for critical chords members

Outside Diameter	Inside Diameter	Thickness	Mass	Sectional Area	Moment of Inertia	Radius of Gyration	Elastic Modulus	Plastis Modulus	Torsional Constants
D	Di	t	M	A	I	i	W_{el}	W_{pl}	It
mm	mm	mm	Kg/m	cm^2	cm^4	cm	cm^3	cm^3	cm^4
406.4	386.4	10.0	97.9	124.5	24475.8	14.0	1204.5	1571.7	48951.6
406.4	382.4	12.0	116.9	148.7	28937.0	14.0	1424.1	1867.2	57874.0
457.0	425.0	16.0	174.2	221.7	53959.4	15.6	2361.5	3113.1	107918.8
559.0	509.0	25.0	329.7	419.4	149821.6	18.9	5360.3	7134.1	299643.2

Table B.3 – Definition of buckling curve

Cross Section	Buckling Curves	Imperfection Factor α
Hollow Section	a_0	0.13
Hot Finished	**a**	**0.21**
S355	b	0.34
	c	0.49
EN1993-1-1 6.3.1.2 T6.2	d	0.76

Table B.4 – Chord member verification

Chords Verification - Cross Section and Member Verification according EN 1993-1-1							
	Level 1	Level 2	Level 3	Level 4	Level 5	Level 6	Level 7	Units
α	0.21	0.21	0.21	0.21	0.21	0.21	0.21	-
L_{cr}	9.74	9.74	8.84	10.64	9.74	8.35	3.67	m
N_{cr}	5349.5	6324.6	7678.3	9882.5	11793.6	44537.0	230548.0	kN
$\bar{\lambda}$	0.9	0.9	0.8	0.9	0.8	0.6	0.3	**Buckling Effects can't be ignored**
λ	77.2	77.6	70.4	75.8	69.4	44.2	19.4	**Verify**
Φ	1.0	1.0	0.9	1.0	0.9	0.7	0.5	-
χ	0.7	0.7	0.8	0.7	0.8	0.9	1.0	-
N_{Ed}	2858.0	3262.6	3521.5	4504.4	5562.1	10472.6	13428.5	kN
$V_{Ed,y}$	0.0	-0.1	-0.8	-1.6	-3.1	-17.6	-7.4	kN
$V_{Ed,z}$	1.2	0.3	-0.1	-9.1	-11.3	-1.1	35.5	kN
$M_{Ed,y}$	12.1	12.1	10.9	25.6	26.4	126.4	126.5	kN.m
$M_{Ed,z}$	1.4	1.2	-0.7	0.7	1.5	56.0	56.0	kN.m
T_{Ed}	-0.1	-0.1	-0.1	-0.1	-0.1	-0.1	0.0	kN.m
$N_{c,Rd}$	4420.9	5278.3	5278.3	7869.3	7869.3	14888.8	14888.8	kN
$N_{b,Rd}$	3218.2	3826.6	4109.9	5815.1	6184.7	13371.2	14710.2	kN
$M_{c,Rd}$	557.9	662.9	662.9	1105.1	1105.1	2532.6	2532.6	kN.m
$M_{N,Rd}$	292.2	370.3	329.7	677.1	492.5	1140.1	407.6	kN.m
$V_{T,Rd}$	1624.7	1940.3	1940.3	2892.6	2892.6	5472.6	5472.4	kN
Ratio	0.92	0.88	0.88	0.81	0.93	0.86	0.97	**Verify**

C. Appendix III – Design of critical brace members per level

Table C.1 – Robot design for chord members

			Chords				
n	BAR	PROFILE	MATERIAL	LAY	LAZ	RATIO	CASE
1	1	CHS 406.4x10	S 355	77.30	77.30	0.31	2 EO
2	2	CHS 406.4x12	S 355	77.54	77.54	0.32	2 EO
3	3	CHS 406.4x12	S 355	70.39	70.39	0.37	2 EO
4	4	CHS 406.4x12	S 355	70.39	70.39	0.4	2 EO
5	5	CHS 457x16	S 355	69.38	69.38	0.48	2 EO
6	6	CHS 406.4x10	S 355	77.30	77.30	0.49	2 EO
7	7	CHS 406.4x12	S 355	77.54	77.54	0.44	2 EO
8	8	CHS 457x16	S 355	75.78	75.78	0.35	2 EO
9	9	CHS 457x16	S 355	68.23	68.23	0.81	2 EO
10	10	CHS 457x16	S 355	69.38	69.38	0.35	2 EO
11	11	CHS 406.4x10	S 355	77.30	77.30	0.96	2 EO
12	12	CHS 406.4x12	S 355	77.54	77.54	0.91	2 EO
13	13	CHS 457x16	S 355	75.78	75.78	0.34	2 EO
14	14	CHS 406.4x12	S 355	63.31	63.31	0.88	2 EO
15	15	CHS 457x16	S 355	69.38	69.38	0.91	2 EO
16	16	CHS 406.4x10	S 355	77.30	77.30	0.1	2 EO
17	17	CHS 406.4x12	S 355	77.54	77.54	0.12	2 EO
18	18	CHS 406.4x12	S 355	70.39	70.39	0.88	2 EO
19	20	CHS 457x16	S 355	69.38	69.38	0.25	2 EO
20	21	CHS 457x16	S 355	62.44	62.44	0.93	2 EO
21	23	CHS 457x16	S 355	75.78	75.78	0.82	2 EO
22	24	CHS 406.4x12	S 355	69.78	69.78	0.88	2 EO
23	25	CHS 406.4x10	S 355	69.56	69.56	0.92	2 EO
24	26	CHS 406.4x10	S 355	77.30	77.30	0.35	2 EO
25	27	CHS 406.4x12	S 355	77.54	77.54	0.36	2 EO
26	28	CHS 406.4x12	S 355	70.39	70.39	0.15	2 EO
27	30	CHS 457x16	S 355	69.38	69.38	0.55	2 EO
28	31	CHS 406.4x10	S 355	77.30	77.30	0.23	3 EW
29	32	CHS 406.4x12	S 355	77.54	77.54	0.21	3 EW
30	33	CHS 457x16	S 355	75.78	75.78	0.16	2 EO
31	35	CHS 457x16	S 355	69.38	69.38	0.16	3 EW
32	36	CHS 406.4x10	S 355	77.30	77.30	0.64	2 EO
33	37	CHS 406.4x12	S 355	77.54	77.54	0.6	2 EO
34	40	CHS 457x16	S 355	69.38	69.38	0.58	2 EO

35	42	CHS 406.4x12	S 355	70.39	70.39	0.42	2 EO
36	43	CHS 457x16	S 355	75.78	75.78	0.39	2 EO
37	44	CHS 406.4x12	S 355	70.39	70.39	0.18	3 EW
38	45	CHS 457x16	S 355	75.78	75.78	0.16	3 EW
39	46	CHS 406.4x12	S 355	70.39	70.39	0.57	2 EO
40	47	CHS 457x16	S 355	75.78	75.78	0.53	2 EO
41	163	CHS 559x25	S 355	19.43	19.43	0.71	2 EO
42	164	CHS 559x25	S 355	19.43	19.43	0.17	3 EW
43	167	CHS 559x25	S 355	19.43	19.43	0.61	2 EO
44	169	CHS 559x25	S 355	19.43	19.43	0.97	2 EO
45	171	CHS 559x25	S 355	19.43	19.43	0.88	2 EO
46	172	CHS 559x25	S 355	19.43	19.43	0.36	2 EO
47	175	CHS 559x25	S 355	19.43	19.43	0.42	2 EO
48	176	CHS 559x25	S 355	19.43	19.43	0.82	2 EO
49	247	CHS 559x25	S 355	44.17	44.17	0.8	2 EO
50	248	CHS 559x25	S 355	44.17	44.17	0.35	2 EO
51	249	CHS 559x25	S 355	44.17	44.17	0.29	2 EO
52	250	CHS 559x25	S 355	44.17	44.17	0.6	2 EO
53	251	CHS 559x25	S 355	44.17	44.17	0.52	2 EO
54	252	CHS 559x25	S 355	44.17	44.17	0.17	3 EW
55	254	CHS 559x25	S 355	44.19	44.19	0.86	2 EO
56	288	CHS 559x25	S 355	44.17	44.17	0.56	2 EO

Table C.2 – Robot design for brace members

Braces							
n	BAR	PROFILE	MATERIAL	LAY	LAZ	RATIO	CASE
1	291	CHS 355.6x8	S 355	193.32	193.32	0.54	2 EO
2	292	CHS 355.6x8	S 355	193.32	193.32	0.05	2 EO
3	293	CHS 355.6x8	S 355	193.32	193.32	0.03	3 EW
4	294	CHS 355.6x8	S 355	193.32	193.32	0.37	3 EW
5	295	CHS 355.6x8	S 355	193.32	193.32	0.77	2 EO
6	296	CHS 355.6x8	S 355	193.32	193.32	0.1	2 EO
7	297	CHS 355.6x8	S 355	193.32	193.32	0.55	2 EO
8	298	CHS 355.6x8	S 355	193.32	193.32	0.09	2 EO
9	299	CHS 355.6x8	S 355	193.32	193.32	0.17	3 EW
10	300	CHS 355.6x8	S 355	193.32	193.32	0.03	3 EW
11	301	CHS 355.6x8	S 355	193.32	193.32	0.39	2 EO
12	302	CHS 355.6x8	S 355	193.32	193.32	0.08	2 EO

13	303	CHS 355.6x8	S 355	193.32	193.32	0.11	2 EO
14	304	CHS 355.6x8	S 355	193.32	193.32	0.79	2 EO
15	305	CHS 355.6x8	S 355	193.32	193.32	0.75	2 EO
16	306	CHS 355.6x8	S 355	193.32	193.32	0.08	2 EO
17	307	CHS 323.9x8	S 355	185.40	185.40	0.26	3 EW
18	312	CHS 323.9x8	S 355	185.41	185.41	0.07	3 EW
19	314	CHS 323.9x8	S 355	185.41	185.41	0.15	2 EO
20	319	CHS 323.9x8	S 355	185.41	185.41	0.73	2 EO
21	320	CHS 323.9x8	S 355	185.41	185.41	0.16	2 EO
22	325	CHS 323.9x8	S 355	185.41	185.41	0.66	2 EO
23	326	CHS 323.9x8	S 355	185.41	185.41	0.08	2 EO
24	333	CHS 323.9x8	S 355	185.41	185.41	0.98	2 EO
25	334	CHS 323.9x8	S 355	185.41	185.41	0.31	3 EW
26	336	CHS 323.9x8	S 355	185.41	185.41	0.03	3 EW
27	344	CHS 323.9x8	S 355	185.41	185.41	0.11	2 EO
28	345	CHS 323.9x8	S 355	185.41	185.41	0.81	2 EO
29	350	CHS 323.9x8	S 355	185.41	185.41	0.89	2 EO
30	351	CHS 323.9x8	S 355	185.41	185.41	0.15	2 EO
31	358	CHS 323.9x8	S 355	185.40	185.40	0.41	2 EO
32	360	CHS 323.9x8	S 355	185.41	185.41	0.11	2 EO
33	308	CHS 323.9x10	S 355	160.53	160.53	0.04	3 EW
34	311	CHS 323.9x10	S 355	160.52	160.52	0.38	3 EW
35	315	CHS 323.9x10	S 355	160.52	160.52	0.77	2 EO
36	318	CHS 323.9x10	S 355	160.52	160.52	0.12	2 EO
37	321	CHS 323.9x10	S 355	160.52	160.52	0.82	2 EO
38	324	CHS 323.9x10	S 355	160.52	160.52	0.11	2 EO
39	327	CHS 323.9x10	S 355	160.52	160.52	0.41	2 EO
40	332	CHS 323.9x10	S 355	160.52	160.52	0.16	2 EO
41	335	CHS 323.9x10	S 355	160.52	160.52	0.05	3 EW
42	337	CHS 323.9x10	S 355	160.52	160.52	0.18	3 EW
43	343	CHS 323.9x10	S 355	160.52	160.52	0.57	2 EO
44	346	CHS 323.9x10	S 355	160.52	160.52	0.14	2 EO
45	352	CHS 323.9x10	S 355	160.52	160.52	0.8	2 EO
46	353	CHS 323.9x10	S 355	160.52	160.52	0.15	2 EO
47	359	CHS 323.9x10	S 355	160.53	160.53	0.07	2 EO
48	361	CHS 323.9x10	S 355	160.52	160.52	0.56	2 EO
49	309	CHS 323.9x10	S 355	136.75	136.75	0.25	3 EW
50	310	CHS 323.9x10	S 355	136.78	136.78	0.11	3 EW
51	316	CHS 323.9x10	S 355	136.76	136.76	0.23	2 EO

52	317	CHS 323.9x10	S 355	136.76	136.76	0.67	2 EO
53	322	CHS 323.9x10	S 355	136.76	136.76	0.25	2 EO
54	323	CHS 323.9x10	S 355	136.76	136.76	0.62	2 EO
55	328	CHS 323.9x10	S 355	136.76	136.76	0.13	2 EO
56	331	CHS 323.9x10	S 355	136.76	136.76	0.91	2 EO
57	338	CHS 323.9x10	S 355	136.76	136.76	0.29	3 EW
58	339	CHS 323.9x10	S 355	136.76	136.76	0.05	3 EW
59	342	CHS 323.9x10	S 355	136.76	136.76	0.17	2 EO
60	347	CHS 323.9x10	S 355	136.76	136.76	0.75	2 EO
61	354	CHS 323.9x10	S 355	136.76	136.76	0.82	2 EO
62	355	CHS 323.9x10	S 355	136.76	136.76	0.24	2 EO
63	362	CHS 323.9x10	S 355	136.75	136.75	0.38	2 EO
64	363	CHS 323.9x10	S 355	136.78	136.78	0.16	2 EO
65	329	CHS 355.6x16	S 355	113.99	113.99	0.43	2 EO
66	330	CHS 355.6x16	S 355	113.99	113.99	0.31	2 EO
67	340	CHS 355.6x16	S 355	113.99	113.99	0.1	3 EW
68	341	CHS 355.6x16	S 355	113.99	113.99	0.18	3 EW
69	348	CHS 355.6x16	S 355	113.99	113.99	0.25	2 EO
70	349	CHS 355.6x16	S 355	113.99	113.99	0.59	2 EO
71	356	CHS 355.6x16	S 355	113.99	113.99	0.28	2 EO
72	357	CHS 355.6x16	S 355	113.99	113.99	0.8	2 EO
73	365	CHS 355.6x16	S 355	114.01	114.01	0.13	2 EO
74	366	CHS 355.6x16	S 355	113.99	113.99	0.54	2 EO
75	367	CHS 355.6x16	S 355	114.01	114.01	0.08	3 EW
76	368	CHS 355.6x16	S 355	113.99	113.99	0.36	3 EW
77	369	CHS 355.6x16	S 355	113.99	113.99	0.23	2 EO
78	370	CHS 355.6x16	S 355	113.99	113.99	0.76	2 EO
79	371	CHS 355.6x16	S 355	113.99	113.99	0.82	2 EO
80	372	CHS 355.6x16	S 355	113.99	113.99	0.21	2 EO
81	179	CHS 323.9x16	S 355	76.41	76.41	0.45	2 EO
82	182	CHS 323.9x16	S 355	76.41	76.41	0.86	2 EO
83	188	CHS 323.9x16	S 355	76.41	76.41	0.3	3 EW
84	191	CHS 323.9x16	S 355	76.41	76.41	0.44	2 EO
85	194	CHS 323.9x16	S 355	76.41	76.41	0.32	2 EO
86	197	CHS 323.9x16	S 355	76.41	76.41	0.13	3 EW
87	200	CHS 323.9x16	S 355	76.41	76.41	0.82	2 EO
88	203	CHS 323.9x16	S 355	76.41	76.41	0.63	2 EO
89	206	CHS 323.9x16	S 355	76.41	76.41	0.38	2 EO
90	209	CHS 323.9x16	S 355	76.41	76.41	0.25	3 EW

91	215	CHS 323.9x16	S 355	76.41	76.41	0.97	2 EO
92	218	CHS 323.9x16	S 355	76.41	76.41	0.64	2 EO
93	221	CHS 323.9x16	S 355	76.41	76.41	0.68	2 EO
94	224	CHS 323.9x16	S 355	76.41	76.41	0.32	3 EW
95	245	CHS 323.9x16	S 355	76.41	76.41	0.69	2 EO
96	246	CHS 323.9x16	S 355	76.41	76.41	0.61	2 EO
97	181	CHS 355.6x16	S 355	35.80	35.80	0.84	2 EO
98	184	CHS 355.6x16	S 355	35.80	35.80	0.65	2 EO
99	189	CHS 355.6x16	S 355	35.80	35.80	0.47	3 EW
100	190	CHS 355.6x16	S 355	35.80	35.80	0.7	2 EO
101	193	CHS 355.6x16	S 355	35.80	35.80	0.44	2 EO
102	198	CHS 355.6x16	S 355	35.80	35.80	0.16	3 EW
103	204	CHS 355.6x16	S 355	35.80	35.80	0.97	2 EO
104	205	CHS 355.6x16	S 355	35.80	35.80	0.34	2 EO
105	210	CHS 355.6x16	S 355	35.80	35.80	0.22	3 EW
106	211	CHS 355.6x16	S 355	35.80	35.80	0.95	2 EO
107	216	CHS 355.6x16	S 355	35.80	35.80	0.96	2 EO
108	219	CHS 355.6x16	S 355	35.80	35.80	0.97	2 EO
109	220	CHS 355.6x16	S 355	35.80	35.80	0.71	2 EO
110	225	CHS 355.6x16	S 355	35.80	35.80	0.34	3 EW
111	243	CHS 355.6x16	S 355	35.80	35.80	0.65	2 EO
112	244	CHS 355.6x16	S 355	35.80	35.80	0.83	2 EO

D. Appendix IV – Dynamic analysis results

Table D.1 – Dynamic analysis results

Case	Mode	Frequency (Hz)	Period (sec)	Rel.mas. UX (%)	Rel.mas. UY (%)	Rel.mas. UZ (%)	Cur.mas. UX (%)	Cur.mas. UY (%)	Cur.mas. UZ (%)	Total mass UX	Total mass UY	Total mass UZ
5	1	0.16	6.09	58.01	1.74	0	58.01	1.74	0	874068.8	874068.8	874068.8
5	2	0.16	6.09	59.75	59.75	0	1.74	58.01	0	874068.8	874068.8	874068.8
5	3	2.65	0.38	63.4	88.04	0	3.65	28.29	0	874068.8	874068.8	874068.8
5	4	2.65	0.38	91.69	91.69	0	28.29	3.65	0	874068.8	874068.8	874068.8
5	5	3.29	0.3	91.69	91.69	0	0	0	0	874068.8	874068.8	874068.8
5	6	3.3	0.3	91.69	91.69	91.73	0	0	91.73	874068.8	874068.8	874068.8
5	7	3.69	0.27	91.69	91.69	91.73	0	0	0	874068.8	874068.8	874068.8
5	8	3.69	0.27	91.69	91.69	91.73	0	0	0	874068.8	874068.8	874068.8
5	9	5.2	0.19	91.69	91.69	91.73	0	0	0	874068.8	874068.8	874068.8
5	10	5.2	0.19	91.69	91.69	91.73	0	0	0	874068.8	874068.8	874068.8
5	11	6.18	0.16	91.69	91.69	91.75	0	0	0.01	874068.8	874068.8	874068.8
5	12	6.47	0.15	91.69	91.69	91.75	0	0	0	874068.8	874068.8	874068.8
5	13	6.47	0.15	91.69	91.69	91.75	0	0	0	874068.8	874068.8	874068.8
5	14	6.98	0.14	91.69	91.69	91.75	0	0	0	874068.8	874068.8	874068.8
5	15	7.48	0.13	91.69	91.69	91.75	0	0	0	874068.8	874068.8	874068.8
5	16	7.48	0.13	91.69	91.69	91.75	0	0	0	874068.8	874068.8	874068.8
5	17	7.7	0.13	91.69	91.69	91.75	0	0	0	874068.8	874068.8	874068.8
5	18	7.7	0.13	91.69	91.69	91.75	0	0	0	874068.8	874068.8	874068.8
5	19	8.84	0.11	97.32	92.61	91.75	5.63	0.92	0	874068.8	874068.8	874068.8
5	20	8.84	0.11	98.24	98.24	91.75	0.92	5.63	0	874068.8	874068.8	874068.8
5	21	9.33	0.11	98.24	98.24	91.79	0	0	0.04	874068.8	874068.8	874068.8
5	22	9.85	0.1	98.24	98.24	91.79	0	0	0	874068.8	874068.8	874068.8
5	23	9.85	0.1	98.24	98.24	91.79	0	0	0	874068.8	874068.8	874068.8
5	24	10.02	0.1	98.27	98.35	91.79	0.03	0.1	0	874068.8	874068.8	874068.8
5	25	10.03	0.1	98.37	98.37	91.79	0.1	0.03	0	874068.8	874068.8	874068.8
5	26	10.13	0.1	98.37	98.37	91.79	0	0	0	874068.8	874068.8	874068.8
5	27	10.13	0.1	98.37	98.37	91.79	0	0	0	874068.8	874068.8	874068.8
5	28	11.15	0.09	98.37	98.37	93.87	0	0	2.08	874068.8	874068.8	874068.8
5	29	11.41	0.09	98.37	98.37	93.87	0	0	0	874068.8	874068.8	874068.8
5	30	11.61	0.09	98.37	98.37	93.87	0	0	0	874068.8	874068.8	874068.8

E. Appendix V – Towers concepts comparison

Table E.1 – Towers concepts comparison (addapted from Rebelo et al. 2014)

Concept	Name	Type	External Diameter (mm) Bottom/0,5Height/Top	Thickness (mm) Bottom/0,5Height/Top	Number of tendons Bottom/0,5Height/Top	Mass of Steel S355 (ton) / Volume of Concrete C40/50 (m3)	Steel Rebars/ Prestressing tendons	Flange/ Bolts (Ton/Number)
Steel Towers	WFC20	5.0 MW 150 m	10,100/-/4500	47/-/25	-	1025 ton	-	21.43/911
	FrC20	5.0 MW 150 m	9400/-/4500	44/-/20	-	871.9 ton	-	4.24/6280
	FrC40	5.0 MW 150 m	9600/-/4500	47/-/25	-	987.6 ton	-	4.27/6323
Concrete Towers	CT20	5.0 MW 150 m	12,000/8400/4500	620/425/300	56/42/10	1778.9 m3	12.9/74.2	-
	CT40	5.0 MW 150 m	12,000/8400/4500	620/425/300	56/42/10	1778.9 m3	12.9/74.2	-
Hybrid Concrete-Steel Towers	Concrete Part CT20	5.0 MW 150 m	11,800/9200/-	600/400/-	60/60/-	1187.5 m3	8.6/59.3	-
	Concrete Part CT40	5.0 MW 150 m	11,800/9200/-	600/400/-	60/60/-	1187.5 m3	8.6/59.3	-
	Steel Part WFC20	5.0 MW 150 m	-/7300/4500	-/36/25	-	342.5 ton	-	9.41/368
	Steel Part FrC20	5.0 MW 150 m	-/6950/4500	-/32/20	-	284.1 ton	-	1.41/2090
	Steel Part FrC40	5.0 MW 150 m	-/7050/4500	-/36/25	-	334.8 ton	-	1.42/2099
Hybrid Lattice-Tubular Steel Tower	Lattice Part	5.0 MW 150 m	-	-	-	233.6 ton	-	-
	FrC20	5.0 MW 150 m	4500/-/2350	23/-/10	-	139 ton	-	1.25/1845